The Application of Broadband Constant Beamwidth Transducer (CBT) Theory to Loudspeaker Arrays

D. B. (Don) Keele, Jr.
DBK Associates
Niles, MI 49120, USA

Presented at
the 109th Convention
2000 September 22-25
Los Angeles, California, USA

A U D I O
ES

AN AUDIO ENGINEERING SOCIETY PREPRINT

The Application of Broadband Constant Beamwidth Transducer (CBT) Theory to Loudspeaker Arrays

D. B. (DON) KEELE, JR.

DBK Associates, Niles, MI 49120, USA

A brief tutorial review of CBT theory as first developed by the military for underwater transducers (JASA July 1978 and June 1983) is presented. Here the transducer is a circular spherical cap of arbitrary half angle with Legendre function shading. This provides a constant beam pattern and directivity with extremely low sidelobes for all frequencies above a certain cutoff frequency. This paper extends the theory by simulation to discrete-source loudspeaker arrays including 1) circular wedge line arrays of arbitrary sector angle which provide controlled coverage in one plane only, 2) circular spherical caps of arbitrary half angle which provide controlled axially-symmetric coverage, and 3) elliptical toriodal caps which provide controlled coverage for arbitrary and independent vertical and horizontal angles.

0.   INTRODUCTION

The holy grail of loudspeakers is a sound source that provides a sound field whose three-dimensional radiation pattern is constant over a wide frequency range. This type of source provides an acoustic output whose spectral content does not vary with direction. Particularly challenging is a speaker that couples these characteristics with high directivity. Traditionally, these speakers are called constant-directivity or constant-beamwidth devices.

Various methods have been used in the sound industry to approximate this behavior including horns [1], [2], omnidirectional sources [3], and arrays [4] [5], higher-order sources [6], etc. Underwater transducers have much the same problems as in-the-air transducers. Here, one excellent solution to this problem is described in two papers written by authors at the U. S. Navel Research Laboratory (now at the Naval Undersea Warfare Center) [7], [8]. This research, which describes spherical transducers with shaded caps, is described in the next section.

This paper extends this research to arrays of loudspeakers via computer simulation and prediction of radiation patterns using three-dimensional discrete arrays of point sources.

1.   BRIEF REVIEW OF CBT THEORY

Rogers and Van Buren [7], and Buren et. al. [8] describe the theory and experiments of what they call broadband "constant beamwidth transducers" (CBT) for use as underwater projectors and receivers for sonar use. Here the transducer is in the form of a circular spherical cap of arbitrary half angle whose normal surface velocity (or pressure) is shaded with a Legendre function. The Legendre shading is independent of frequency. This transducer provides a broadband symmetrical directional coverage whose beam pattern and directivity is essentially

independent of frequency over all frequencies above a certain cutoff frequency, and also change very little with distance from the source. The transducer can be designed to cover any arbitrary coverage angle with a constant beamwidth that extends over an operating bandwidth which is, in theory, virtually unlimited.

Figure 1 shows a circular spherical cap of half angle θ_0 on the surface of a sphere of radius a. Rogers and Van Buren [7] determined that if the radial velocity (or equivalently the surface pressure) on the surface of a rigid sphere of radius a conforms to

$$u(\theta) = \begin{cases} P_v(\cos\theta) & \text{for} \quad \theta \le \theta_0 \\ 0 & \text{for} \quad \theta > \theta_0 \end{cases} \tag{1}$$

where

$u(\theta)$ = radial velocity distribution

θ = elevation angle in spherical coordinates,

$\quad$ ($\theta = 0$ is center of circular spherical cap)

θ_0 = half angle of spherical cap

$P_v(x)$ = Legendre function of order v ($v > 0$) of argument x,

then an approximation to the farfield pressure pattern, above a cutoff frequency which depends on the size of the sphere and the wavelength, will be

$$p(\theta) \cong \begin{cases} P_v(\cos\theta) & \text{for} \quad \theta \le \theta_0 \\ 0 & \text{for} \quad \theta > \theta_0 \end{cases} \tag{2}$$

where

$p(\theta)$ = radial pressure distribution.

This surprising result shows that the farfield sound pressure distribution is essentially equal to the pressure distribution on the surface of the sphere. Rogers and Van Buren also point out that because the surface pressure and velocity are nearly zero over the inactive part of the outside surface of the sphere, the part of the rigid spherical shell outside the spherical cap region $\theta > \theta_0$ can be removed without significantly changing the acoustic radiation. This means that the ideal constant beamwidth behavior of the spherical cap is retained even though the rest of the sphere is missing!

The Legendre function $P_v(\cos\theta)$ is equal to one at $\theta = 0$ and has its first zero at angle $\theta = \theta_0$, the half angle of the spherical cap. The Legendre function order (v) is chosen so that its first zero occurs at the half angle of the spherical cap. Note that v is normally greater than one, and not necessarily an integer.

Rogers and Van Buren calculate an approximate lower limit for the constant beamwidth operation which they call the cutoff frequency Ω_v. They point out that intuitively the spherical cap must be large enough to support a sound beam of the required width.

Rogers and Van Buren also point out that the constant beamwidth behaviour of a rigid spherical cap also applies as well to an acoustically transparent spherical shell. However the acoustic radiation is bidirectional, generating the same beam pattern front and rear.

Rogers and Van Buren go on to design three example CBTs for Legendre orders of $v = 5, 7.5,$ and 10 called respectively P_5 CBT, $P_{7.5}$ CBT, and P_{10} CBT. These values result in transducers having total cap angles of roughly 50º, 34º, and 26º. These three CBTs are shown in Fig. 2 (which is a copy of Fig. 1 of ref. [7]). Figure 3 shows the three velocity shading functions for these CBTs (which is a copy of Fig. 2 of [7]). Figures 4, 5, and 6 show plots of the range of beam patterns for these three CBTs (which are copies of ref. [7]'s Figs. 5, 7, and 8). Note the extreme uniformity of the beam patterns exhibited in these plots.

To sum up the advantages of the CBT I quote from [7]:

> "We enumerate the expected properties of the CBT above cutoff:
>
> (1) Essentially constant beam pattern.
>
> (2) Very low sidelobes.
>
> (3) The surface distribution as well as the pressure distribution at all distances out to the farfield is approximately equal to the surface distribution. Thus in a sense, there is no nearfield.
>
> (4) Since both the surface velocity and surface pressure have the same dependence on θ, the local specific acoustic impedance is independent of θ (and equal to $\rho_0 c$). Thus the entire transducer is uniformly loaded."

Advantages (3) and (4) in this list are extra added bonuses of the CBT. Advantage (3) means that the beam patterns and polars generated by the CBT are not only very uniform with frequency, but stay essentially the same at very far distances, very close distances, and anywhere in between!

2.   APPLICATION TO LOUDSPEAKER ARRAYS

Existing CBT theory applies to a continuous (i.e. non discrete) source on the surface of a rigid sphere. When the theory is extended to discrete arrays of point sources or loudspeakers, an upper bandwidth limitation exists where the center-to-center spacing of the sources is on the order of a wavelength at the upper operating frequency. At higher frequencies, the constant beamwidth behavior falls apart. In this higher-frequency range, the individual elements that make up the array must individually provide narrow coverage, so that the total array at high

frequencies can approximate its behavior at lower frequencies. This aspect is not dealt with in this paper.

The theory is found to apply equally well to circular wedge-shaped line arrays, which provide constant-beamwidth operation in one plane only, and to elliptical toriodal caps that provide asymmetrical coverage for arbitrary and independent vertical and horizontal angles, over arbitrary frequency ranges. The array shape in the latter case is an ellipse on the surface of a torus. The torus (a doughnut shape), has two independent radii of curvature which allows the vertical and horizontal coverage's of the array to be independently set.

In all cases, the size of the array and its angular coverage set the low-frequency limit of the constant beamwidth operation range, while the center-to-center spacing of the array elements sets the upper operating limit.

The relationship between the size of the array, the angular coverage, and the low frequency cutoff is approximately the same as the corresponding relationships for constant directivity horns shown in [1, Eq. (10), Figs. 17 and 18]:

$$ X = \frac{K}{\theta\, f_i} \tag{3} $$

where

X = horn mouth width (or height)

θ = coverage angle of horn

f_i = frequency down to which coverage angle is maintained

(assumed same as CBT cutoff frequency)

K = a constant (= 2.5 x 10^4 meters-degs-Hz, or

1 x 10^6 inches-degs-Hz).

Example: this relationship indicates that a source must be about 0.34 m (13.5 in.) high to provide 65 deg coverage down to 1.15 kHz (the same dimension used in most of the following simulations).

The following three subsections describe the array configurations that were analyzed by simulation with point-source arrays.

2.1   Circular-Wedge Line Arrays

Figure 7 shows the configuration of the circular segment line array. The sources are equally spaced around the arc of a circle of radius b and wedge angle θ.

2.2   Spherical Cap Arrays

Figure 8 shows the configuration of the spherical cap array. The spherical cap of radius a and total angle θ_M is circular, and has sources spaced in concentric circles with a point density that is approximately equal over the surface of the cap.

2.3   Toriodal Cap Arrays

Figure 9 shows the configuration of the toriodal cap array. The elliptical toriodal cap has width c and height d with angles of θ horizontal and ψ vertical. Usually $d > c$ and $\theta > \psi$. The torus has major and minor radii of α and β. The sources are located on the elliptical cap with a point density that is approximately equal over the surface of the cap.

3.   ARRAY SIMULATIONS

3.1   Introduction

A comprehensive point-source array simulator program was written using the program Igor Pro 3.1 by WaveMetrics. (Details on Igor are found in the Appendix.) This program calculates the pressure distribution at a specific distance for a 3-D array of point sources of arbitrary magnitude and phase. Program outputs include:

1. Source configuration views as seen from front, top, and sides with magnitude shading indicated by source size.

2. Horizontal and vertical beamwidth (-6dB) vs. frequency plots at each one-third-octave center from 20 Hz to 16 kHz.

3. Directivity index and Q vs. frequency plots at each one-third-octave center from 20 Hz to 16 kHz.

4. On-axis response loss plot vs. frequency (compared to all sources on and in-phase at the pressure sampling point). This plot indicates how much on-axis attenuation the array imposes as compared to the situation where all the sources add in phase at the sampling point.

5. Complete set of horizontal and vertical polar plots at all one-third octaves over the frequency range of 20 Hz to 20 kHz. The polar displays have 0 dB on the outside edge and –40 dB in the center with 10 dB grid circle spacings. The –6dB grid circle is also drawn. All polars are normalized so that the outside edge represents the level of all sources on and in phase. On-axis loss <u>is</u> preserved in the polars.

6. Complete set of ±60º horizontal x ±60º vertical footprint plots at all one-third octaves over the frequency range of 20 Hz to 16 kHz. In each footprint plot, the pressure in dB is normalized to the maximum in the stated angular range and is shown as a grey-scale density plot (high pressure in white and low in black).

This output information allows a complete analysis to be done of the pressure distribution generated by each specific source configuration. This program was used to analyze all the following array configurations. Arrays analyzed include straight line, circular wedge line, circular spherical cap, and toriodal cap. All point sources were equally spaced on the line arrays, and spaced for approximate equal point density on the surface of the spherical cap and toriodal cap arrays.

3.2   Approximation of Legendre Shading Function

To simplify calculation of the Legendre shading functions, a four-term power series was developed that approximates eq. (1). Although Fig. 3 shows slight changes in shape for different Legendre orders v (when normalized to the first zero crossing), the following third-order power-series approximation fits the Legendre shading function acceptably well over all useful orders:

$$U(x) \approx \begin{cases} 1 + 0.066x - 1.8x^2 + 0.743x^3 & \text{for} \quad x \leq 1 \\ 0 & \text{for} \quad x > 1 \end{cases} \tag{3}$$

where

$$x = \text{normalized angle} \left(\frac{\theta}{\theta_0} \right)$$

Note that this function is exactly 1 at $x = 0$ and 0 at $x = 1$ (where $\theta = \theta_0$ the half cap angle). All the following simulations use eq. (3) as a substitute for the Legendre polynomial function.

Fig. 10 shows plots of this function on linear and log vertical scales. Note that the function is one-half or 6-dB down at roughly $x = 0.64$. This implies that the beamwidth generated by a CBT is roughly 64% of the total cap angle, i. e. a 100° cap will generate a 64° beamwidth. Or stated another way, a desired 90° coverage angle requires a much larger total cap angle of about 140° ($\approx 90/0.64$).

3.3   Line Arrays

Several line arrays were simulated including: an 11-point equal-level straight line array, and several 100° circular wedge line arrays with various numbers of points (11, 21, and 81) and types of shading. Shading variations included: equal level (no shading), Legendre [using Eq. (3)], and two- and three-level stepped approximations (0, -6 dB and 0, -6, -12 dB). The height of most of the circular-wedge line arrays was set to one-wavelength at 1 kHz, i.e. about 0.34 m or 13.5 inches (assuming a speed of sound in air of 343 m/s). The 81-point circular wedge line array was much higher at 1.37 m (54 in.), which is one wavelength at 250 Hz. All line arrays were oriented with their longest dimension vertical (z axis) and faced towards the positive x axis.

3.3.1   Straight Line Array, 11-Point, Equal Levels

Figure 11 displays information and simulation results of the 11-point 13.5-in.-high straight line array with equal level drives (no shading) as follows: (a) front, top, and side configuration views, (b) plot of beamwidth vs. frequency, (c) directivity and Q vs. frequency, (d) on-axis loss plot vs frequency, (e) vertical polar plots of the array from 630 Hz to 16 kHz at one-third-octave centers, and (f) footprint plots from 630 Hz to 16 kHz at one-third-octave centers.

The beamwidth plot (b) exhibits the classic straight line array narrowing of vertical coverage of the main beam as frequency increases. Directivity (c) continues to increase up to 8 kHz where the source-to-source spacing becomes comparable to wave length. No on-axis loss (d)

is evident as all sources arrive in phase at on-axis points far from the array. Horizontally, the array is omnidirectional (not shown). Vertical polars (e) show the complex off-axis behaviour as frequency rises with multiple lobes. The footprint plots (f) clearly show the omnidirectional horizontal response and the fragmented vertical response.

3.3.2   Circular-Wedge Line Array, 11-Point, Equal Levels (No shading)
Figure 12 displays information and simulation results of the 11-point circular-wedge line array with equal level drives (no shading) as follows: (a) configuration views, (b) beamwidth, (c) directivity and Q, (d) on-axis loss, (e) horizontal polars, (f) vertical polars, and (g) footprints.

The vertical beamwidth plot (b) exhibits the classic coverage of a curved line source: above a certain frequency the angular coverage is roughly equal to the wedge angle (100º in this case) with a slight amount of midrange narrowing in the lower part of the control range. At higher frequencies of 8 kHz and above, the beamwidth control falls apart due to the spacing of the sources. The vertical polars (f), although not narrowing as frequency increases as the straight line source, exhibits much fingering and lobing. The footprint plots (f) show much interference and banding.

3.3.3   Circular-Wedge Line Array, 11-Point, Legendre Shading
Figure 13 displays information and simulation results of the 11-point circular-wedge line array with Legendre shading. This is the same array configuration as Fig. 12 but Legendre shading was used (eq. 3).

Here the vertical beamwidth (b) is much more well behaved. The coverage angle has narrowed and the midrange narrowing is minimal. The vertical polars (f) in the range of 1.6 to 6.3 kHz are extremely uniform and lobe free. As before, the vertical coverage falls apart at 8 kHz and above due to the spacing of the sources. Note also the symmetrical front-rear polars, this is because the point sources radiate equally well front and rear and thus simulate an acoustically transparent spherical shell (as pointed out in section 1.). The footprint plots (g) are extremely uniform up to 6.3 kHz.

3.3.4   Circular-Wedge Line Array, 21-Point, Equal Levels (No shading)
Figure 14 displays information and simulation results of the 21-point circular-wedge line array with equal level drives (no shading). Here the height of the array is the same as the previous array but filled with more point sources. The closer spacing of the sources allow the array to operate well up to a higher 12.5 kHz. The vertical beamwidth (b), although fairly well behaved as compared to previous speakers, still exhibits some midrange narrowing and high-frequency drop off. The directivity (c) bobs up and down due to non-uniform polars. As with the 11-point non shaded wedge, the vertical polars (f) exhibit much non uniformity, ripple, and lobes. The interference in the forward direction is clearly shown in the footprint plots (g).

3.3.5   Circular-Wedge Line Array, 21-Point, Legendre Shading
Figure 15 displays information and simulation results of the 21-point circular-wedge line array with Legendre shading.

The Legendre shading works wonders here, all data plots are extremely uniform up to 16 kHz! Interestingly, the on-axis loss plot shows a uniform rolloff of 3-dB/octave starting at 2 kHz.

At higher frequencies, the horizontal polar plots (e) exhibit a characteristic two-petal shape with bulges in the right and left directions (up and down on the polar graphs).

3.3.6   Circular-Wedge Line Array, 21-Point, 0, -6, -12 dB Step Shading

Figure 16 displays information and simulation results of the 21-point circular-wedge line array with three-stepped shading of 0, -6, and -12 dB. Here the Legendre shading is crudely approximated with three 6-dB steps as follows: assuming the sources are numbered 0 to 20, points 0,1,19, and 20 are set to 0.25, points 2-4 and 16-18 are set to 0.5, and the remaining central points 5-15 are set to unity (the center source is number 10).

Surprisingly the results are still quite good as compared to the equal level (no shading) situation of Fig. 14.

3.3.7   Circular-Wedge Line Array, 21-Point, 0, -6 dB Step Shading

Figure 17 displays information and simulation results of the 21-point circular-wedge line array with two-stepped shading of 0, -6 dB. This simulation approximates the Legendre shading with only two steps of 0, and –6 dB as follows: points 0-4 and 16-20 are set to 0.5, and the remaining central points 5 to 15 are set to unity.

Although not nearly as good as full Legendre shading, a definite improvement over the equal level (no shading) situation of Fig. 14 is evident. This and the previous shading are easy to implement by simple series-parallel wiring of speakers that make up an array.

3.3.8   Circular-Wedge Line Array, 81-Point, Legendre Shading

Figure 18 displays information and simulation results of the 81-point circular-wedge line array with Legendre shading. This array was intended to be a no-holds-bared configuration with enough point sources to provide wide-band coverage from 250 Hz to 16 kHz. This array is four times higher than the previous ones at 1.37 m (54 in.), which is one wavelength at 250 Hz. As evidenced by the simulation, the results are nearly perfect! The configuration does however exhibit significant on-axis loss of nearly 17 dB at 16 kHz.

3.4   Spherical Cap Arrays

Two 100º spherical cap arrays were simulated with Legendre shading [using Eq. (3)] with 121 and 381 point sources. Both arrays were 0.34 m (13.5 inches) in diameter, which is one wavelength at 1 kHz.

3.4.1   Circular Spherical Cap Array, 121-Point, Legendre Shading

This array has one central point source with six concentric rings of additional sources. Point center-to-center spacing is roughly 33 mm (1.3 inches). Figure 19 displays information and simulation results of the 121-point spherical cap array with Legendre shading.

Here the results are very good in the range of 1 to 8 kHz. At higher frequencies the results degrade due to spacing of the sources. Note that coverage is symmetrical in both planes. Up to 8 kHz, the horizontal and vertical polars (e) and (f) are essentially exactly the same. Above this frequency however, asymmetries are evident because the source is not exactly symmetrical up-down vs. right-left. The footprint plots are very well behaved from 1 to 8 kHz, but exhibit extremely interesting patterns at higher frequencies.

3.4.2   Circular Spherical Cap Array, 381-Point, Legendre Shading

This array has one central point source with 11 concentric rings of additional sources. Point center-to-center spacing is roughly 18 mm (0.7 inches). Figure 20 displays information and simulation results of the 381-point spherical cap array with Legendre shading.

Like the array of Fig. 18, this one was intended to provide exemplary performance above 1 kHz. Results are extremely good.

3.5 Toriodal Cap Array

A 100º horizontal x 50º vertical toroidal cap array was simulated with Legendre shading [Eq. (3)] with 372 point sources. To maintain beamwidth control down to the same frequency in both planes, the height of the array was set to twice its width. The array has the following characteristics: height (ellipse major axis) = 0.69m (27 inches), width (ellipse minor axis)= 0.34 m (13.5 inches), horizontal radius (torus minor radius) = 0.22 m (8.81 inches), and vertical radius (torus major radius) = 0.81 m (31.94 inches). Note that the width of the array is one wavelength at 1 kHz, and the height is two wavelengths at 1 kHz. This provides beamwidth control down to approximately 1 kHz in both planes.

3.5.1   Elliptical Toriodal Cap Array, 372-Point, Legendre Shading

This array has 15 point sources along the ellipse minor axis (horizontal) and 31 along the ellipse major axis (vertical). Angular coverage is approximately 64º horizontal and 32º vertical. Figure 21 displays information and simulation results of the 372-point elliptical toroidal cap array with Legendre shading.

The beamwidth plot (b) shows that the array provides different angular coverage in both planes as designed. Some midrange narrowing is evident in both planes at 2 kHz. The horizontal beamwidth drops off above 10 kHz. The polar plots (e) and (f) are extremely uniform and lobe free and clearly show that the vertical pattern (f) is significantly narrower than the horizontal (e).

4.   CONCLUSIONS

This paper reviewed the theory of broadband "constant beamwidth transducers" (CBT) as originally applied to underwater transducers by the military. Here the transducer is a continuous Legendre-shaded spherical cap. The applied Legendre shading is independent of frequency. The CBT provides nearly perfect polar behavior with extremely low sidelobes and constant directivity over a very wide frequency range above a certain cutoff frequency. The distribution pattern of the array is found to be essentially independent of distance from the CBT, which effectively means the CBT has no nearfield. The CBT is found to be uniformly loaded because the surface velocity and surface pressure are in phase and exhibit the same dependence on angle.

By simulation, CBT theory was found to apply equally as well to discrete arrays of point sources on a spherical cap and hence can be applied to arrays of transducers such as loudspeakers operating in air or water.

A high frequency limit was found to apply when the point source center-to-center spacing was comparable to a wavelength. At higher frequencies, the CBT array ceases to operate as a constant beamwidth device. In this higher frequency range, the narrowing directivity of real-world transducers may provide control of beamwidth.

Two and three step approximations to the Legendre shading were found to operate acceptably well for some applications. These approximations allow easy hookup of transducers with series/parallel connections to implement the stepped shading.

Simulations also showed that CBT theory and Legendre shading apply equally well to circular wedge line arrays and to elliptical toriodal cap arrays. The circular wedge line arrays provide ideal constant beamwidth coverage in one plane only. The toriodal cap CBT configuration provides constant beamwidth coverage with independent vertical and horizontal coverage angles.

5.   REFERENCES

[1] D. B. Keele, Jr., "What's So Sacred About Exponential Horns?," presented at the 51st Convention of the Audio Engineering Society (1975 May), preprint 1038.

[2] C. A. Henricksen and M. S. Ureda, "The Manta Ray Horns," J. Audio Eng. Soc., vol. 26, no. 9 (1978).

[3] D. Queen, (To be supplied).

[4] M. van der Wal, E.W. Start, D. de Vries, "Design of Logrithmically Spaced Constant-Directivity Transducer Arrays," J. Audio Eng. Soc., vol. 44, no. 6 (1996).

[5] D. G. Meyer, (To be supplied).

[6] J. K. Hilliard, "Unbaffled Loudspeaker Column Arrays," J. Audio Eng. Soc., vol. 32, no. 5 (1970).

[7] P. H. Rogers, and A. L. Van Buren, "New Approach to a Constant Beamwidth Transducer," *J. Acous. Soc. Am.*, vol. 64, no. 1, pp. 38-43 (1978 July).

[8] A. L. Van Buren, L. D. Luker, M. D. Jevnager, and A. C. Tims, "Experimental Constant Beamwidth Transducer," *J. Acous. Soc. Am.*, vol. 73, no. 6, pp. 2200-2209 (1983 June).

6. APPENDIX: GRAPHING and DATA ANALYSIS PROGRAM

All simulations, graphs, and data analysis in this paper were done using the program Igor Pro Version 3.1 by WaveMetrics. I have been using this program since 1990 and give it my highest recommendation (and no, I do not have any stock in the company, just an enthusiastic user!). It is available on both PC and Apple Macintosh platforms (it started out on the Mac, and as a result is very easy to use). Information, a full operating demo, and documentation is available from their Web site at www.wavemetrics.com.

Company contact information:

Address:

> WaveMetrics, Inc.
>
> P.O.Box 2088
>
> Lake Oswego, OR 97035
>
> USA
>
> Voice: (503) 620-3001
>
> Fax: (503) 620-6754

7.   FIGURES
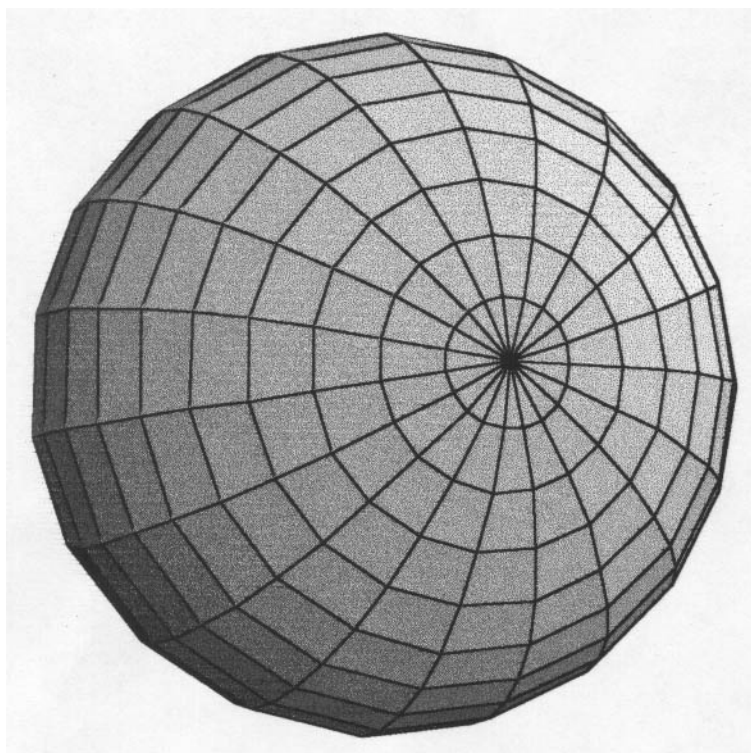
Sphere with cap in place   Cap with sphere removed
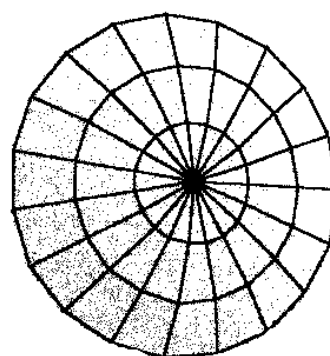
******* Figure not completed!! ********

Fig. 1. Circular spherical cap of half angle θ_0 on the surface of a sphere of radius a.
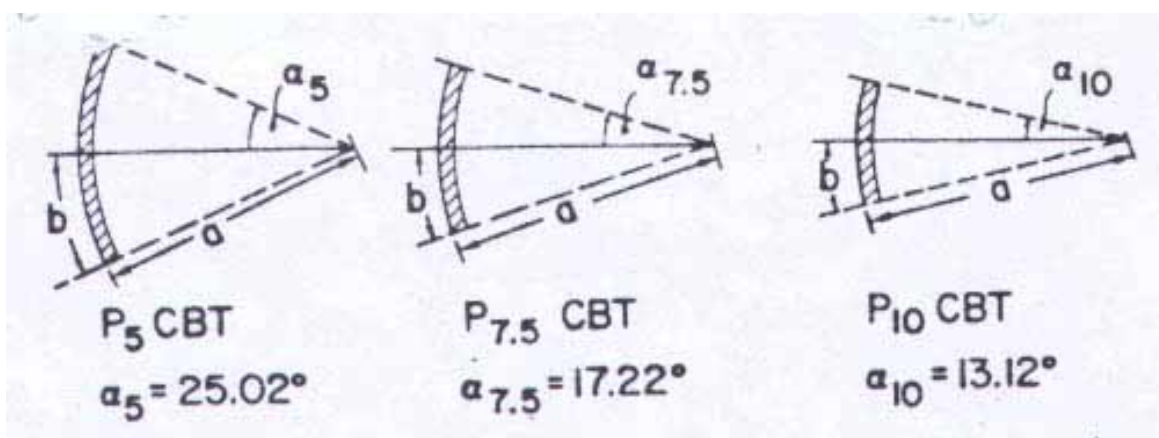
Fig. 2. Geometry of P_5 CBT (left), $P_{7.5}$ CBT (center), and P_{10} CBT (right) spherical cap constant-beamwidth transducers. (Reproduced from Fig. 1 of [7].)
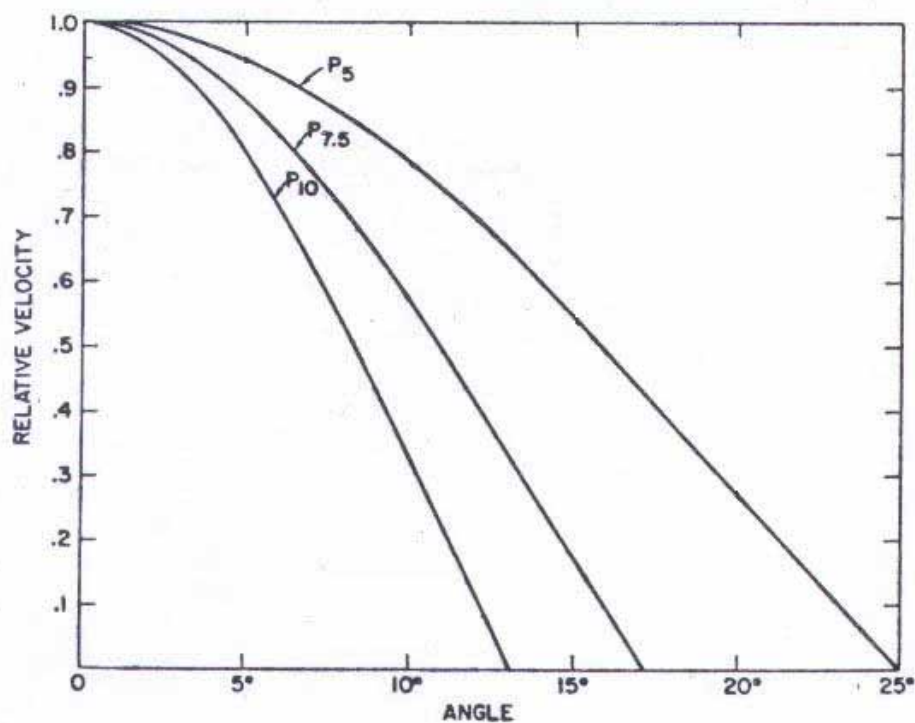
Fig. 3. Velocity shading functions [from Eq. (1)] for Legendre orders of v = 5, 7.5, and 10. (Reproduced from Fig. 2 of [7].)
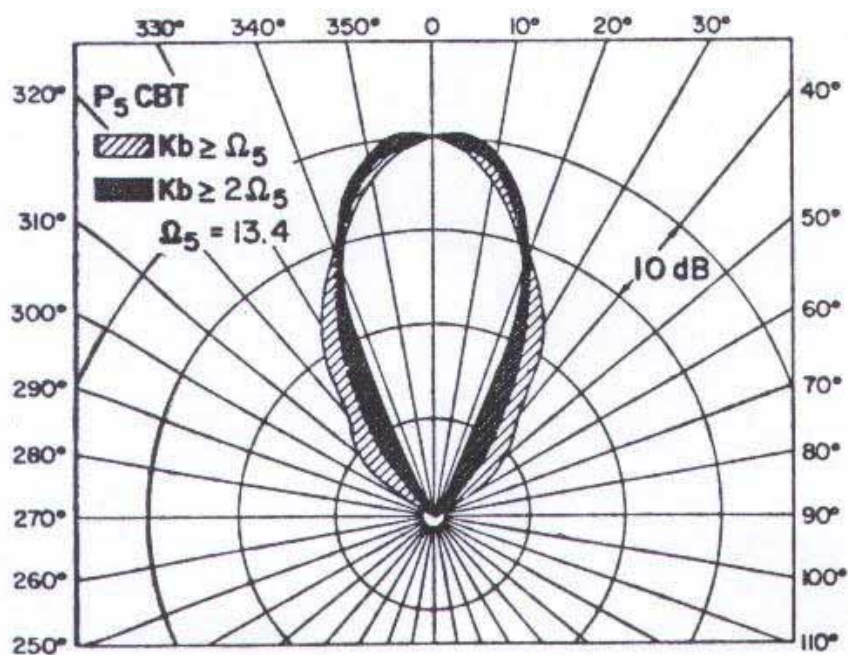
Fig. 4. Range of beam patterns for the P_5 CBT in the range above cutoff (hatched area) and twice the cutoff (solid area). (Reproduced from Fig. 5 of [7].)
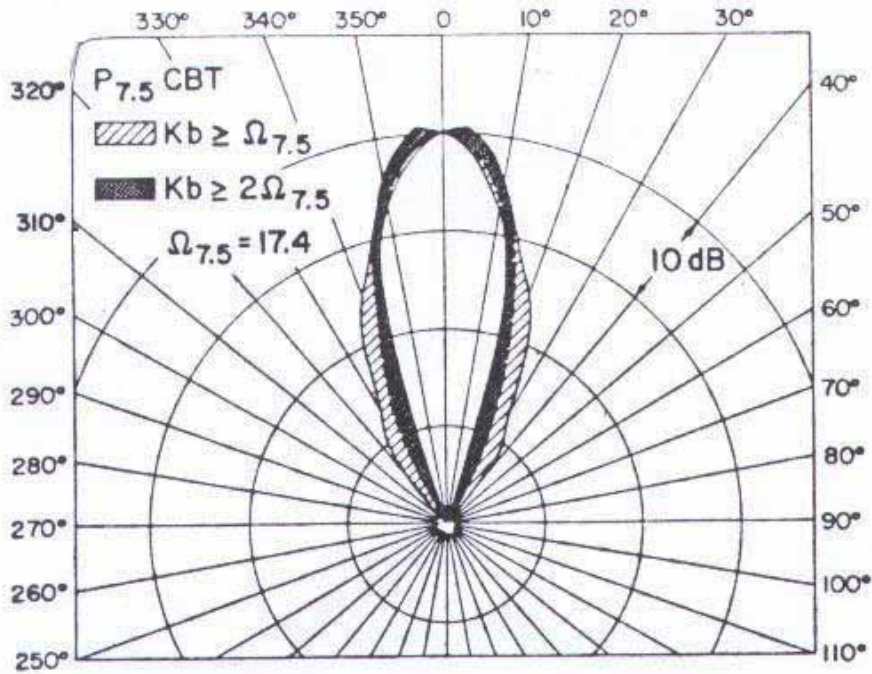
Fig. 5. Range of beam patterns for the $P_{7.5}$ CBT in the range above cutoff (hatched area) and twice the cutoff (solid area). (Reproduced from Fig. 7 of [7].)
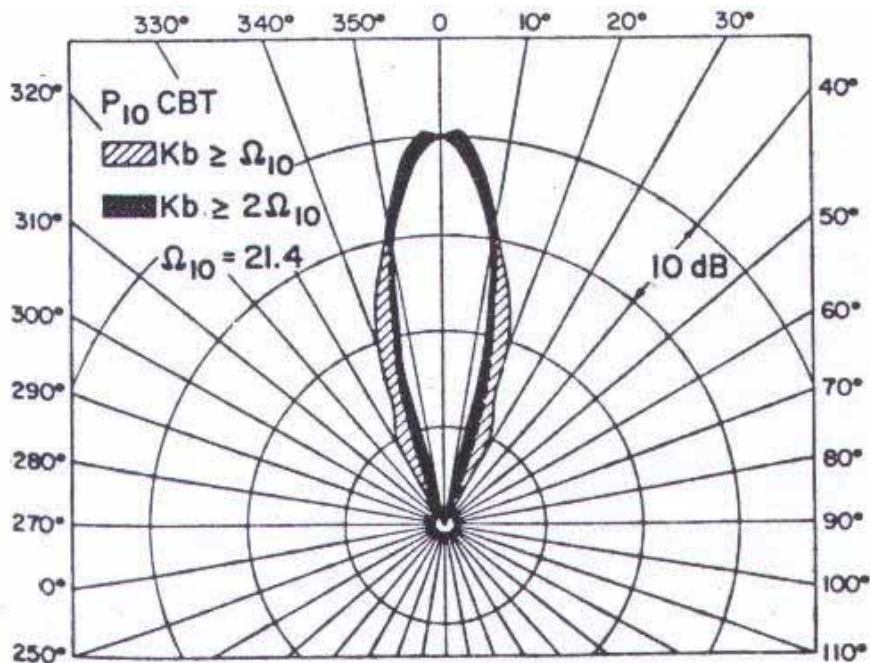
Fig. 6. Range of beam patterns for the P_{10} CBT in the range above cutoff (hatched area) and twice the cutoff (solid area). (Reproduced from Fig. 8 of [7].)

To be supplied.

Fig. 7. Configuration of circular segment line array.

To be supplied.

Fig. 8. Configuration of spherical cap array.
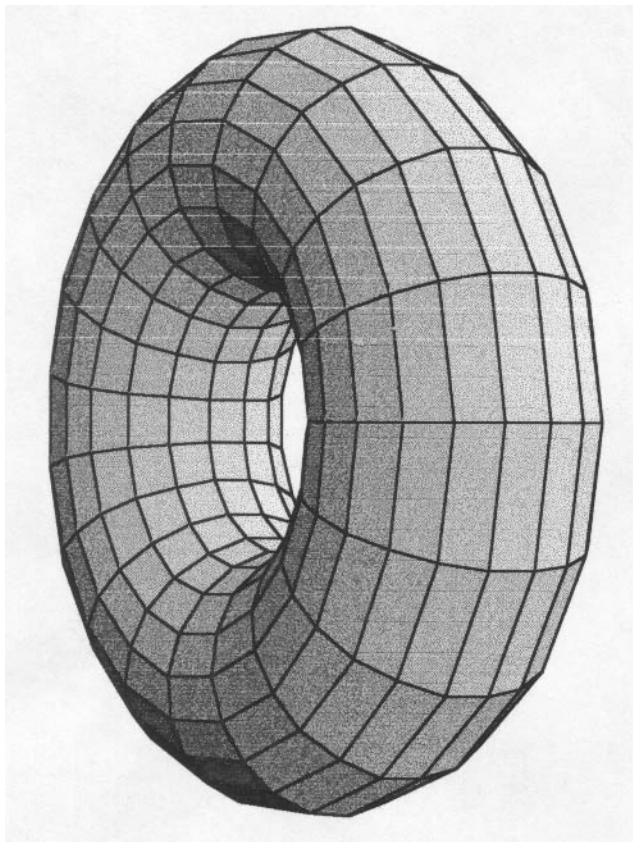
******* Figure not completed!! ********

Fig. 9. Configuration of toriodal cap array.
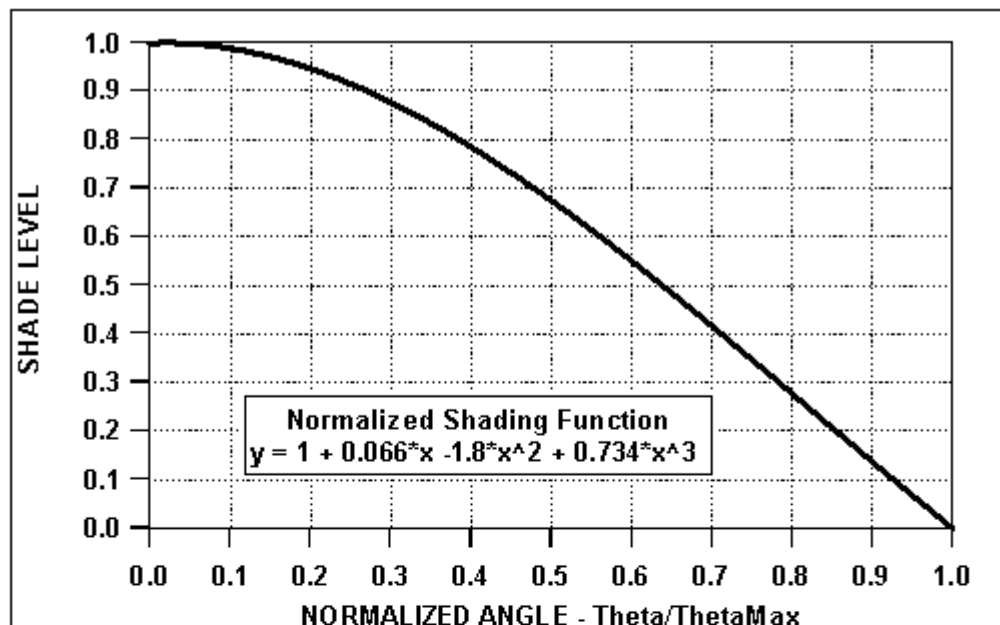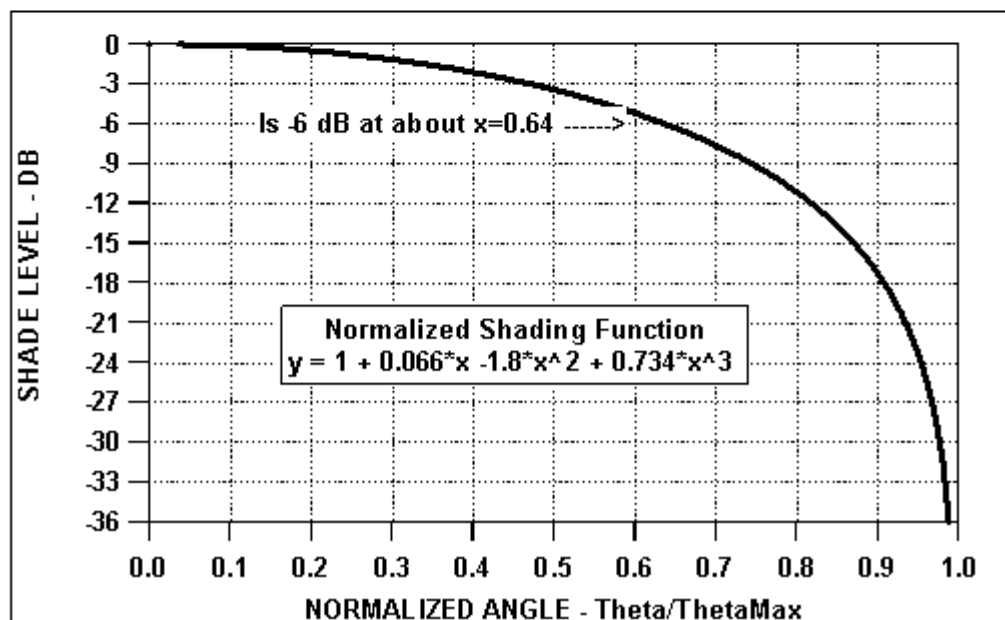
Fig. 10. Plots of the third-order polynomial approximation [Eq. (3)] to the Legendre function shading of Eq. 1. (a) Plot of shading on linear vertical scale. (b) Plot of shading on log vertical scale in dB. Note that the function is one-half or 6-dB down at roughly $x = 0.64$. This implies that the beamwidth generated by a CBT is roughly 64% of the total cap angle.
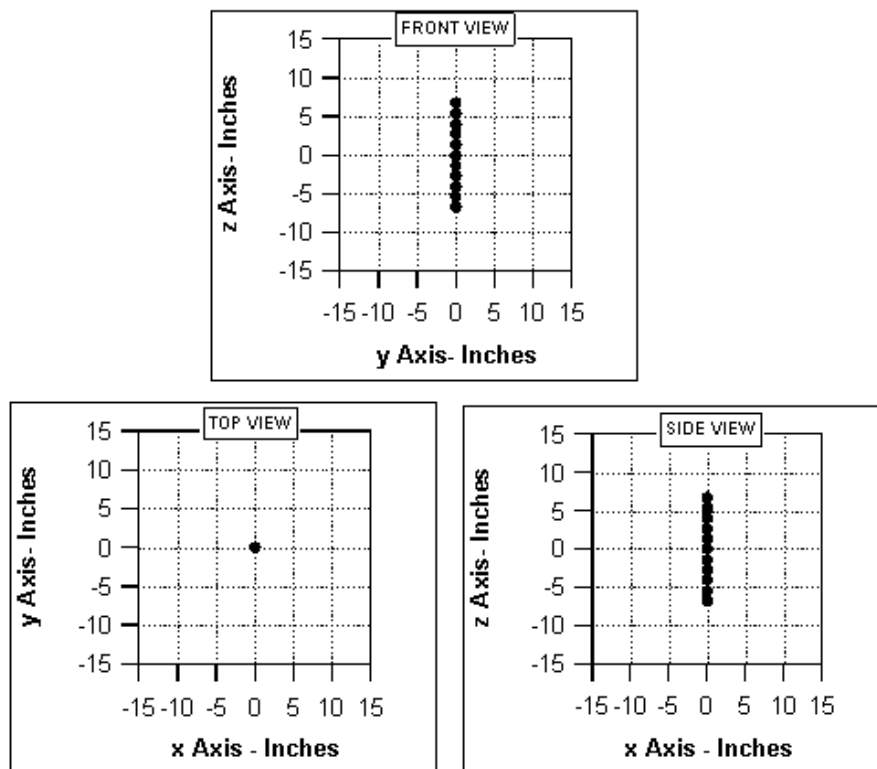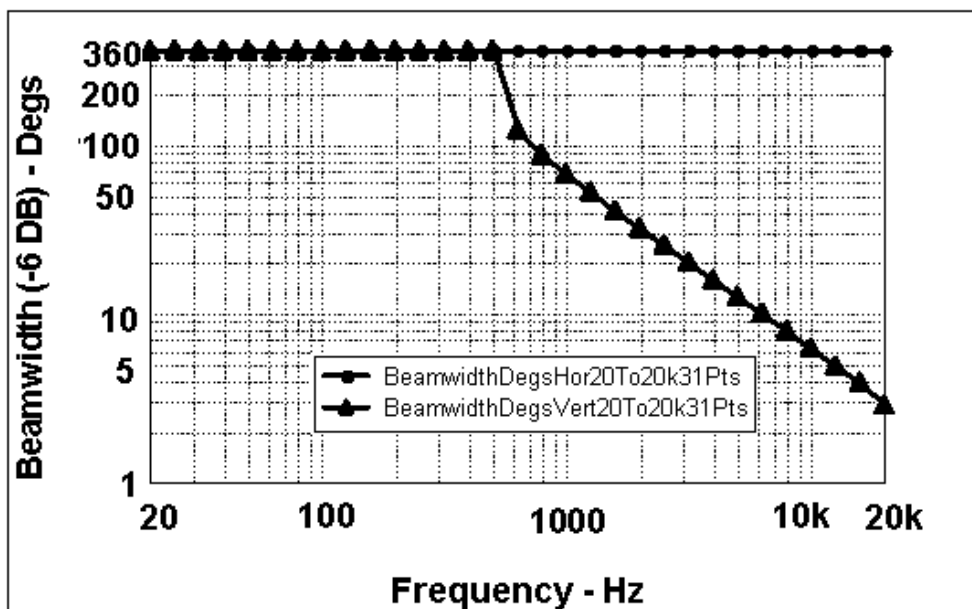
Fig. 11. Simulation results of the 11-point straight line array with equal drive levels (no shading). (a) Front, top, and side configuration views. (b) Plot of beamwidth vs. frequency. (c) Directivity and Q vs. frequency. (d) On-axis loss plot vs. frequency. (e) Vertical polar plots of the array from 630 Hz to 16 kHz at one-third-octave centers. (f) Footprint plots from 630 Hz to 16 kHz at one-third-octave centers.
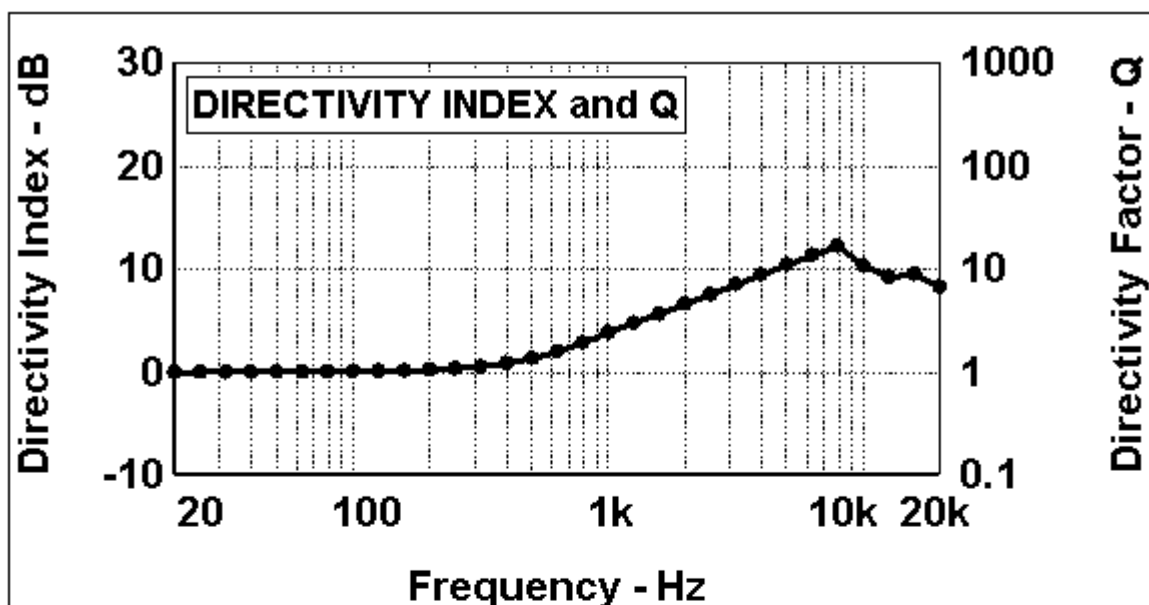
(c)
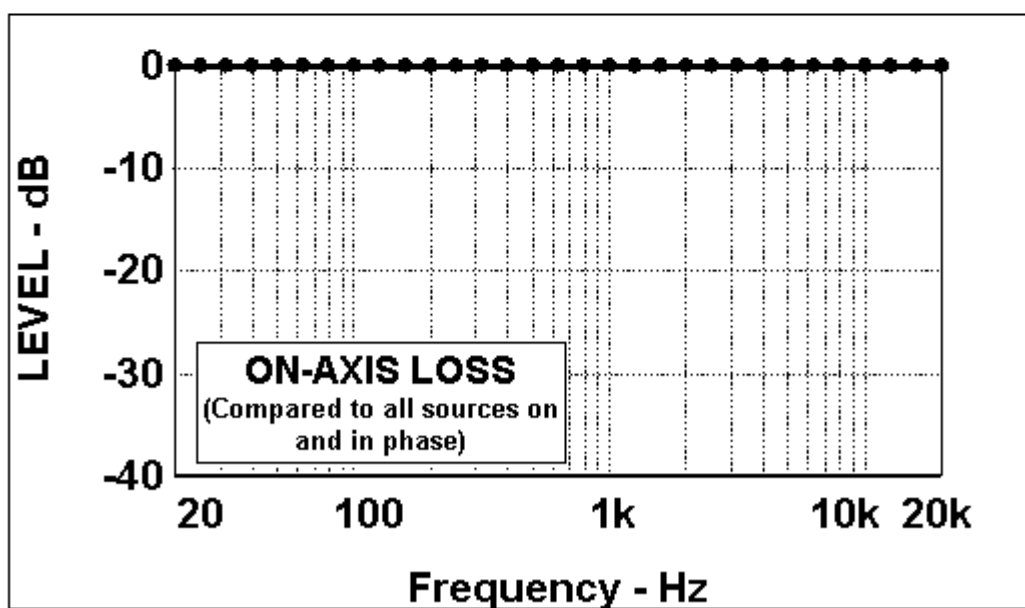
(d)

Fig. 11. (c) Directivity. (d) On-axis loss. See first figure for full caption.
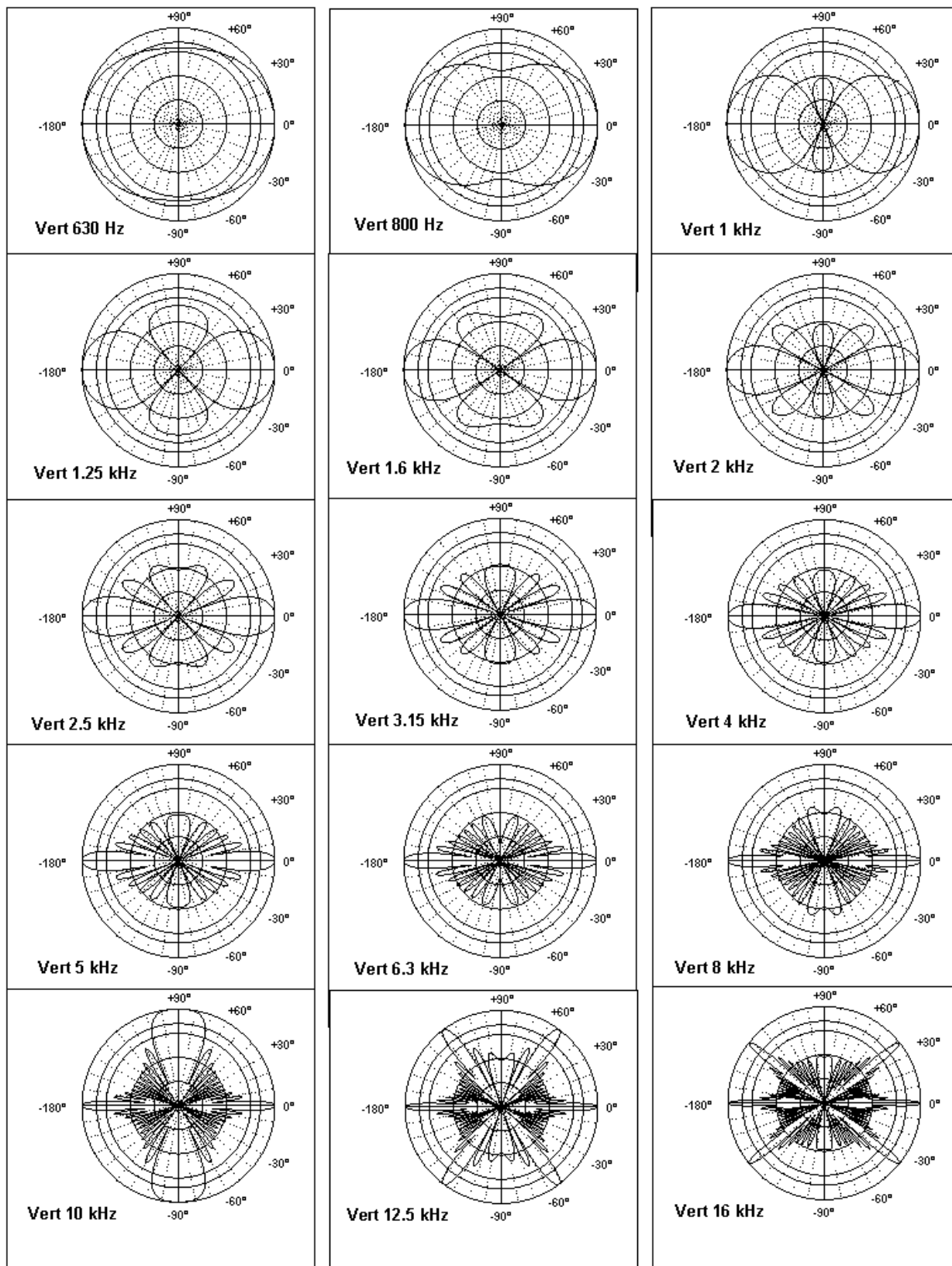
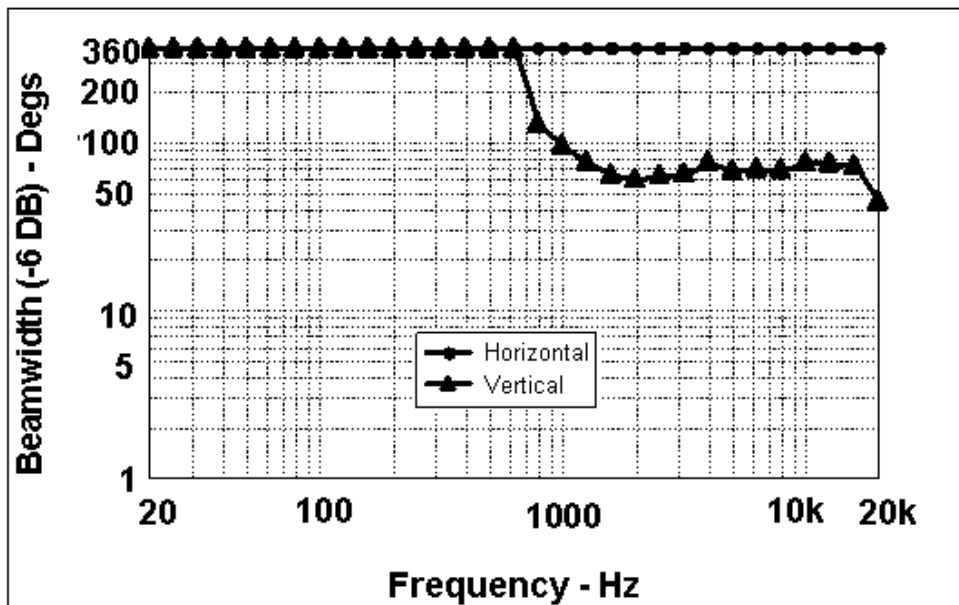Fig. 11 (e) Vertical polars. See first figure for full caption.
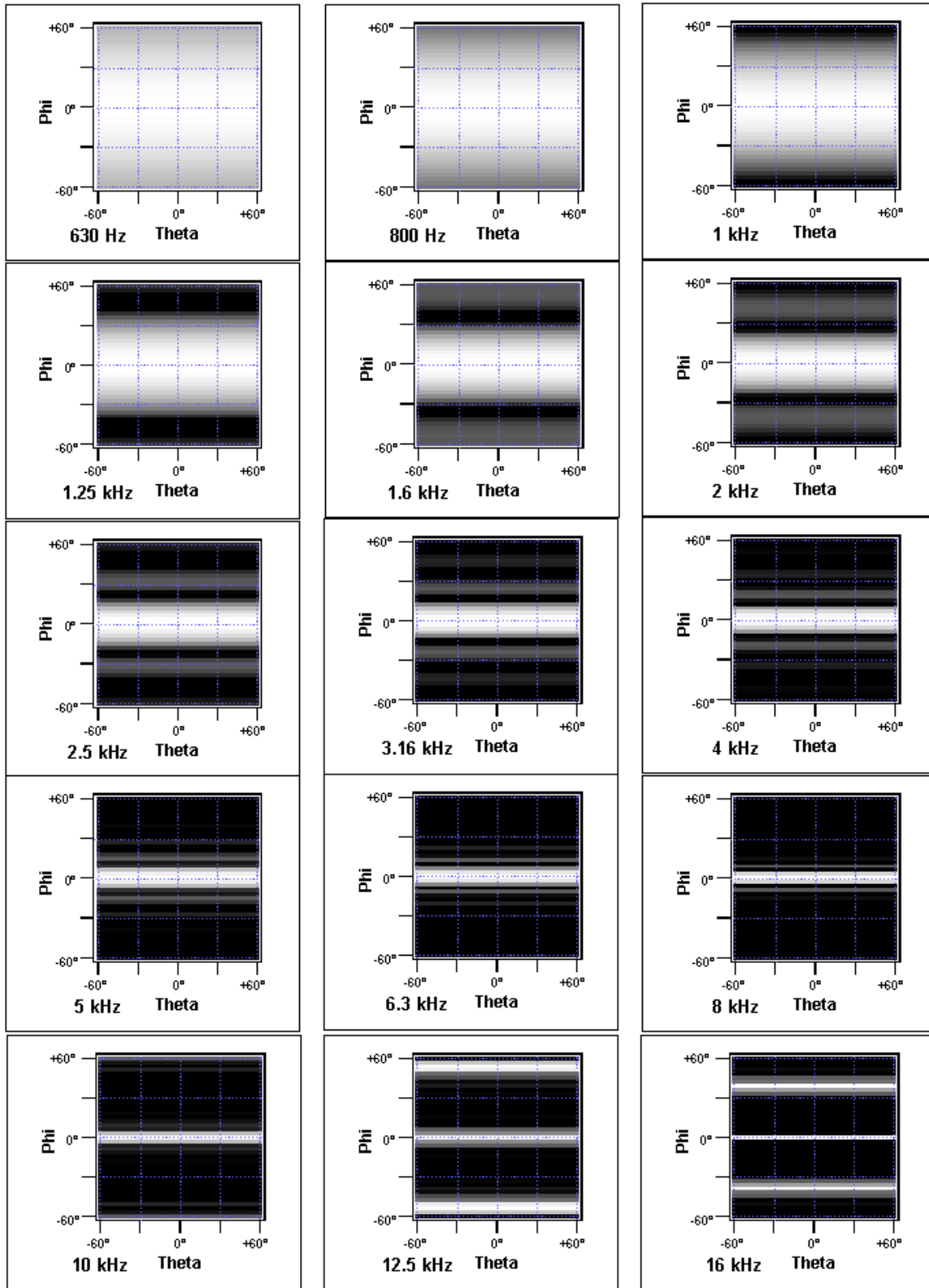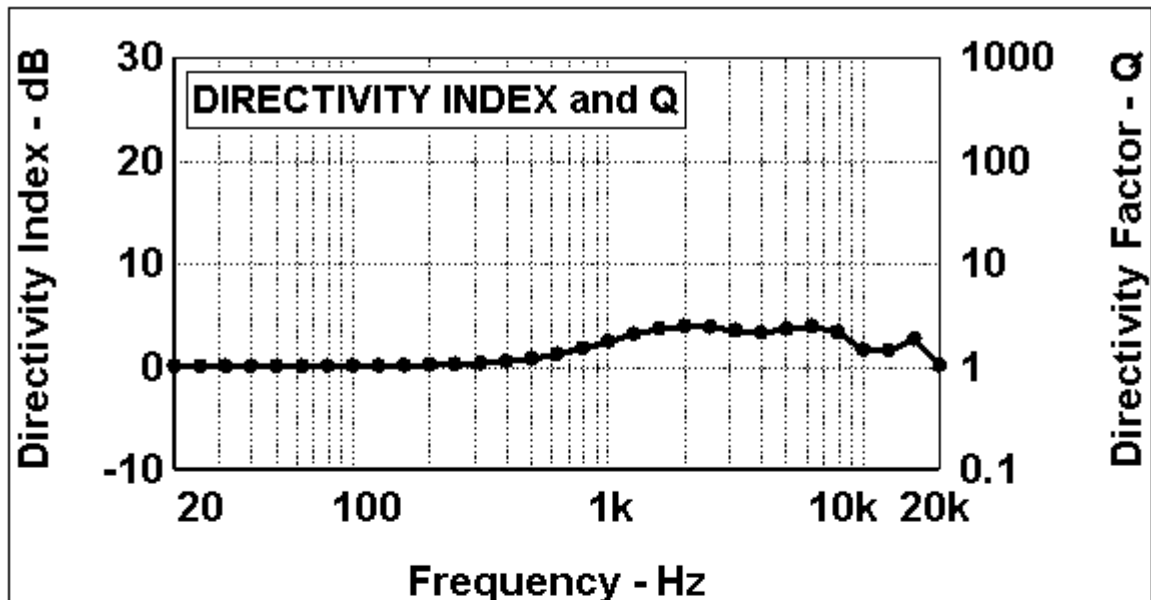
Fig. 11 (f) Footprints. See first figure for full caption.
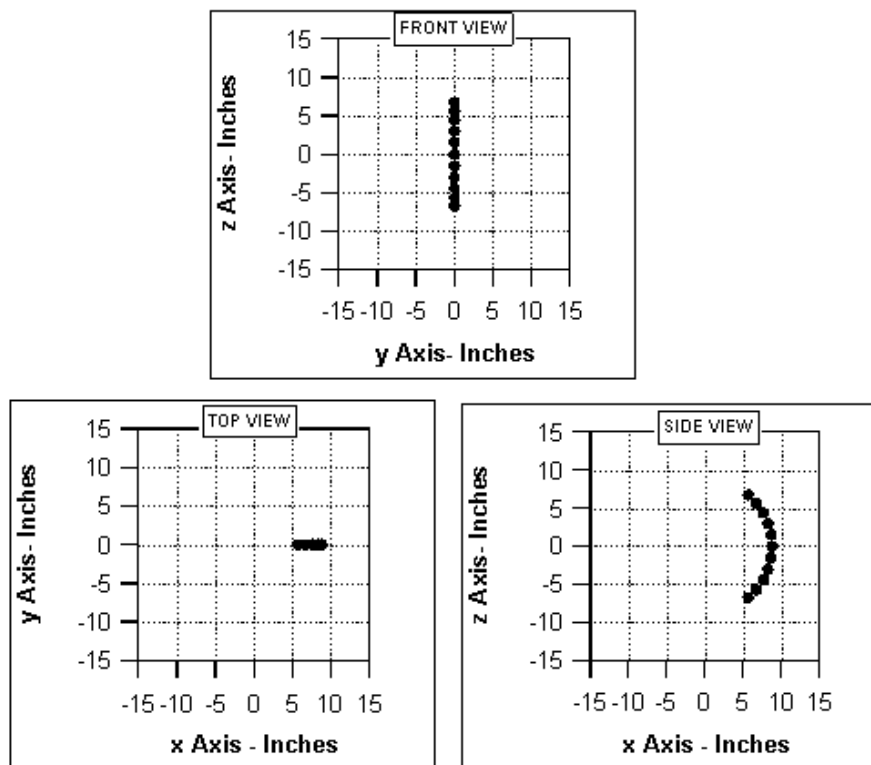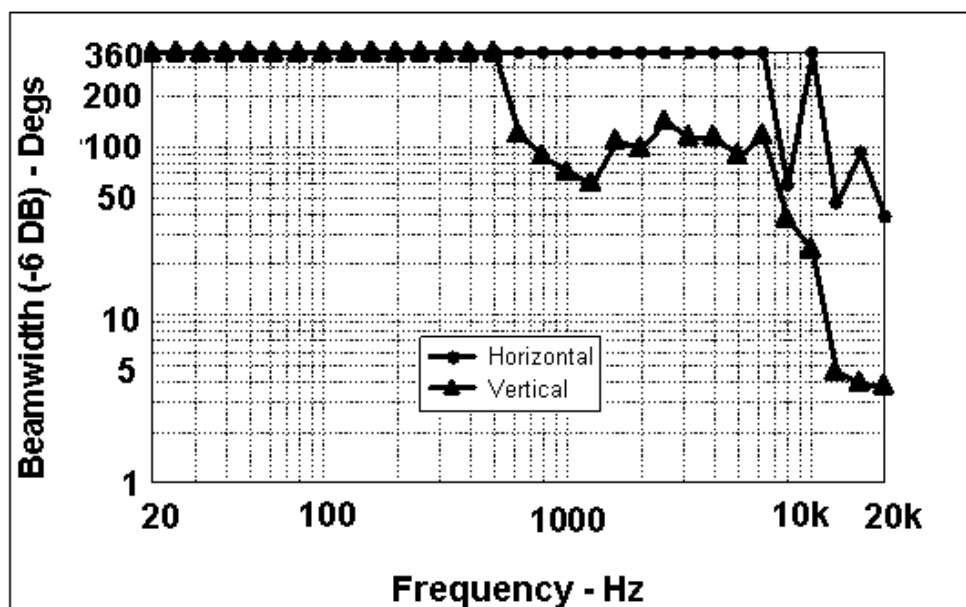
Fig. 12. Simulation results of the 11-point circular wedge line array with equal drive levels (no shading). (a) Front, top, and side configuration views. (b) Plot of beamwidth vs. frequency. (c) Directivity and Q vs. frequency. (d) On-axis loss vs. frequency. (e) Horizontal polar plots of the array from 630 Hz to 16 kHz at one-third-octave centers. (e) Vertical polar plots of the array from 630 Hz to 16 kHz at one-third-octave centers. (f) Footprint plots from 630 Hz to 16 kHz at one-third-octave centers.
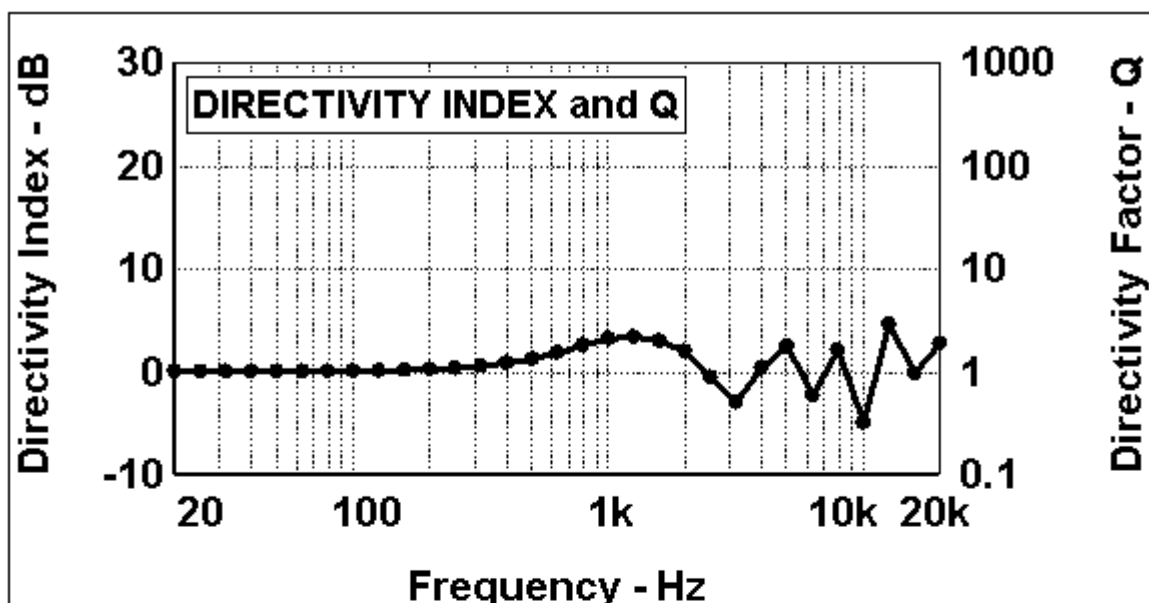
(c)
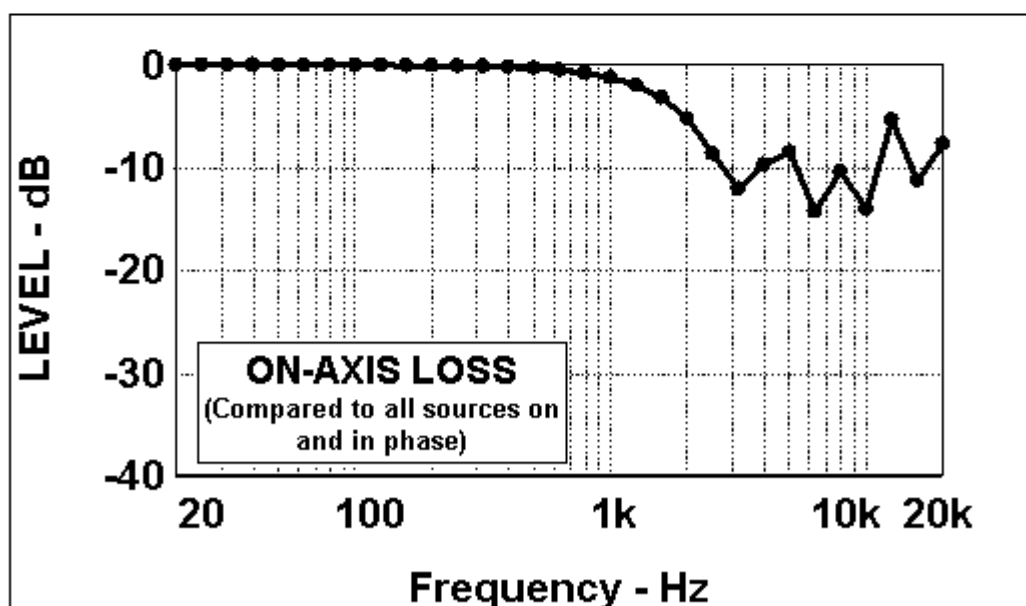
(d)

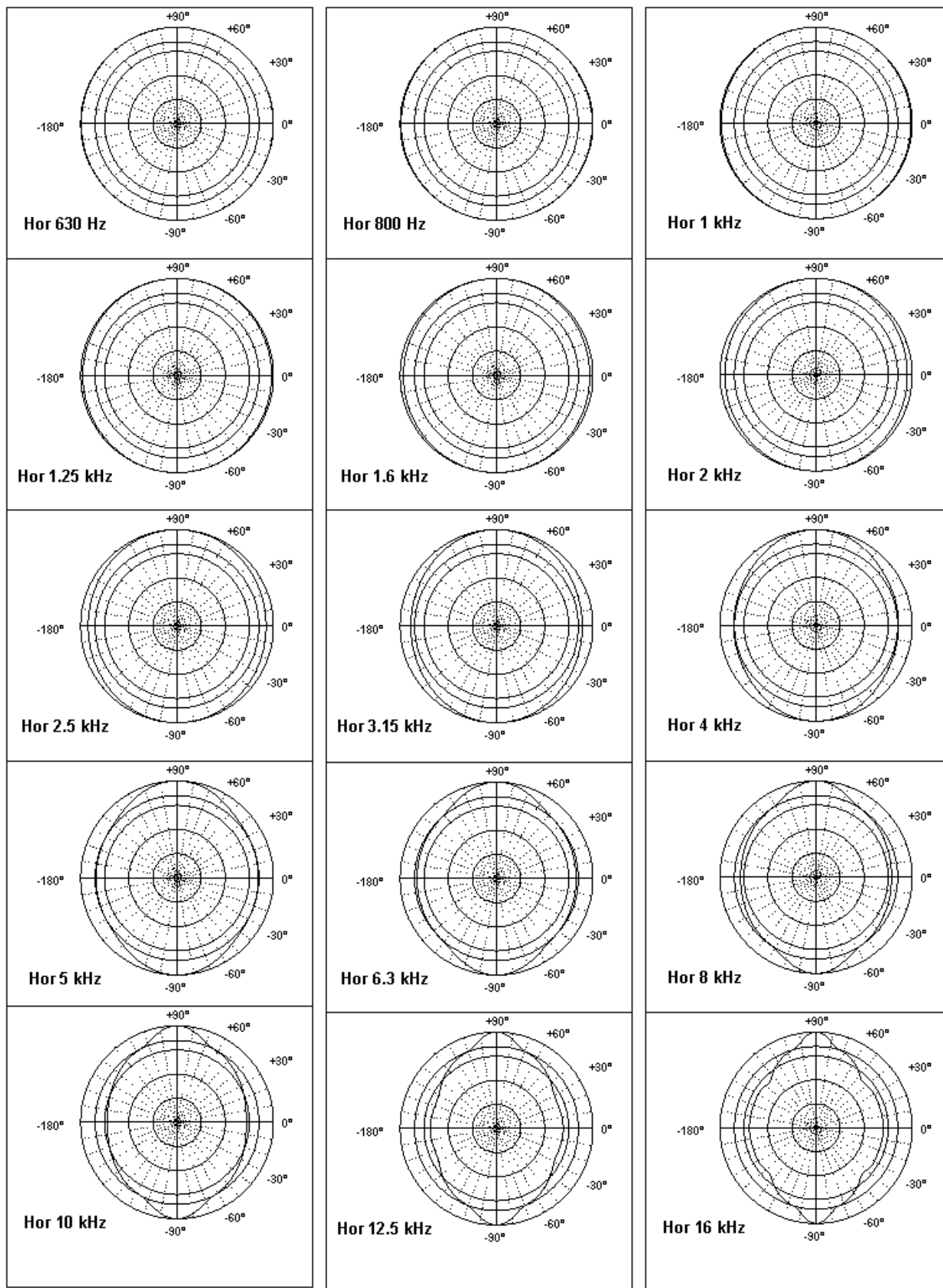Fig. 12. (c) Directivity. (d) On-axis loss. See first figure for full caption.
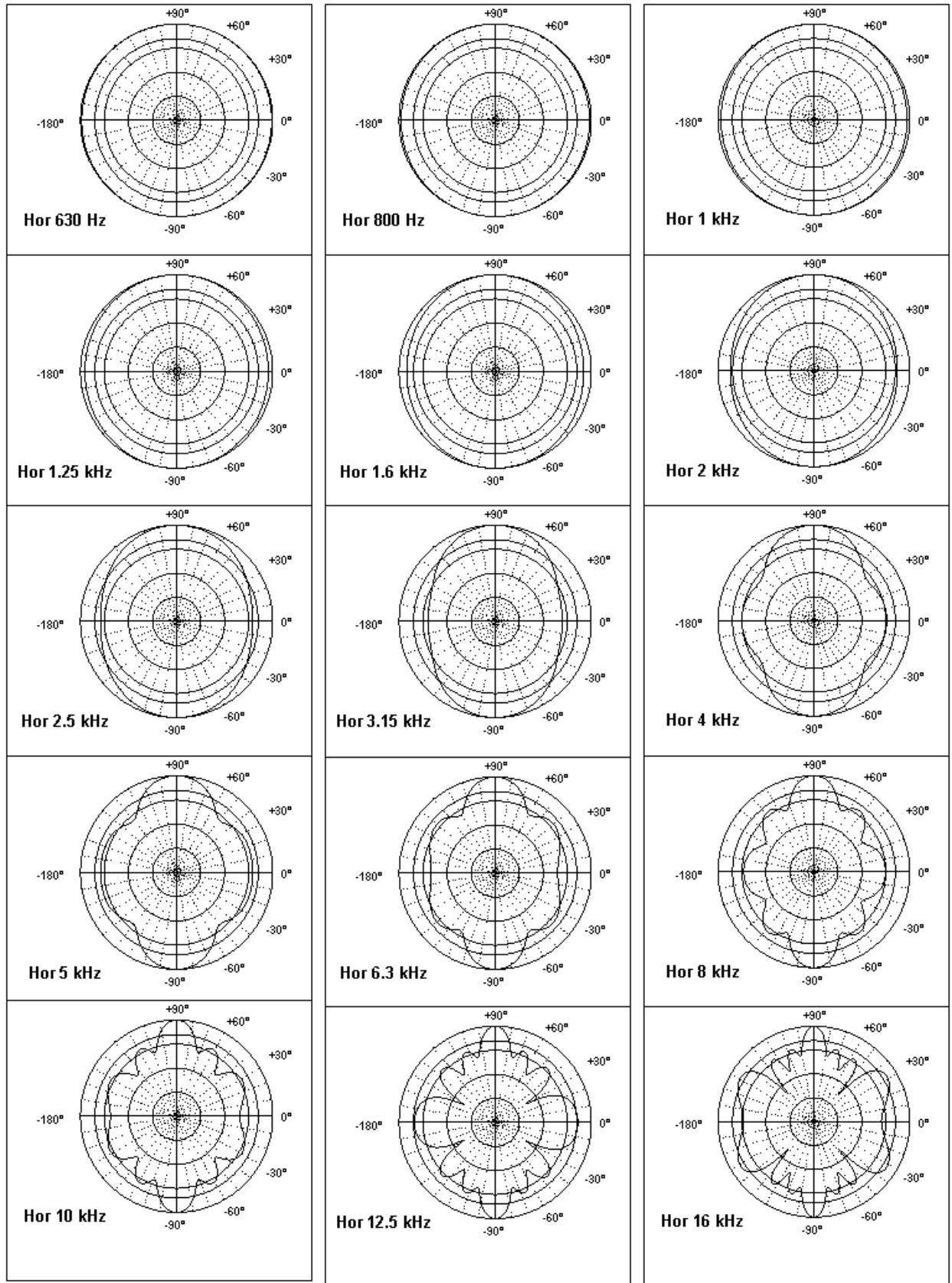
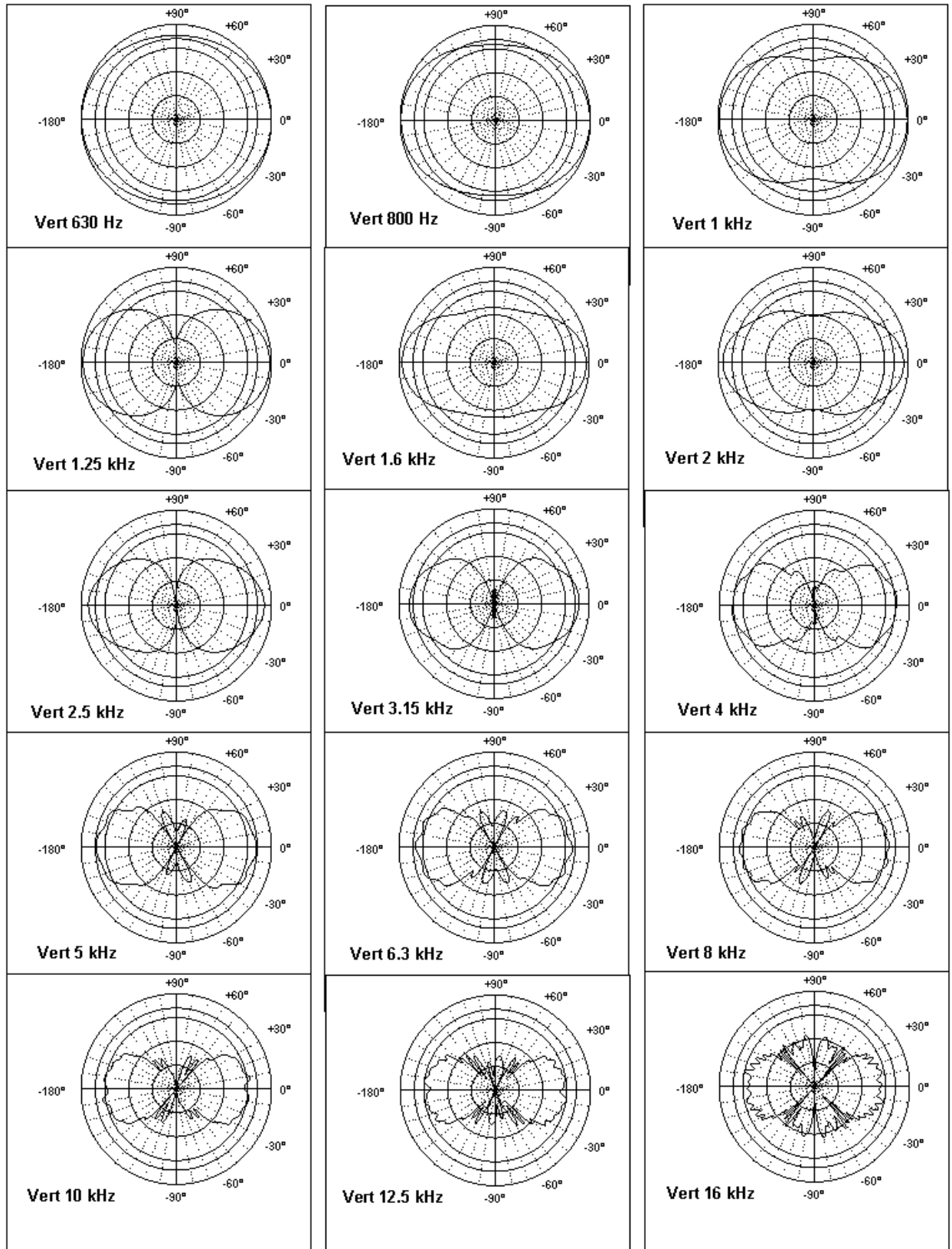Fig. 12 (e) Horizontal polars. . See first figure for full caption.
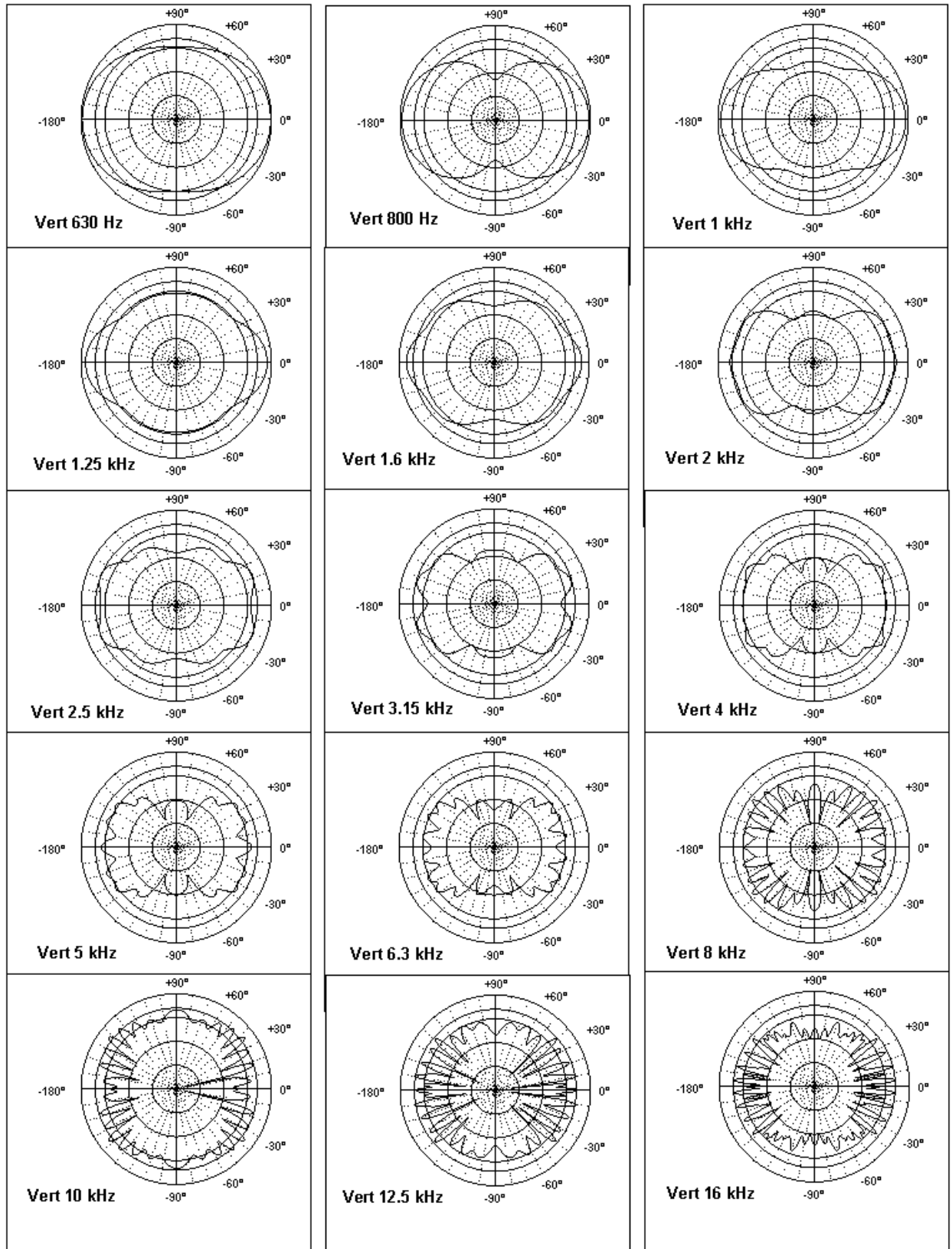
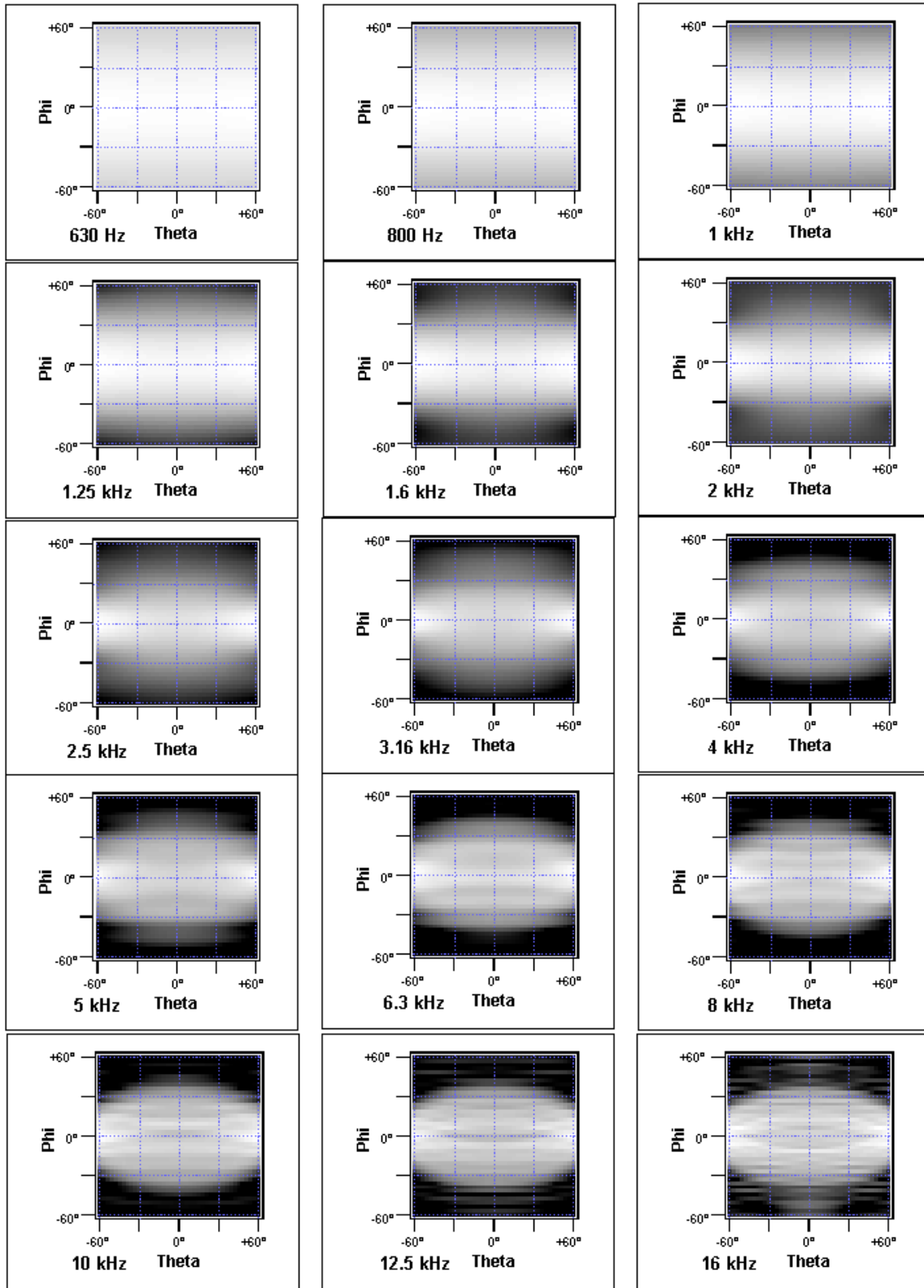Fig. 12 (f) Vertical polars. . See first figure for full caption.
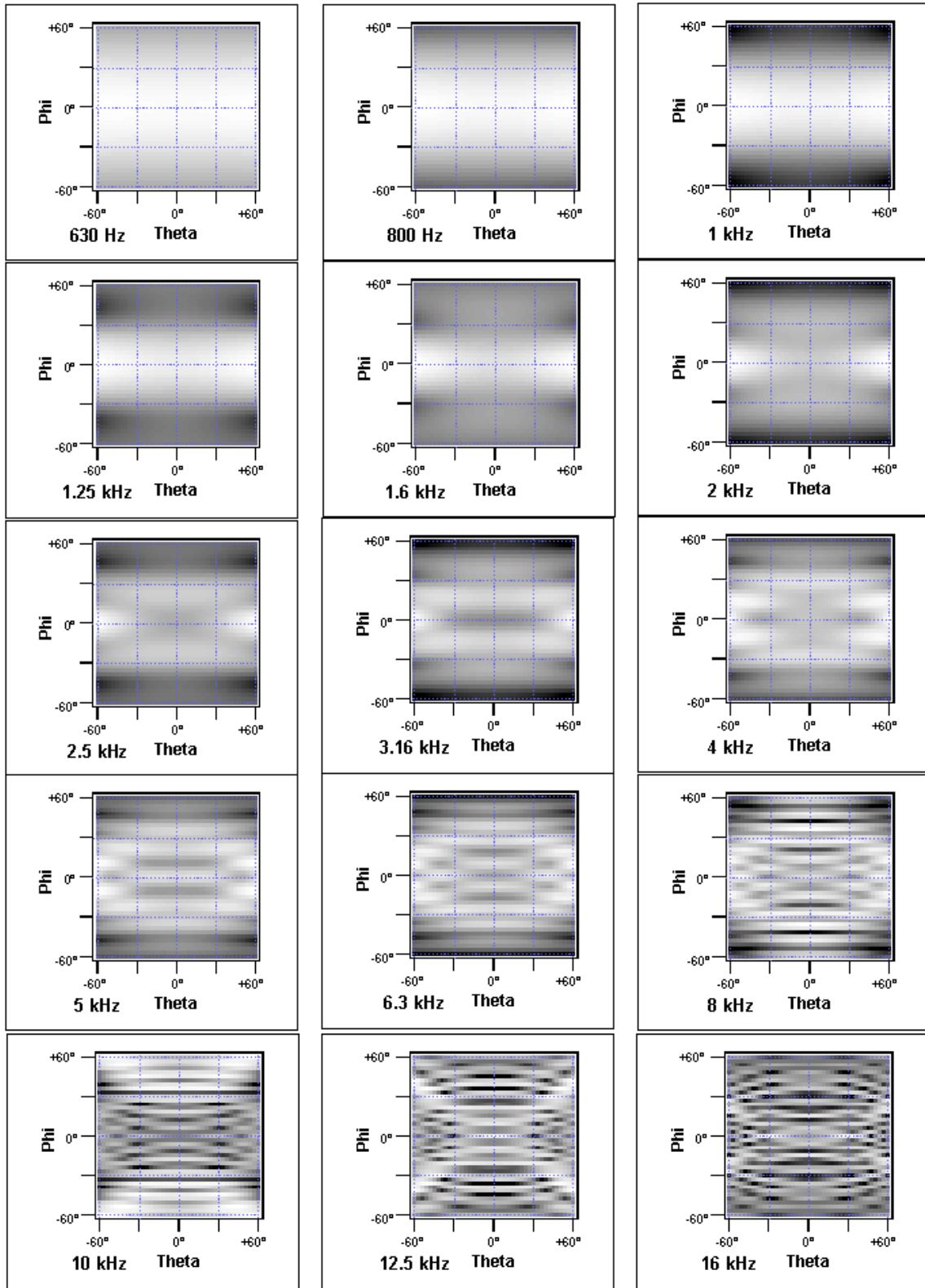
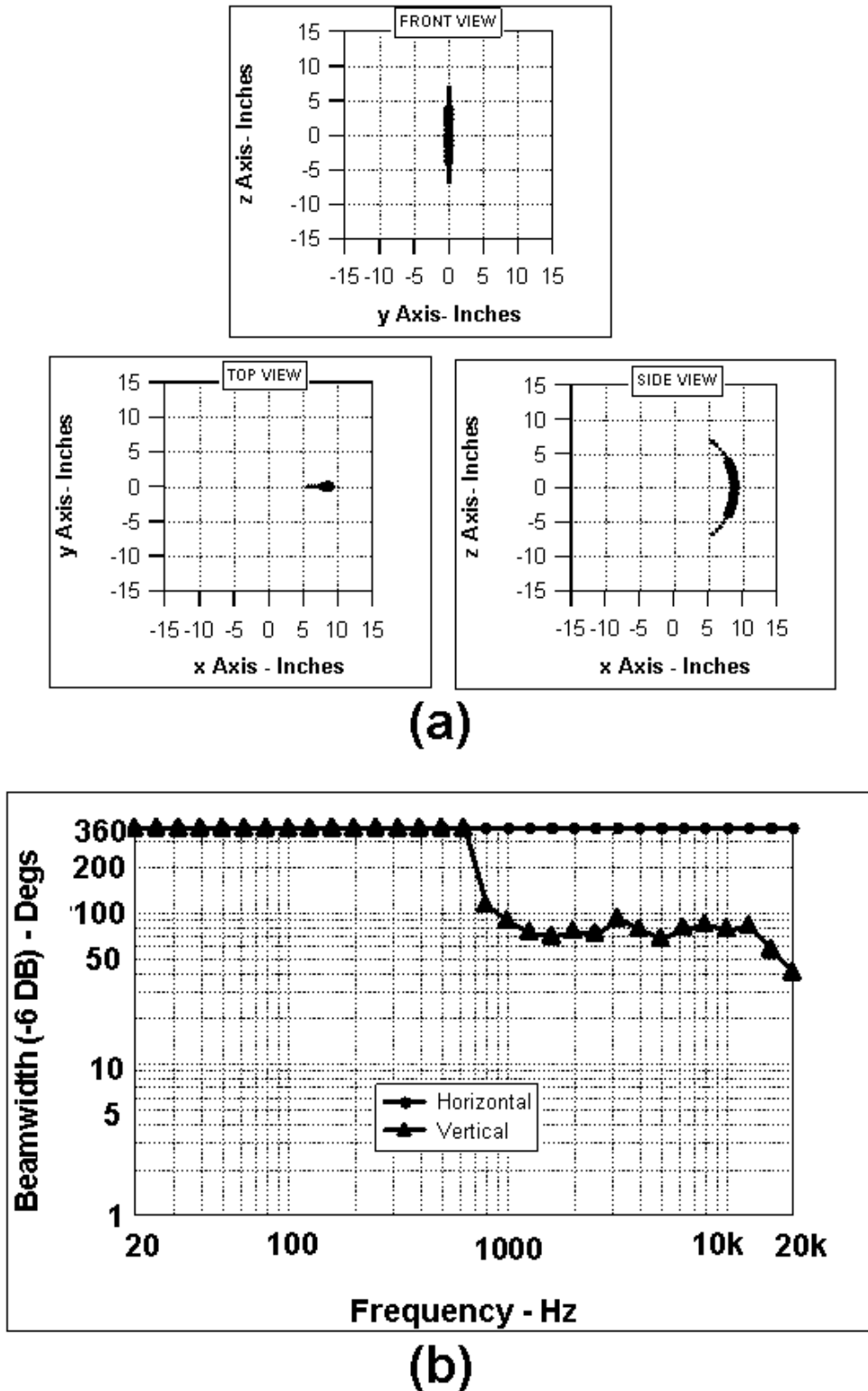Fig. 12 (g) Footprints. See first figure for full caption.
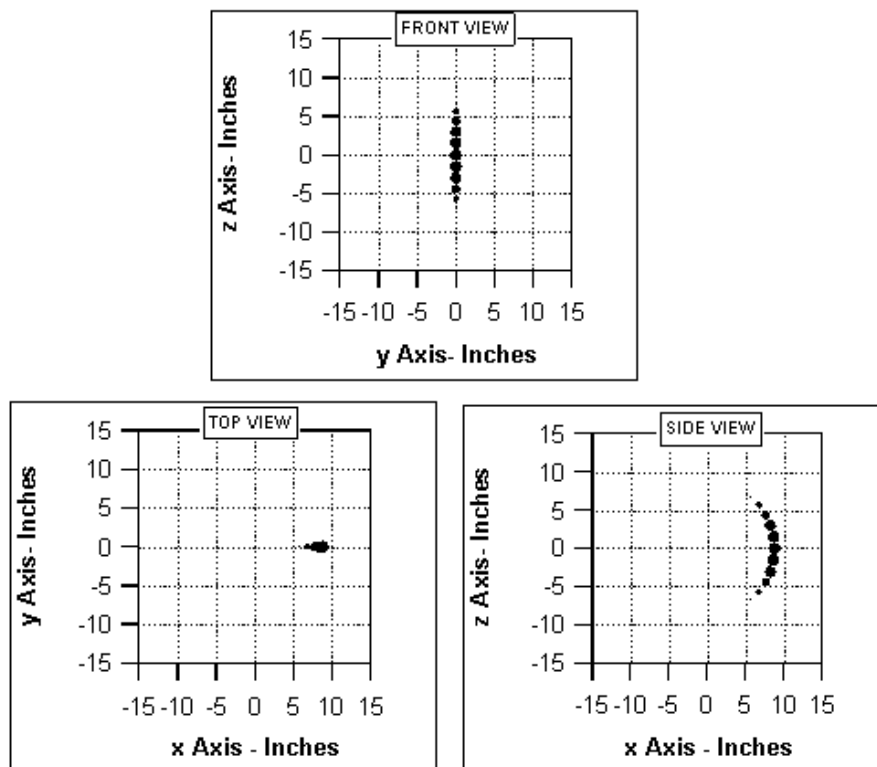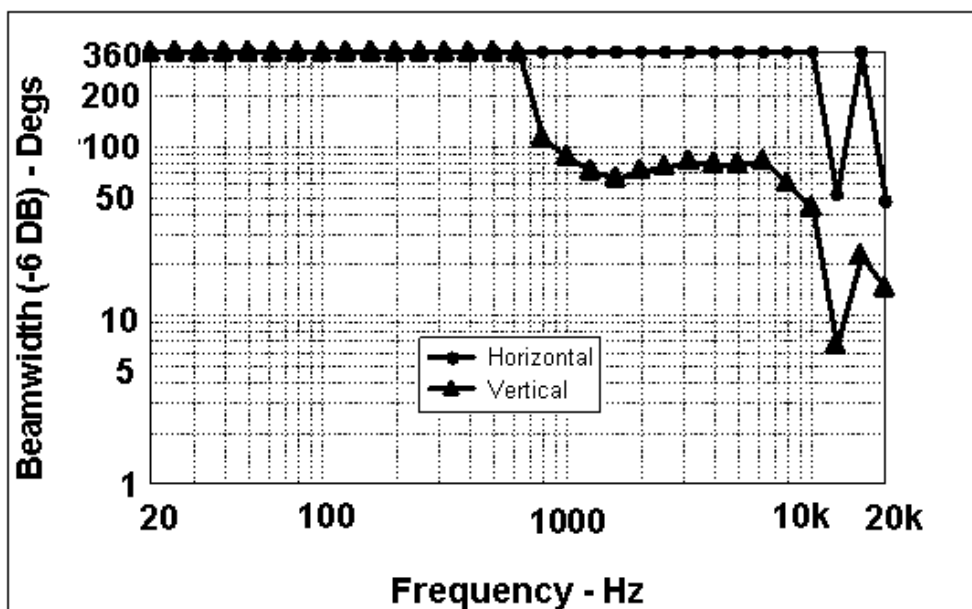
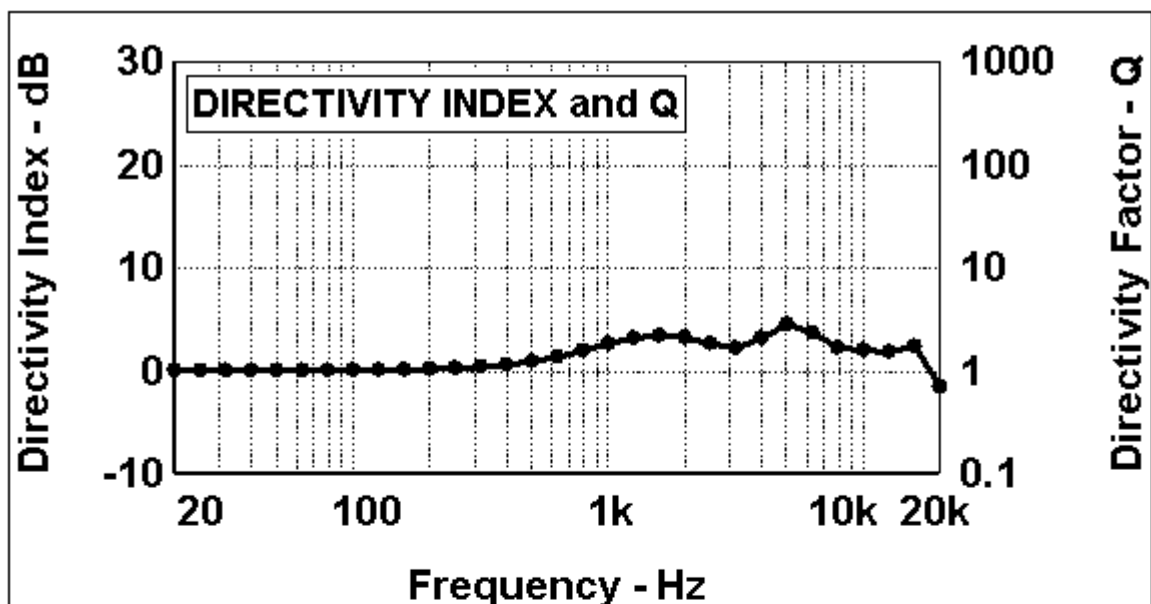Fig. 13. Simulation results of the 11-point circular wedge line array with Legendre shading. (a) Front, top, and side configuration views. (b) Plot of beamwidth vs. frequency. (c) Directivity and Q vs. frequency. (d) On-axis loss vs. frequency. (e) Horizontal polar plots of the array from 630 Hz to 16 kHz at one-third-octave centers. (f) Vertical polar plots of the array from 630 Hz to 16 kHz at one-third-octave centers. (g) Footprint plots from 630 Hz to 16 kHz at one-third-octave centers.
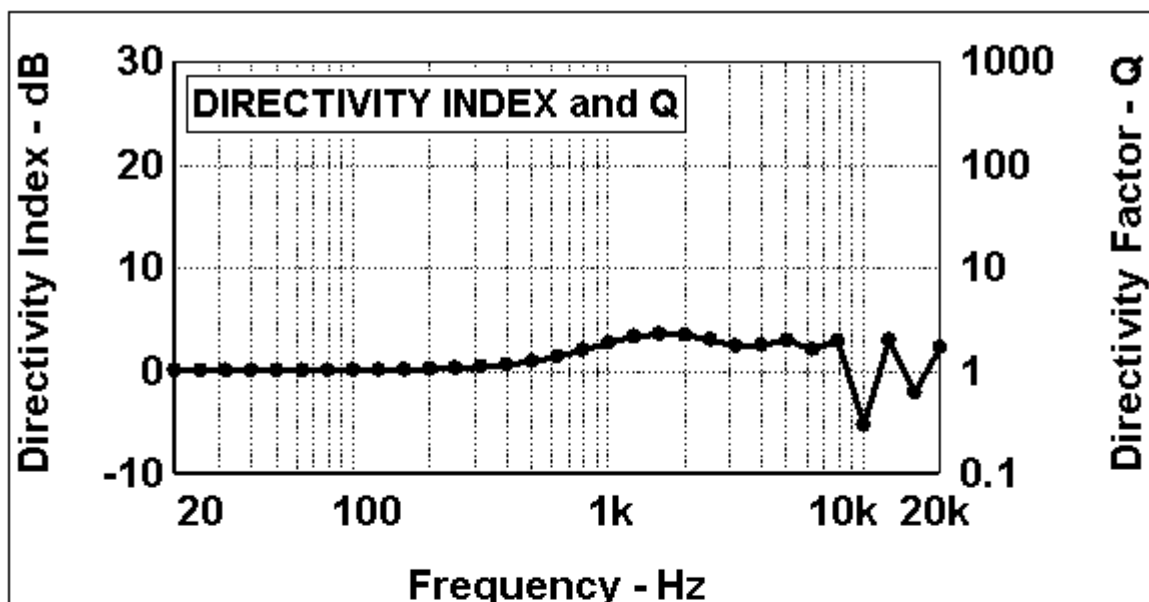
(c)
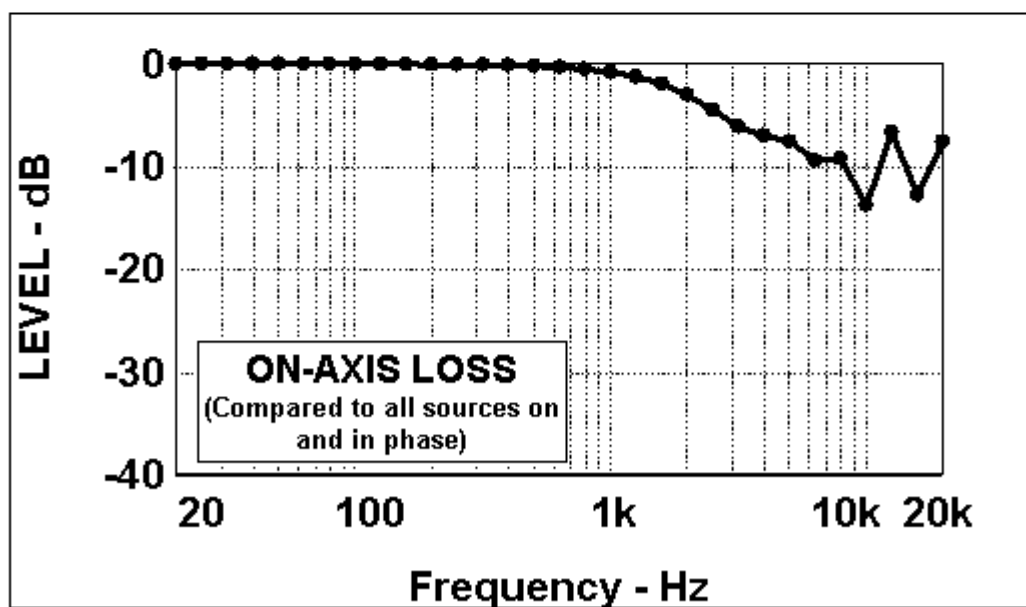
(d)

Fig. 13. (c) Directivity. (d) On-axis loss. See first figure for full caption.
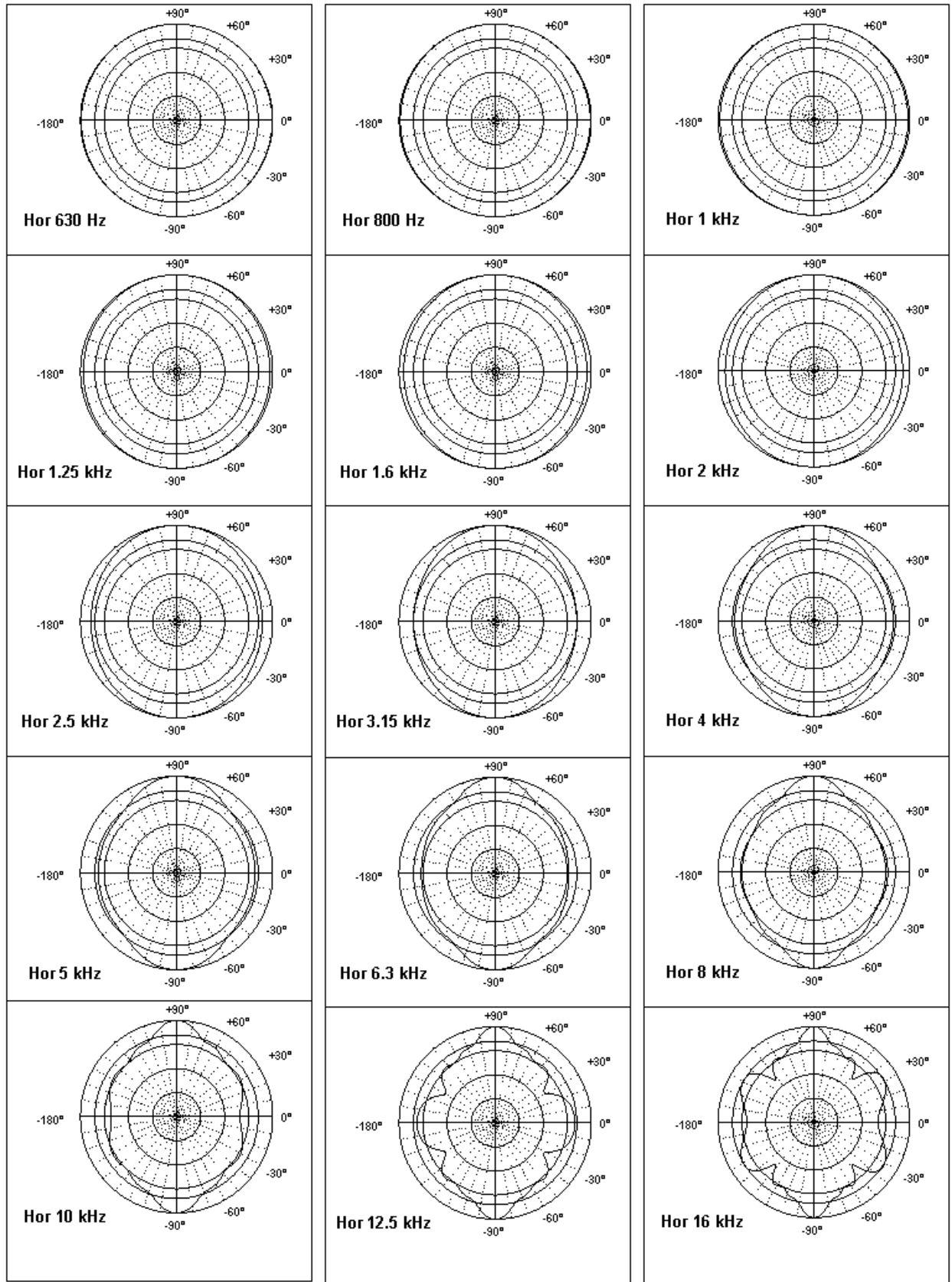
Fig. 13 (e) Horizontal polars. . See first figure for full caption.
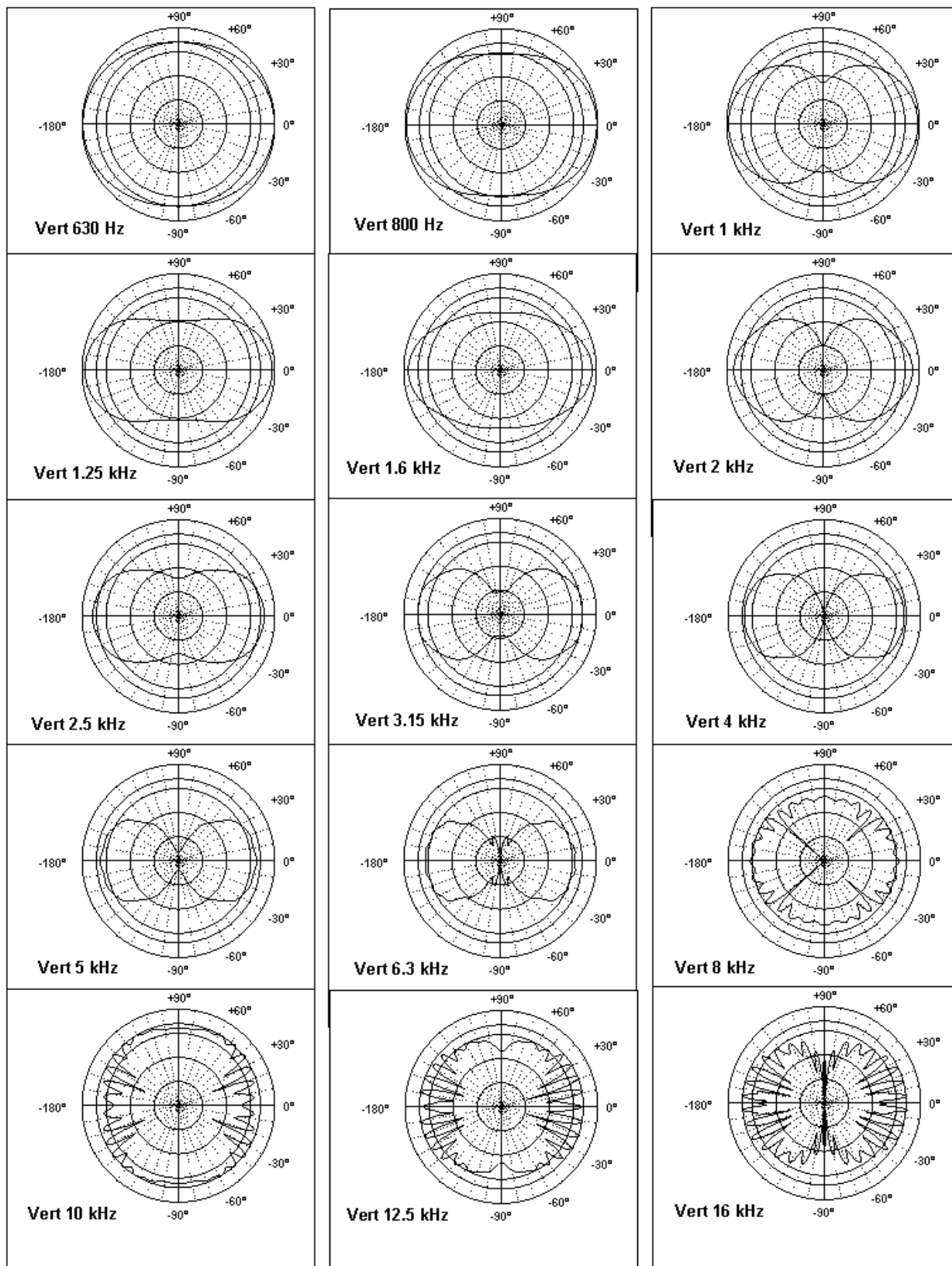
Fig. 13 (f) Vertical polars. . See first figure for full caption.
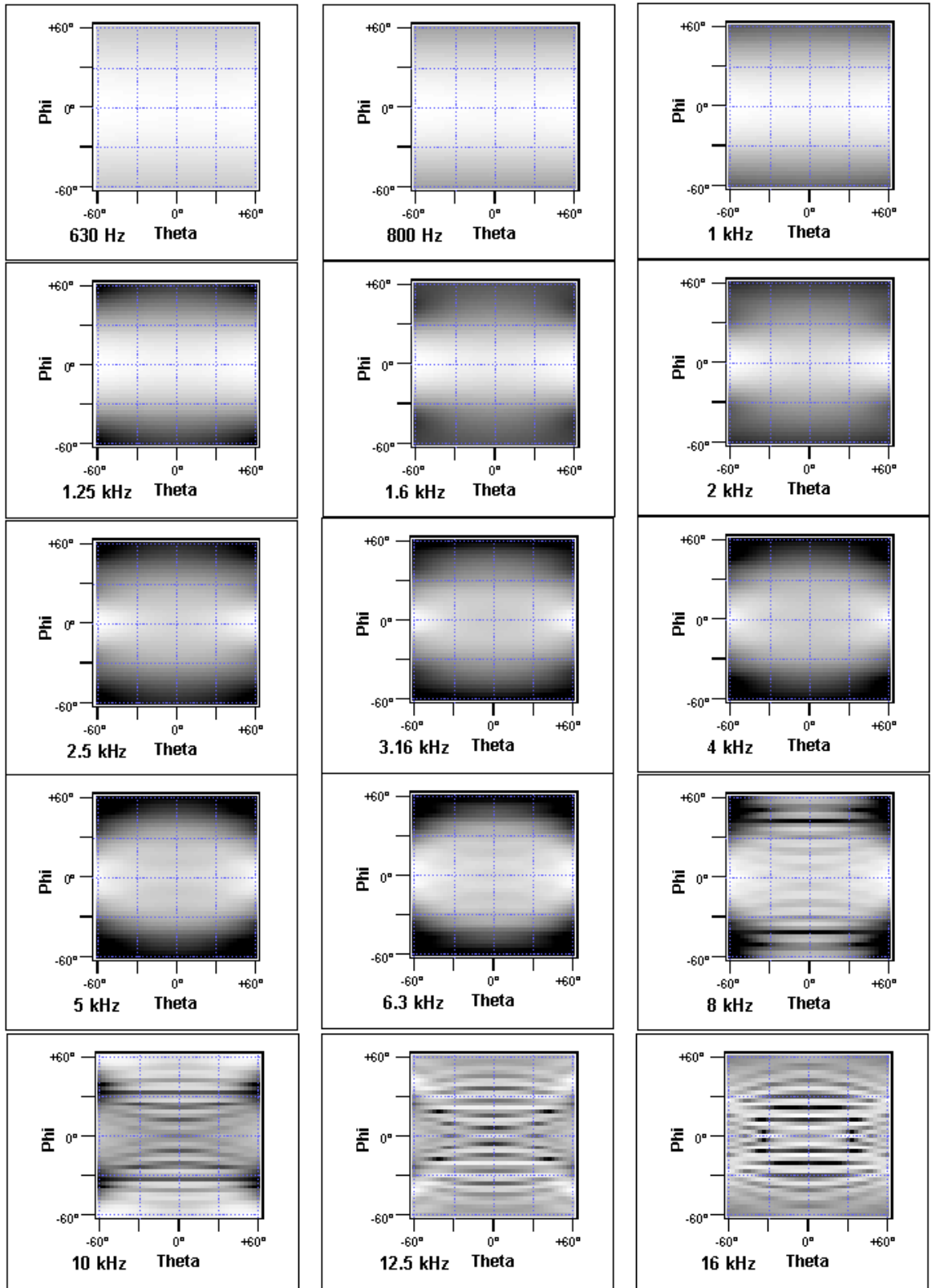
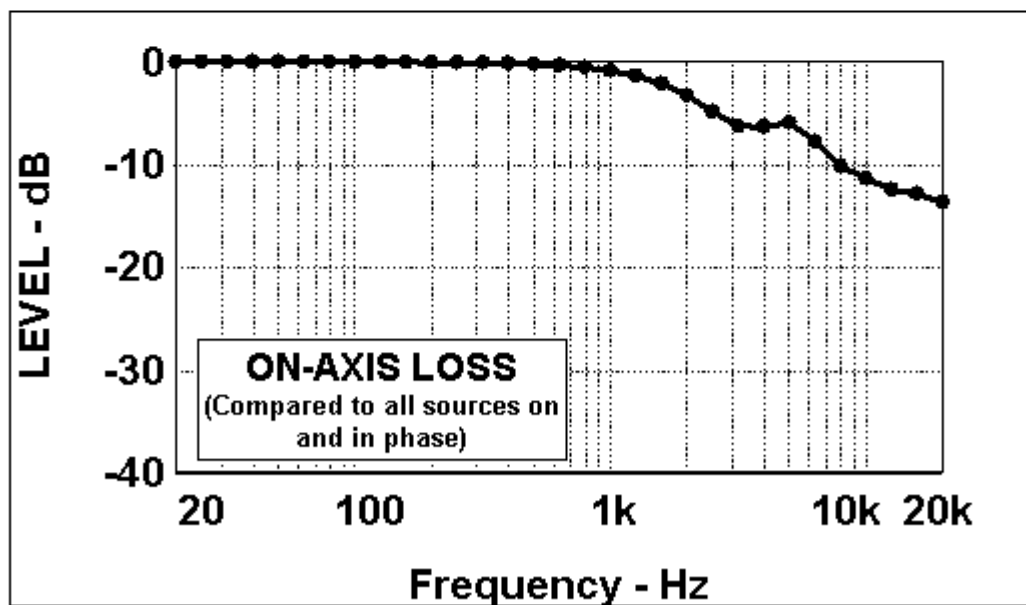Fig. 13 (g) Footprints. See first figure for full caption.
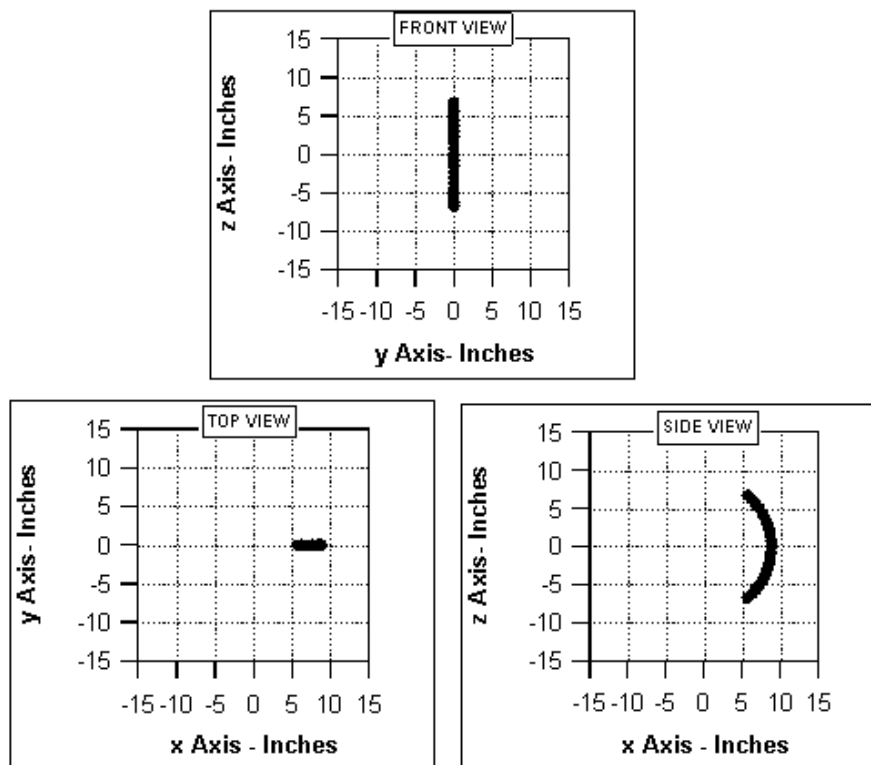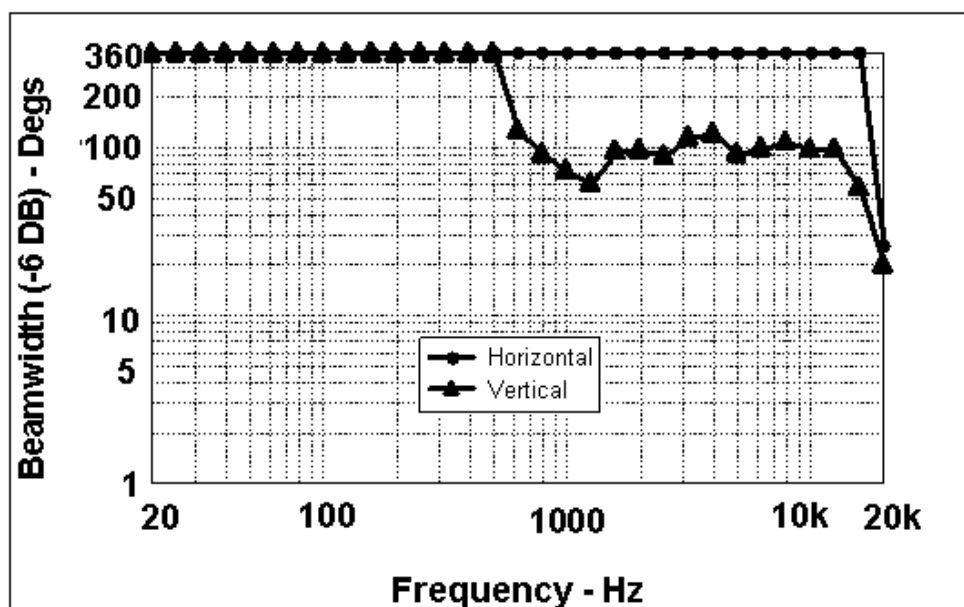
Fig. 14. Simulation results of the 21-point circular wedge line array with equal drive levels (no shading). (a) Front, top, and side configuration views. (b) Plot of beamwidth vs. frequency. (c) Directivity and Q vs. frequency. (d) On-axis loss vs. frequency. (e) Horizontal polar plots of the array from 630 Hz to 16 kHz at one-third-octave centers. (f) Vertical polar plots of the array from 630 Hz to 16 kHz at one-third-octave centers. (g) Footprint plots from 630 Hz to 16 kHz at one-third-octave centers.
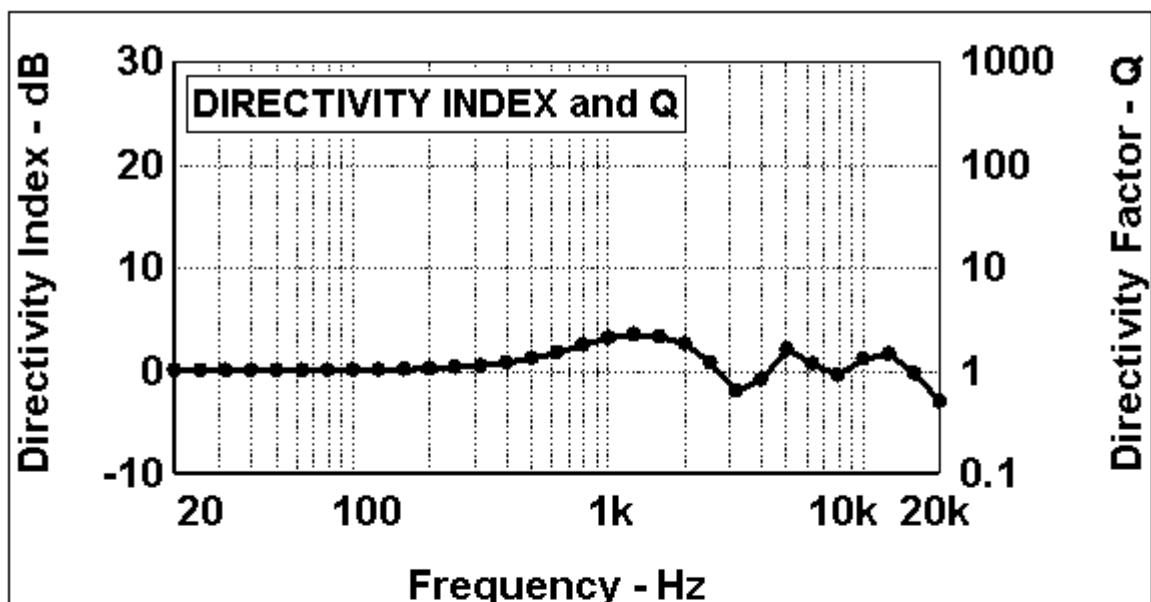
(c)
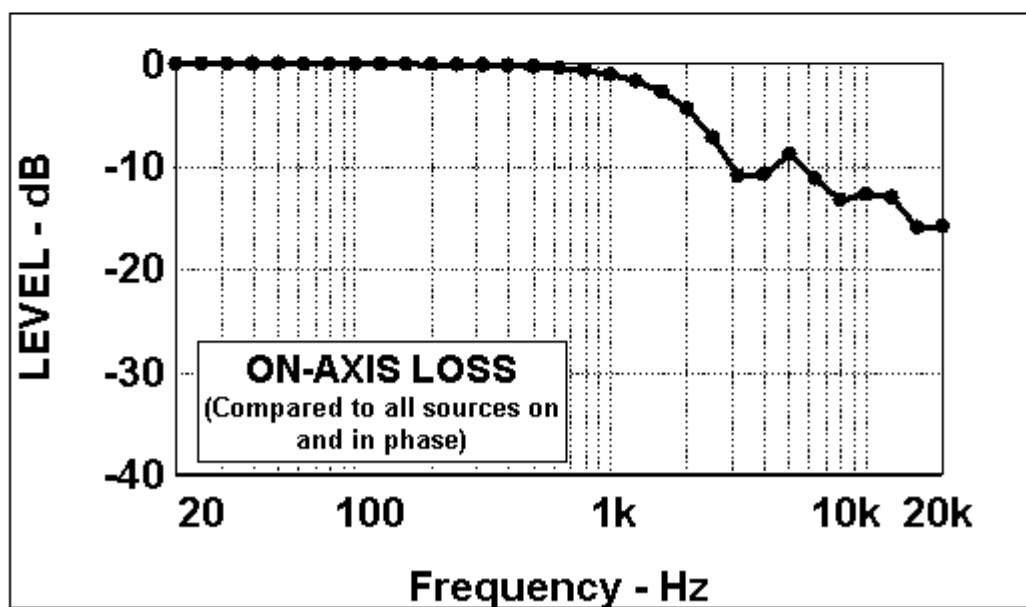
(d)

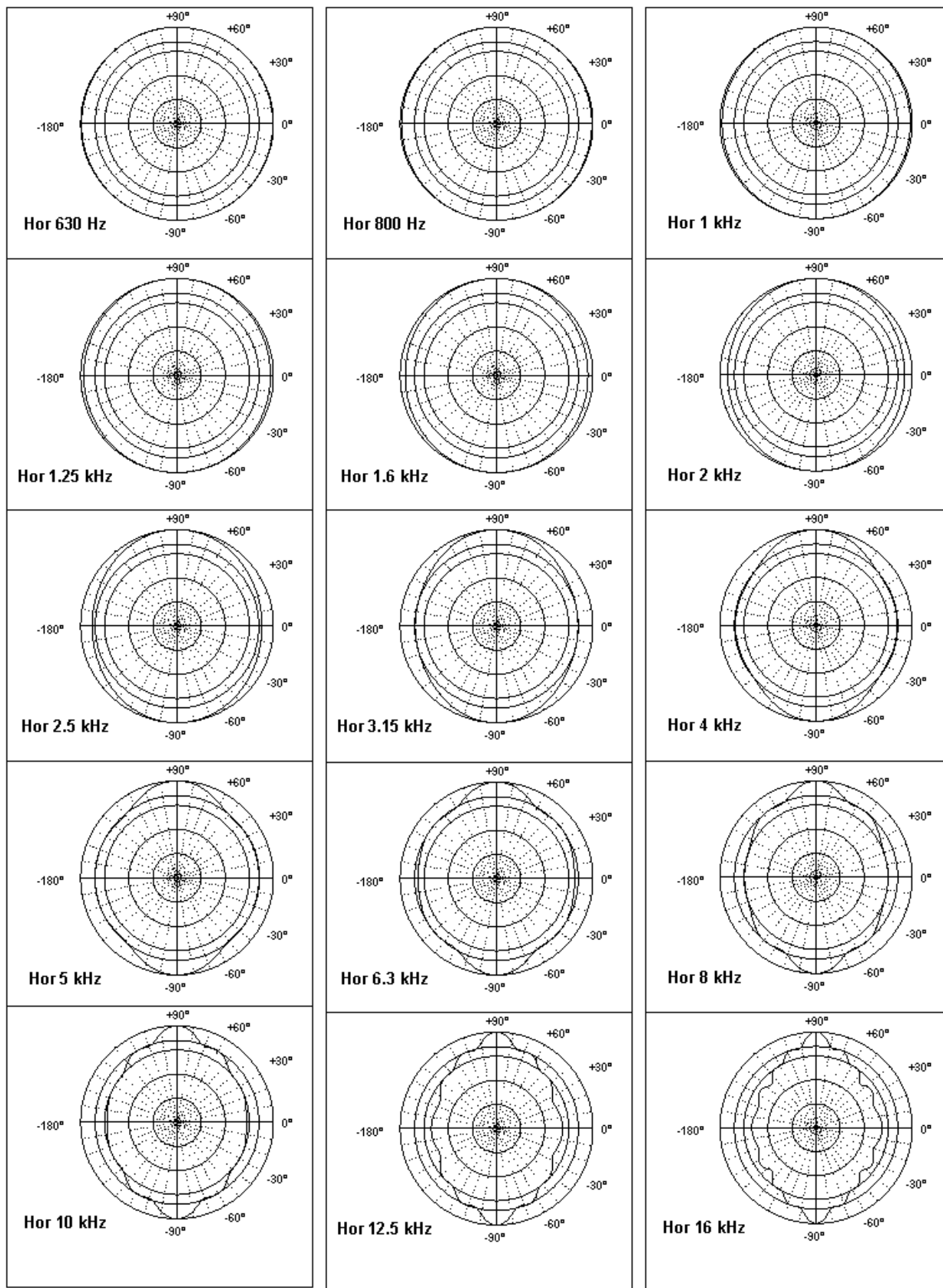Fig. 14. (c) Directivity. (d) On-axis loss. See first figure for full caption.
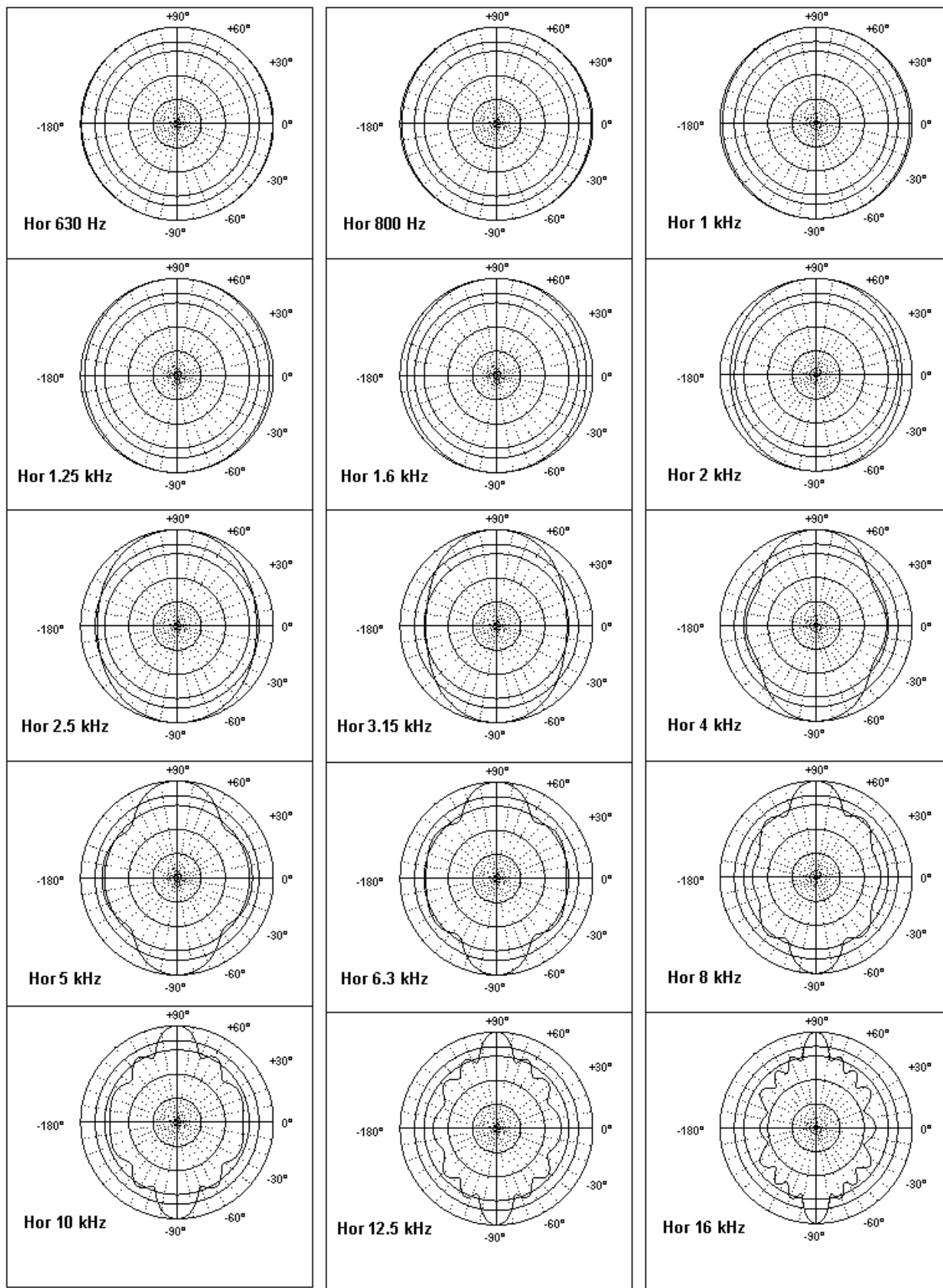
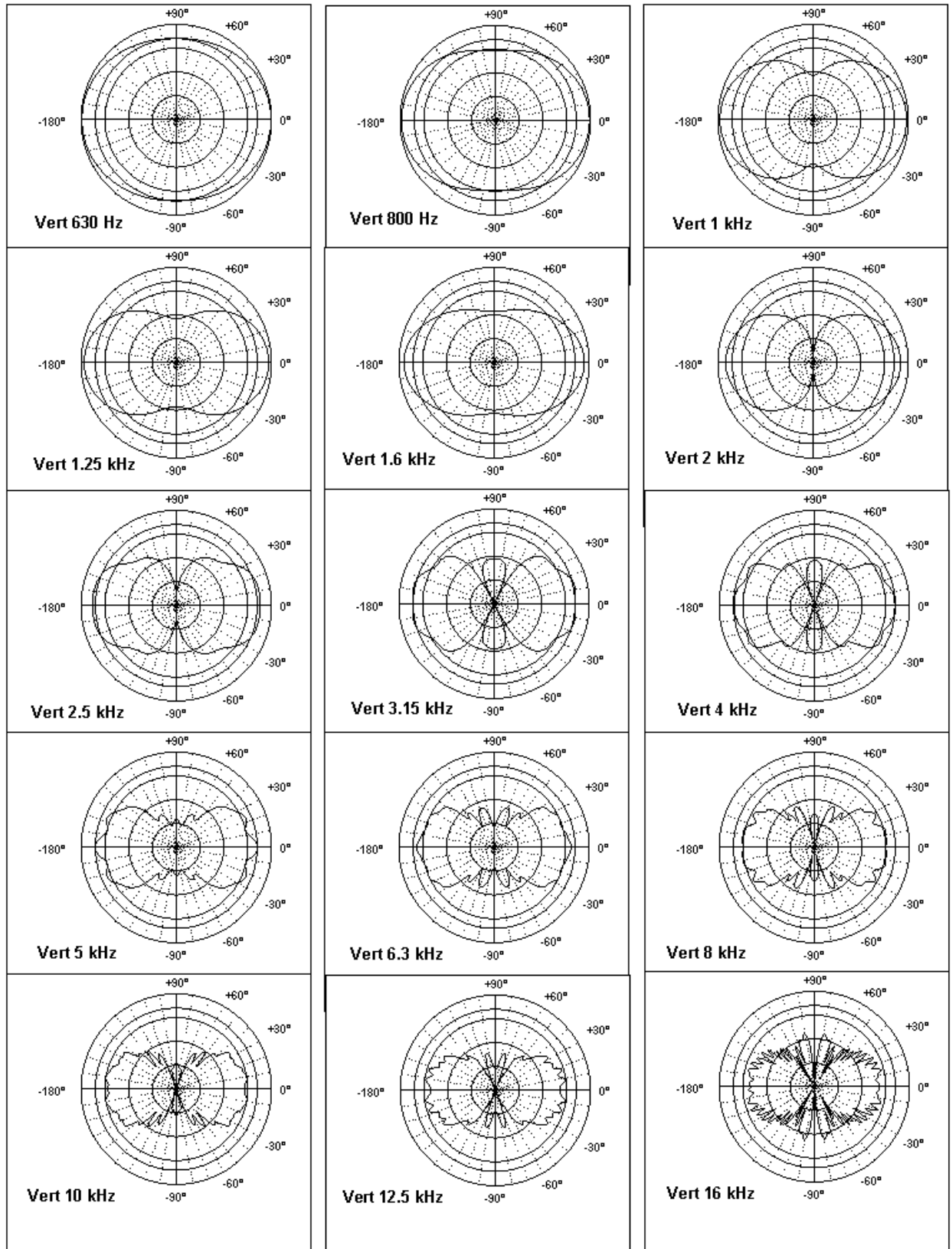Fig. 14 (e) Horizontal polars. . See first figure for full caption.
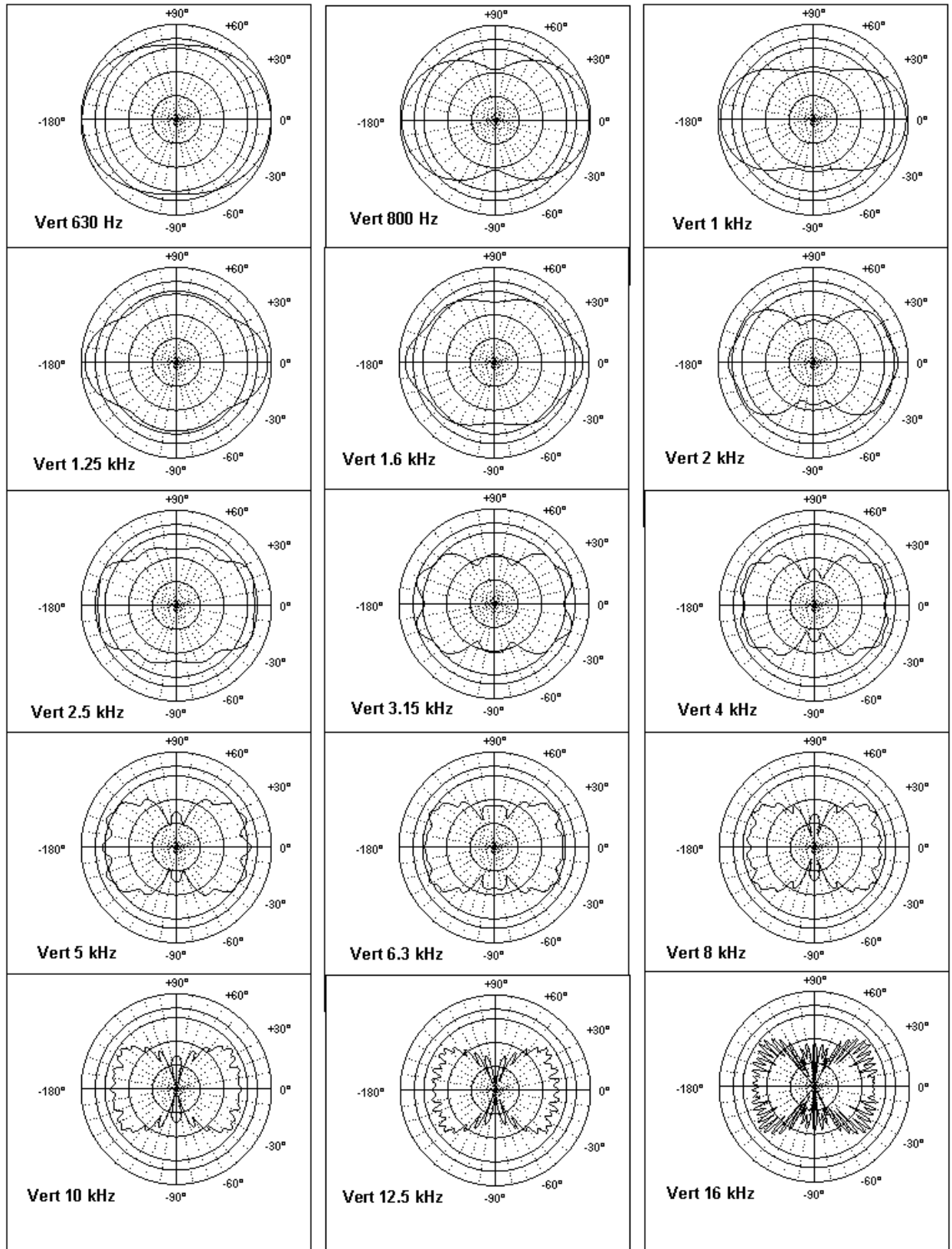
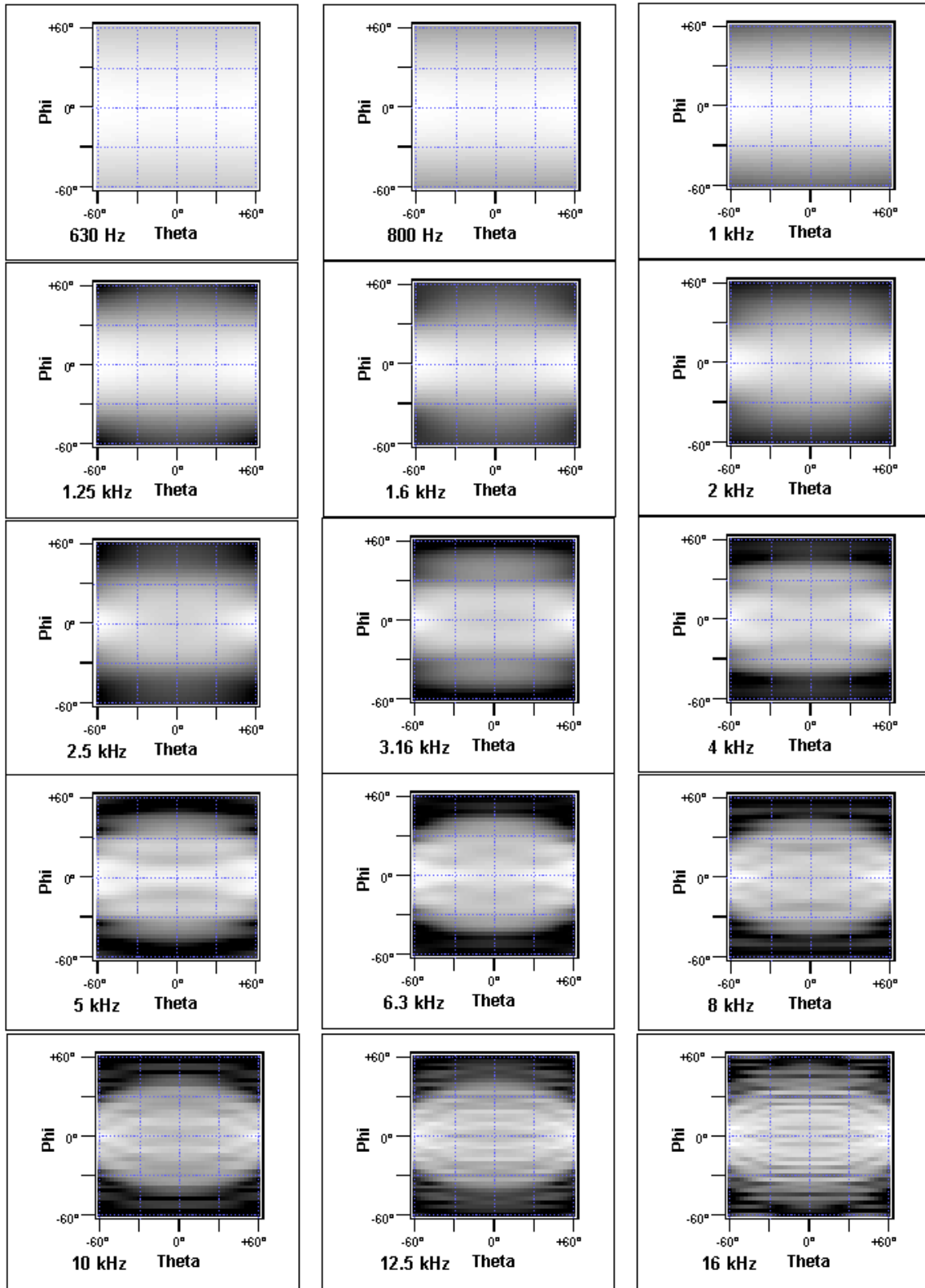Fig. 14 (f) Vertical polars. . See first figure for full caption.
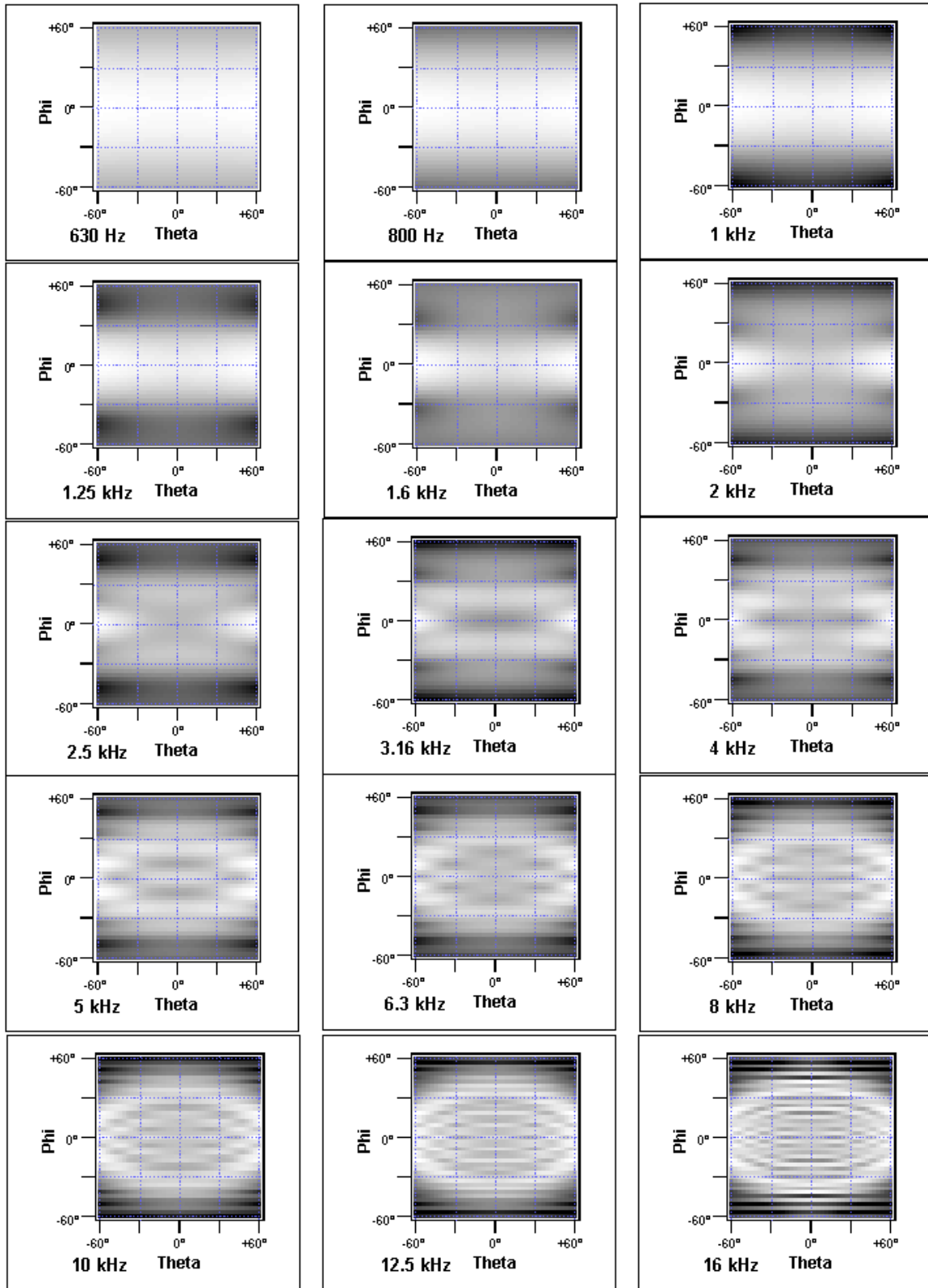
Fig. 14 (g) Footprints. See first figure for full caption.
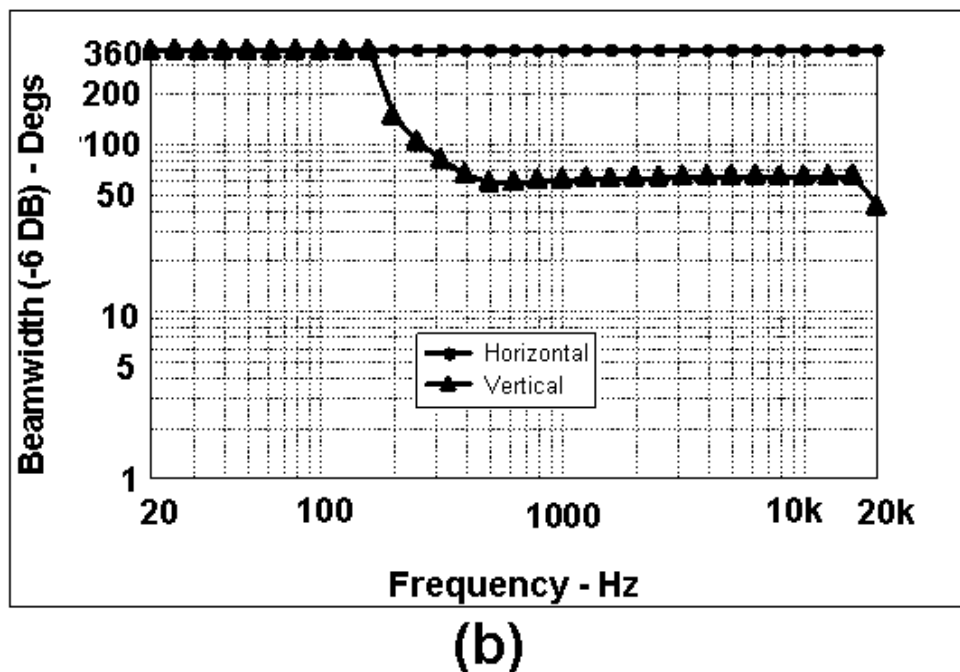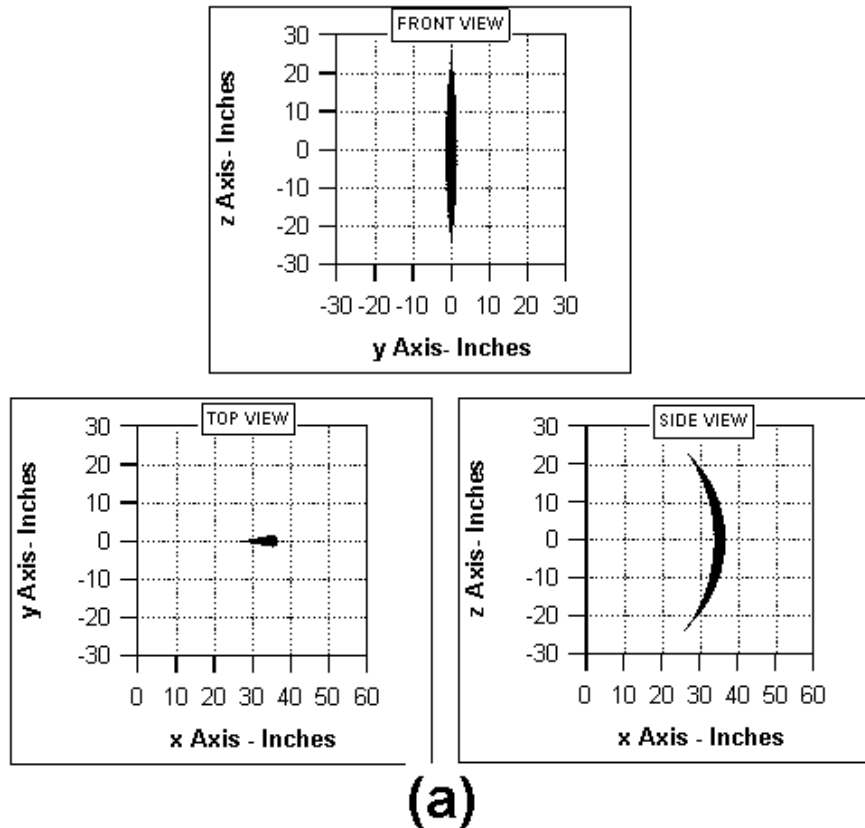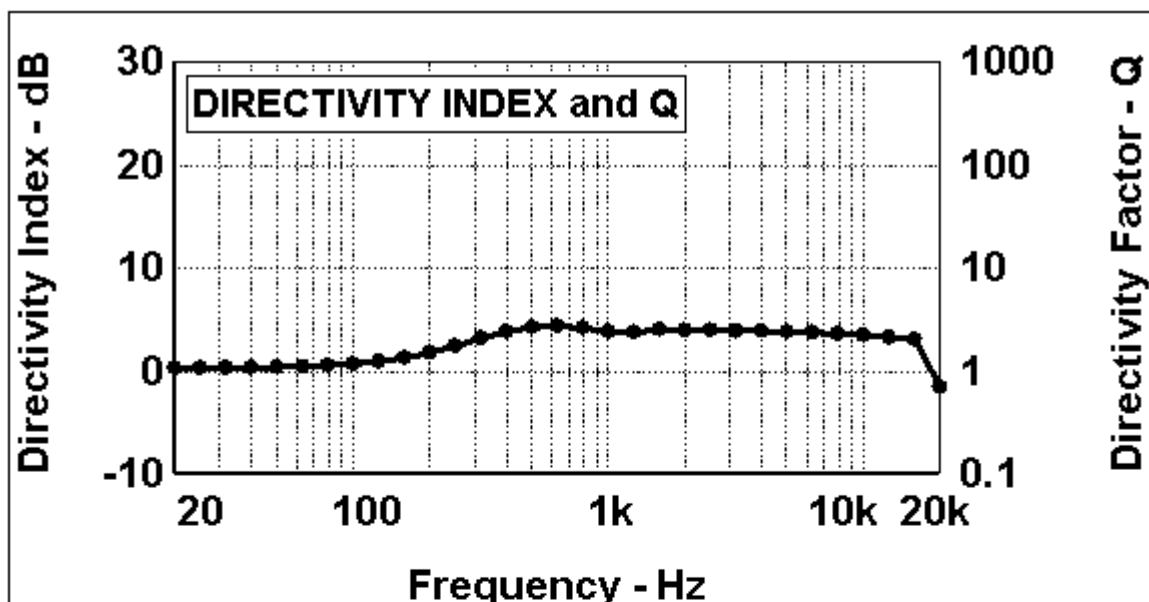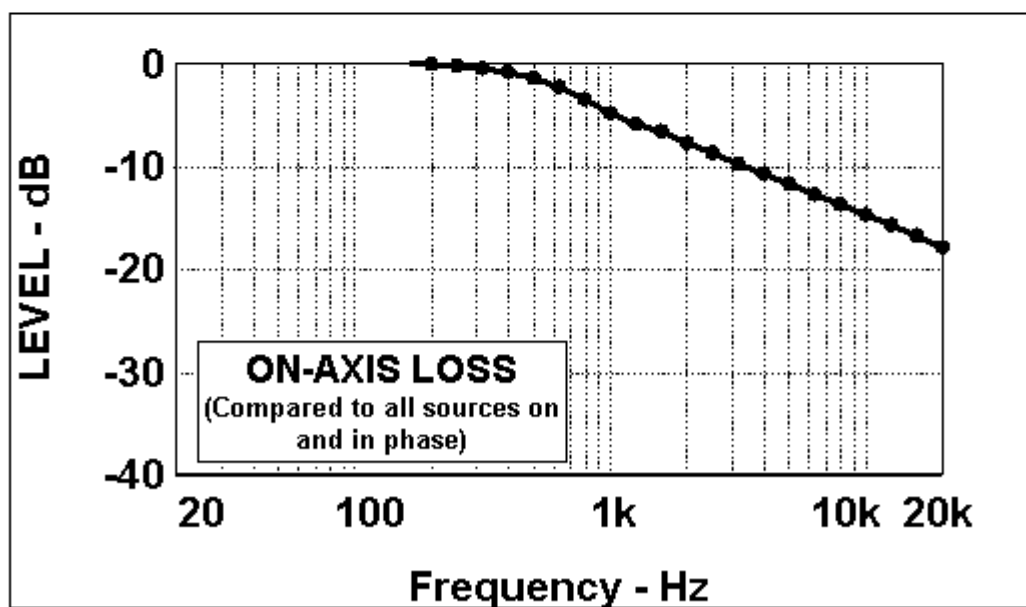
(a)

(b)
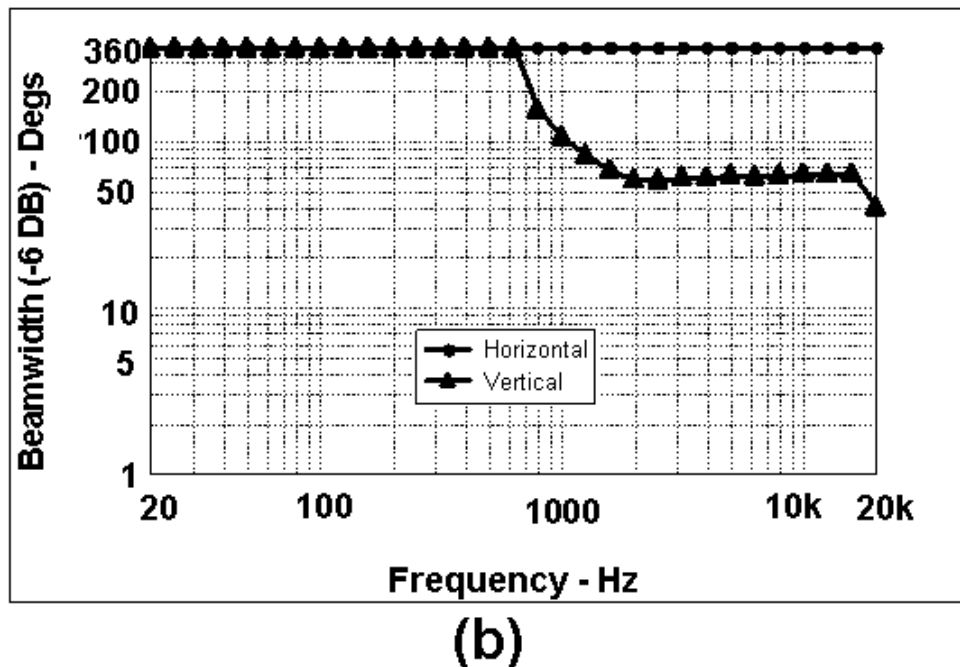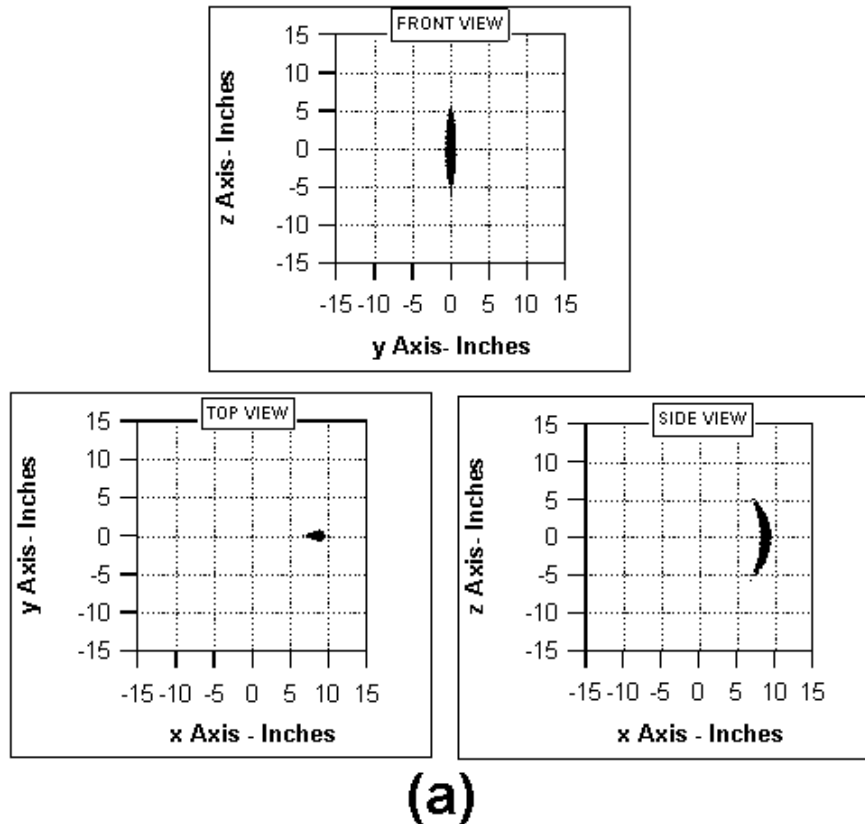
Fig. 15. Simulation results of the 21-point circular wedge line array with Legendre shading. (a) Front, top, and side configuration views. (b) Plot of beamwidth vs. frequency. (c) Directivity and Q vs. frequency. (d) On-axis loss vs. frequency. (e) Horizontal polar plots of the array from 630 Hz to 16 kHz at one-third-octave centers. (f) Vertical polar plots of the array from 630 Hz to 16 kHz at one-third-octave centers. (g) Footprint plots from 630 Hz to 16 kHz at one-third-octave centers.
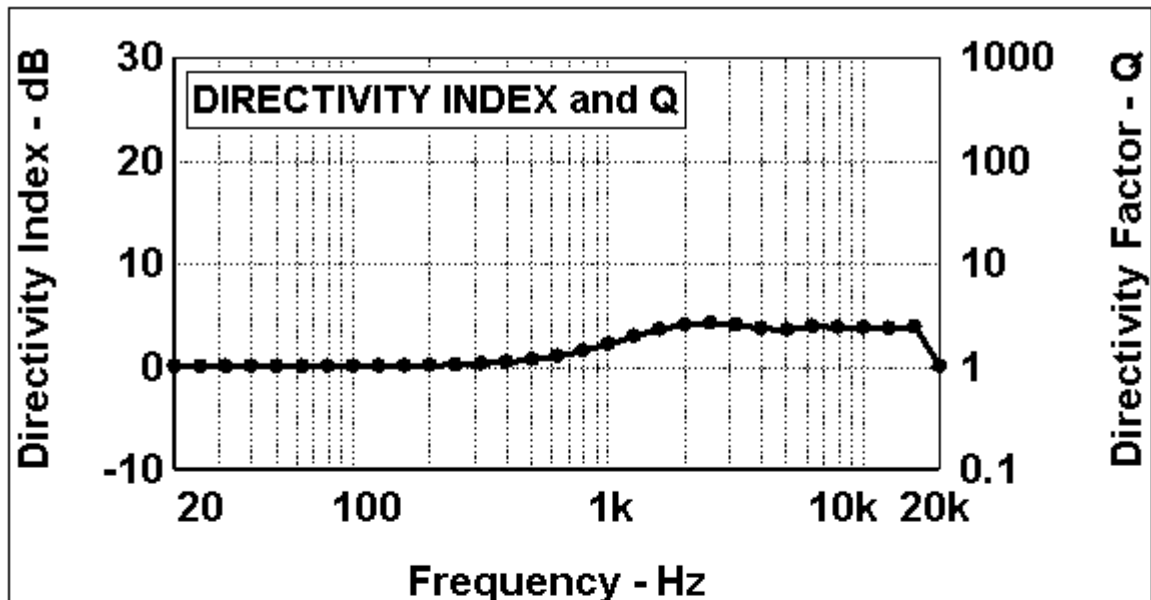
(c)
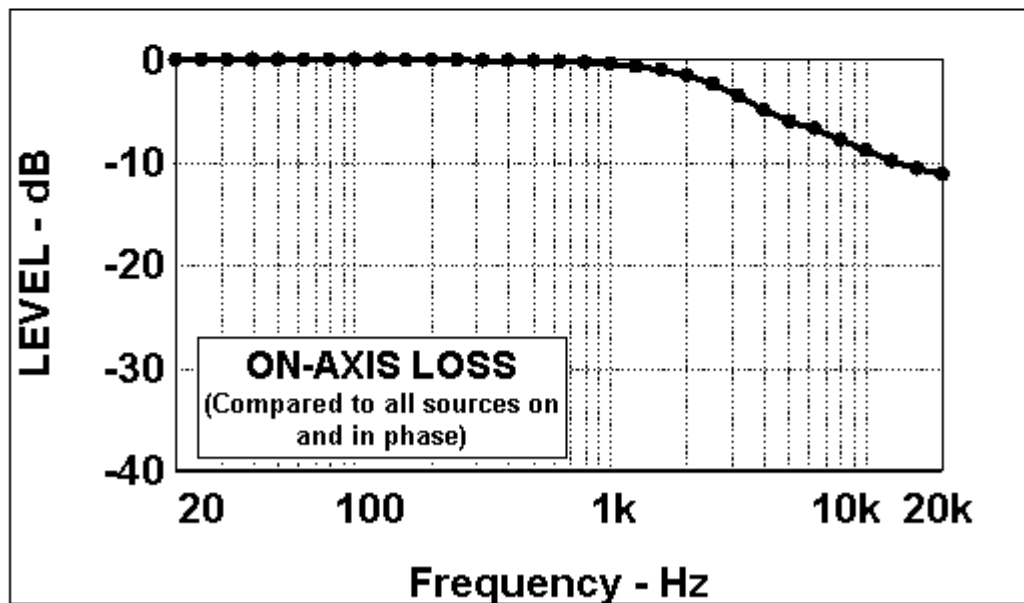
(d)

Fig. 15. (c) Directivity. (d) On-axis loss. See first figure for full caption.
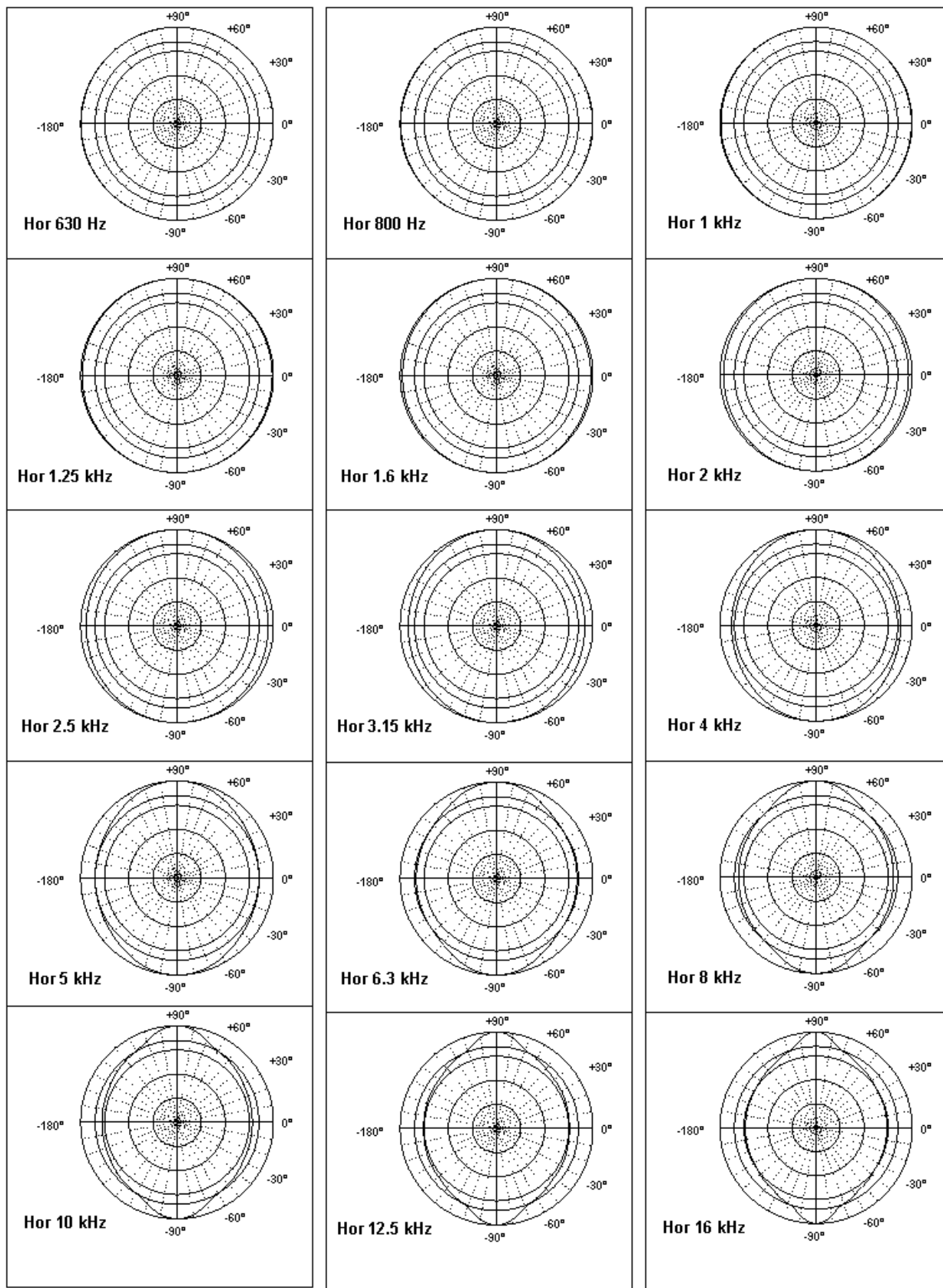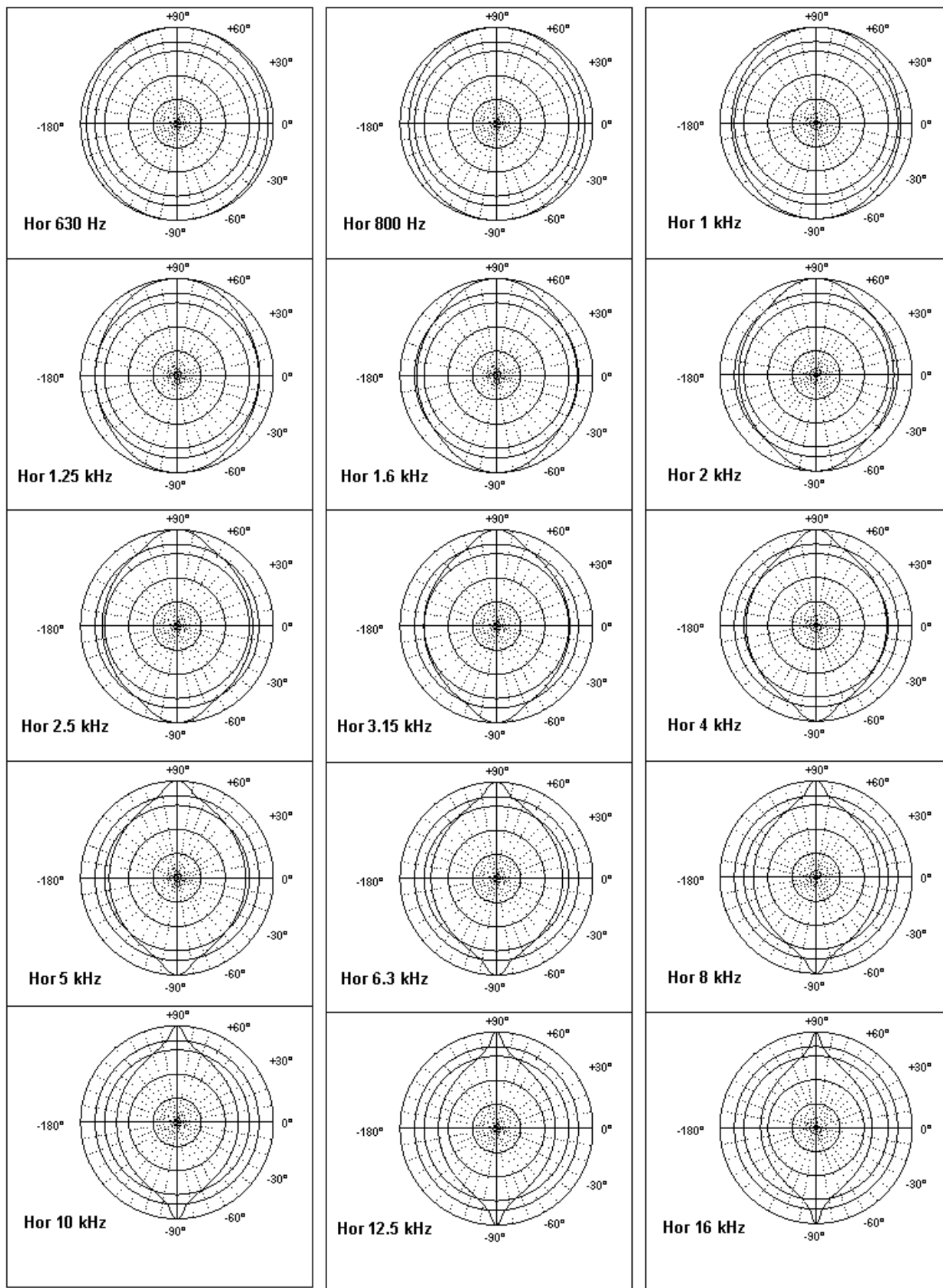
Fig. 15 (e) Horizontal polars. . See first figure for full caption.
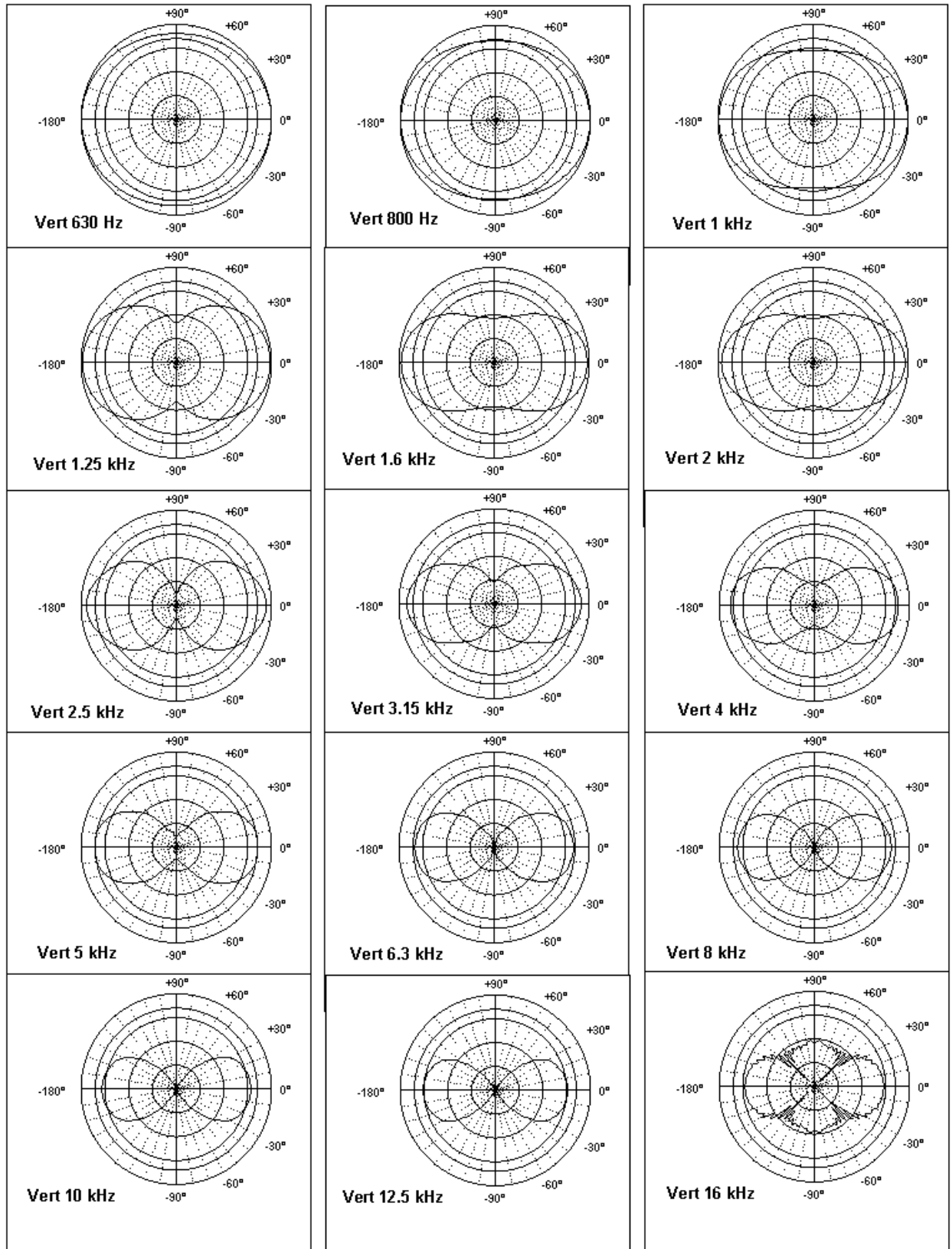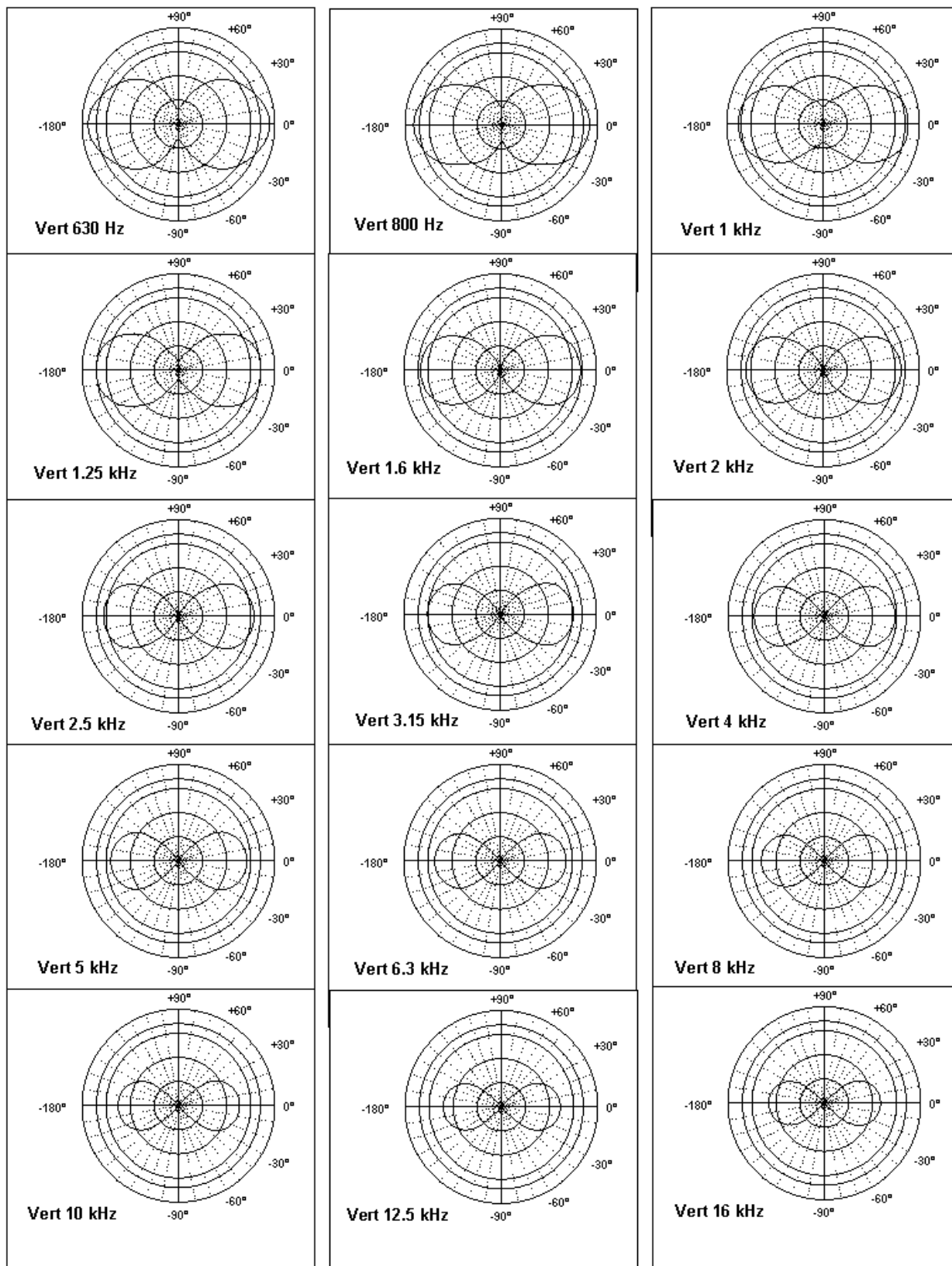
Fig. 15 (f) Vertical polars. . See first figure for full caption.
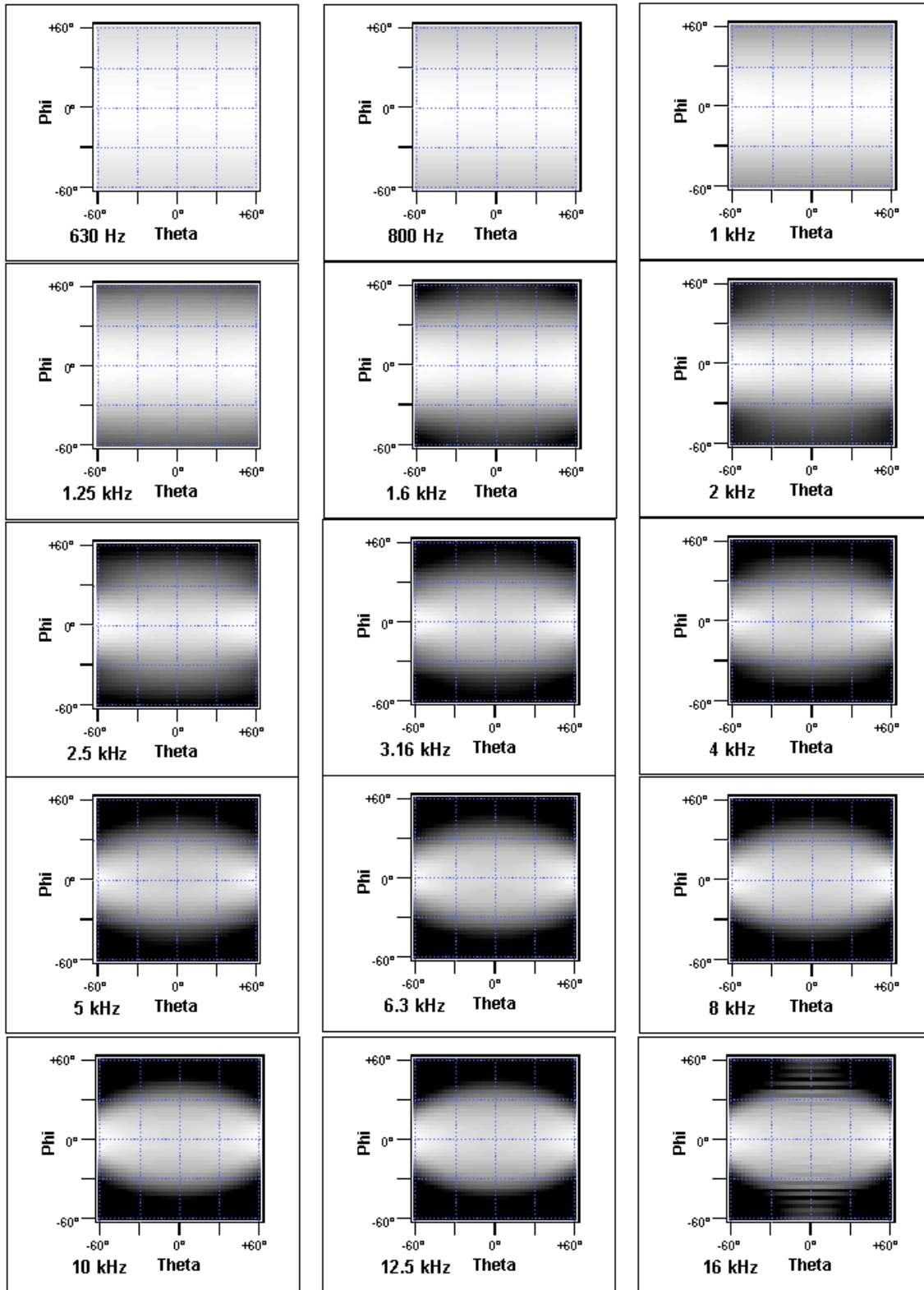
Fig. 15 (g) Footprints. See first figure for full caption.
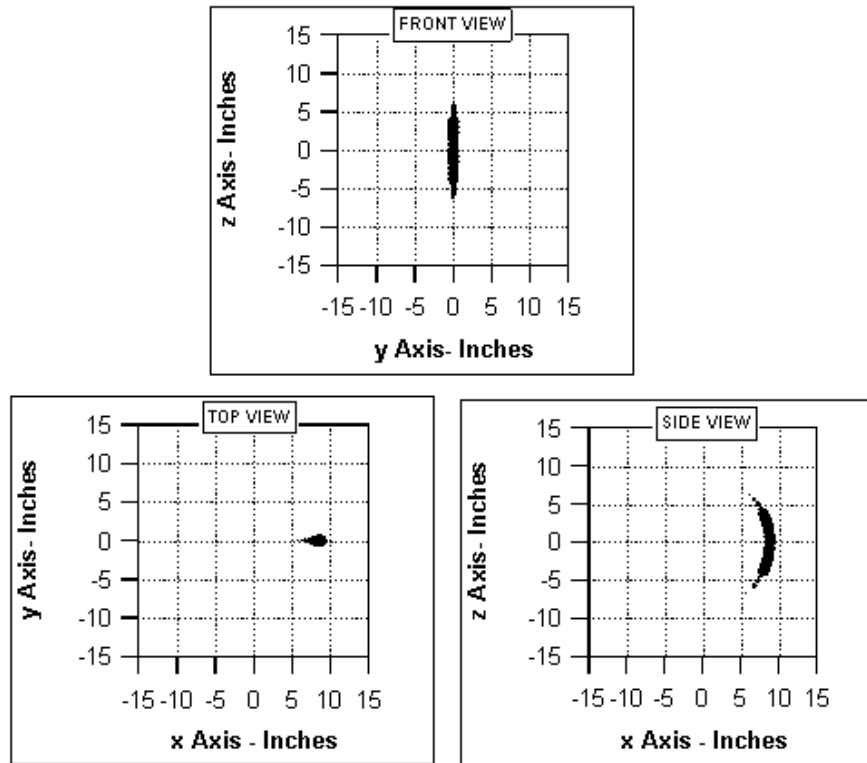
(a)

(b)

Fig. 16. Simulation results of the 21-point circular wedge line array with three-stepped shading of 0, -6, and -12 dB. (a) Front, top, and side configuration views. (b) Plot of beamwidth vs. frequency. (c) Directivity and Q vs. frequency. (d) On-axis loss plot vs frequency. (e) Horizontal polar plots of the array from 630 Hz to 16 kHz at one-third-octave centers. (f) Vertical polar plots of the array from 630 Hz to 16 kHz at one-third-octave centers. (g) Footprint plots from 630 Hz to 16 kHz at one-third-octave centers.

(c)
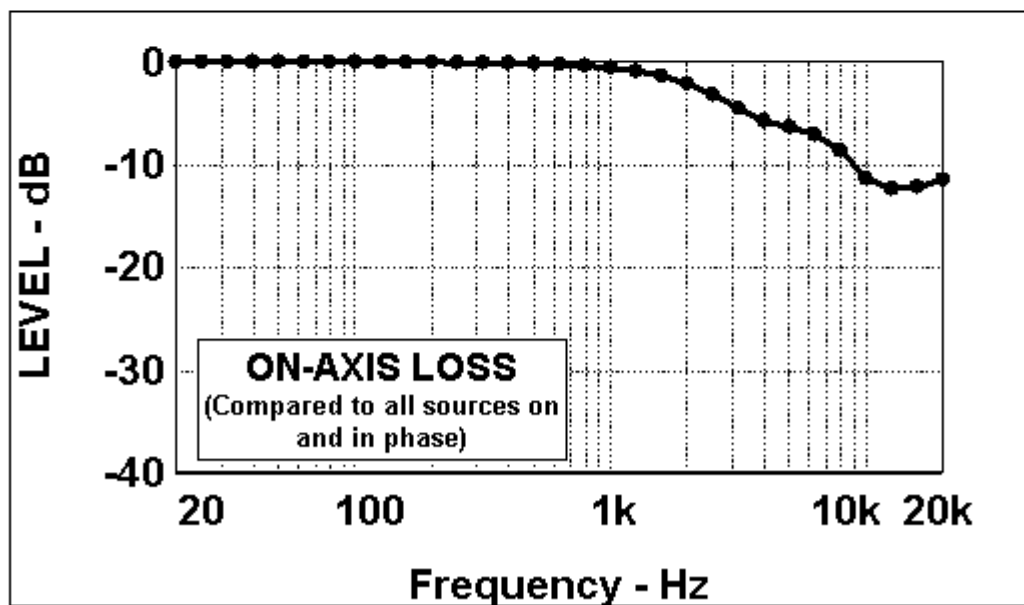
(d)

Fig. 16. (c) Directivity. (d) On-axis loss. See first figure for full caption.

Fig. 16 (e) Horizontal polars. . See first figure for full caption.

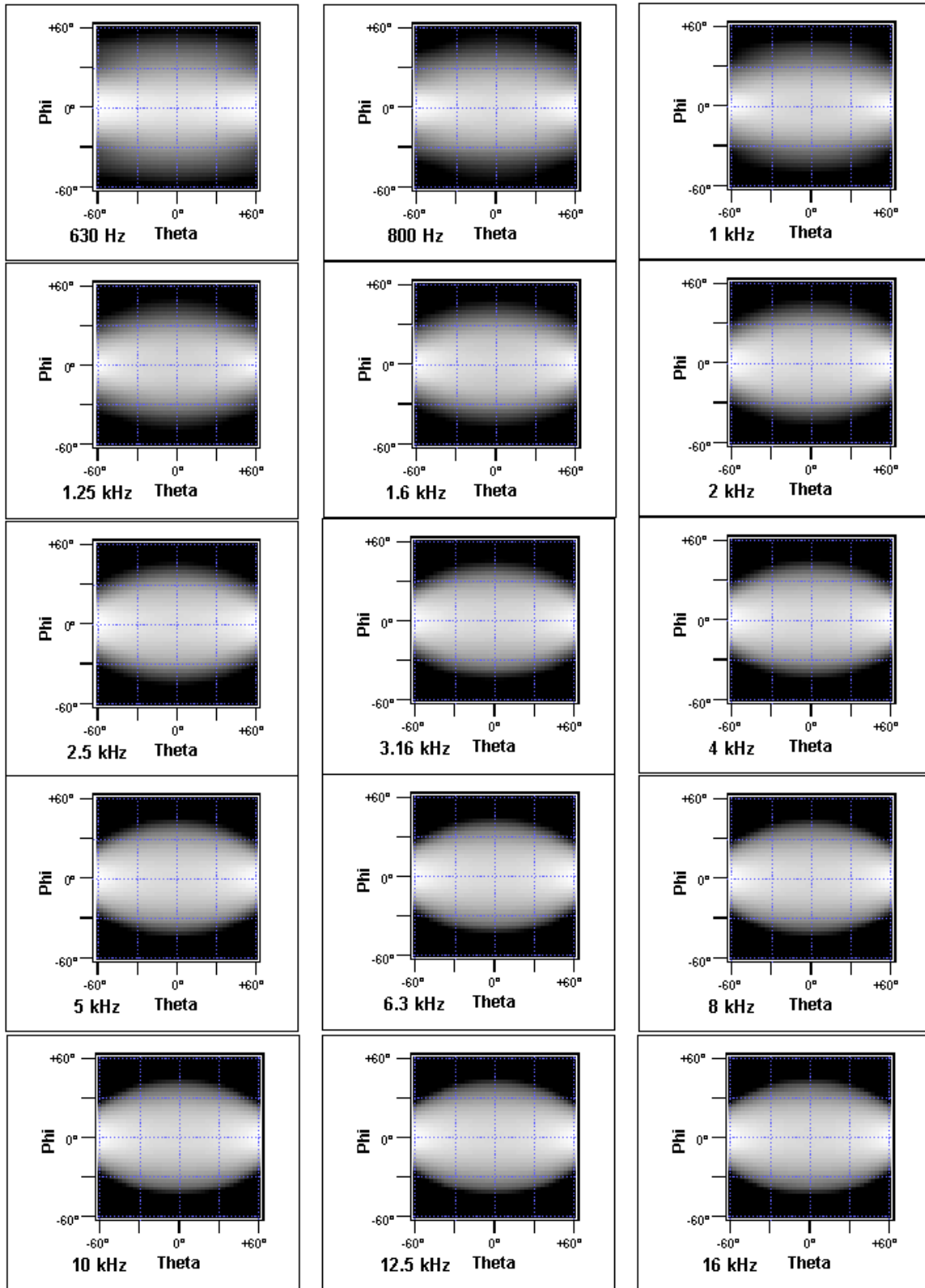Fig. 16 (f) Vertical polars. . See first figure for full caption.
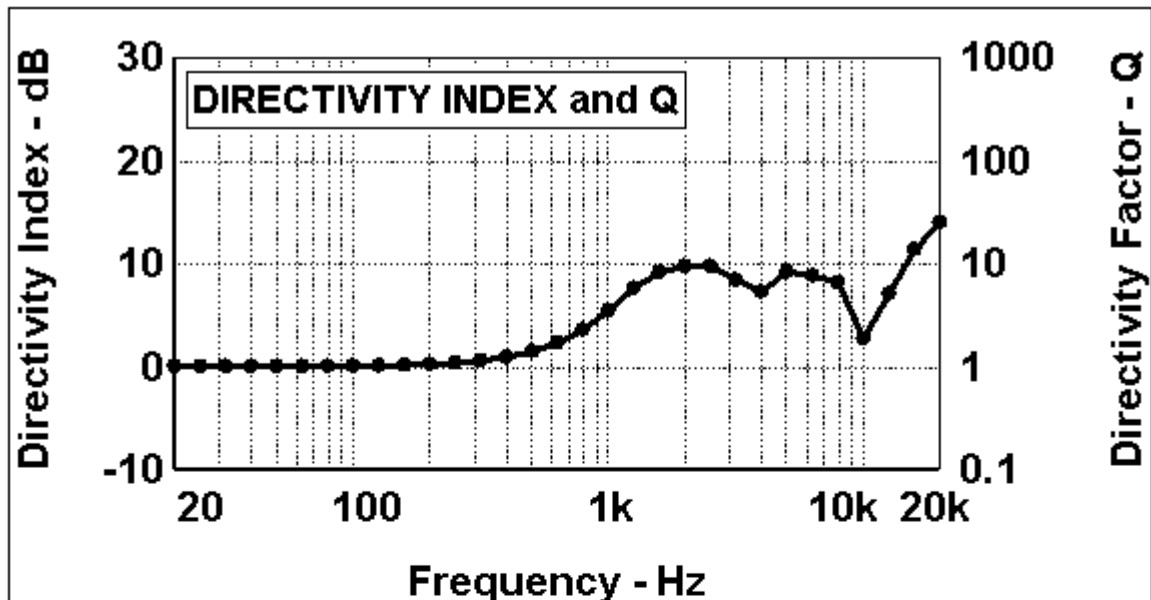
Fig. 16 (g) Footprints. See first figure for full caption.

Fig. 17. Simulation results of the 21-point circular wedge line array with two-stepped shading of 0, -6 dB. (a) Front, top, and side configuration views. (b) Plot of beamwidth vs. frequency. (c) Directivity and Q vs. frequency. (d) On-axis loss plot vs frequency. (e) Horizontal polar plots of the array from 630 Hz to 16 kHz at one-third-octave centers. (f) Vertical polar plots of the array from 630 Hz to 16 kHz at one-third-octave centers. (g) Footprint plots from 630 Hz to 16 kHz at one-third-octave centers.

(c)

(d)

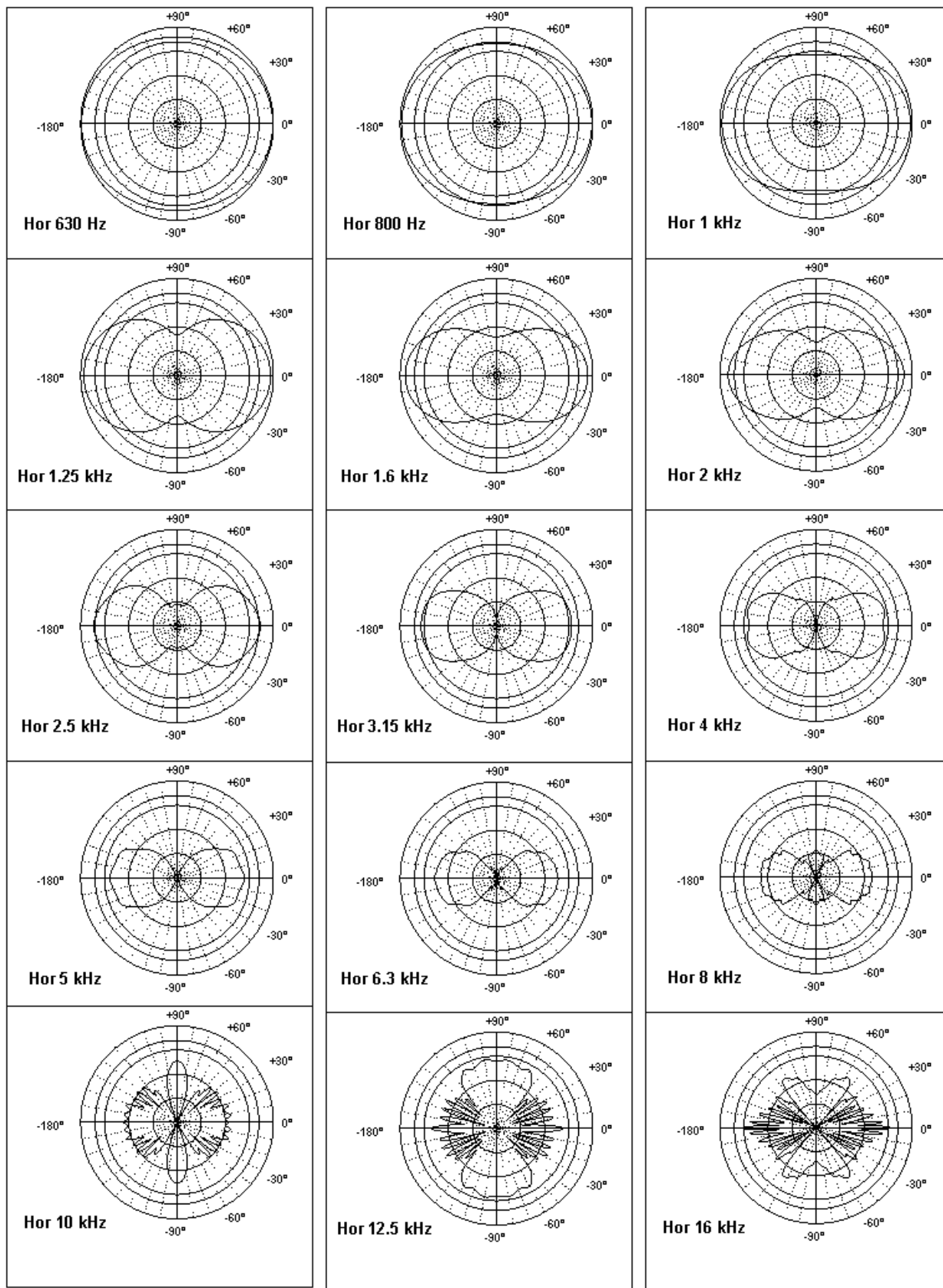Fig. 17. (c) Directivity. (d) On-axis loss. See first figure for full caption.

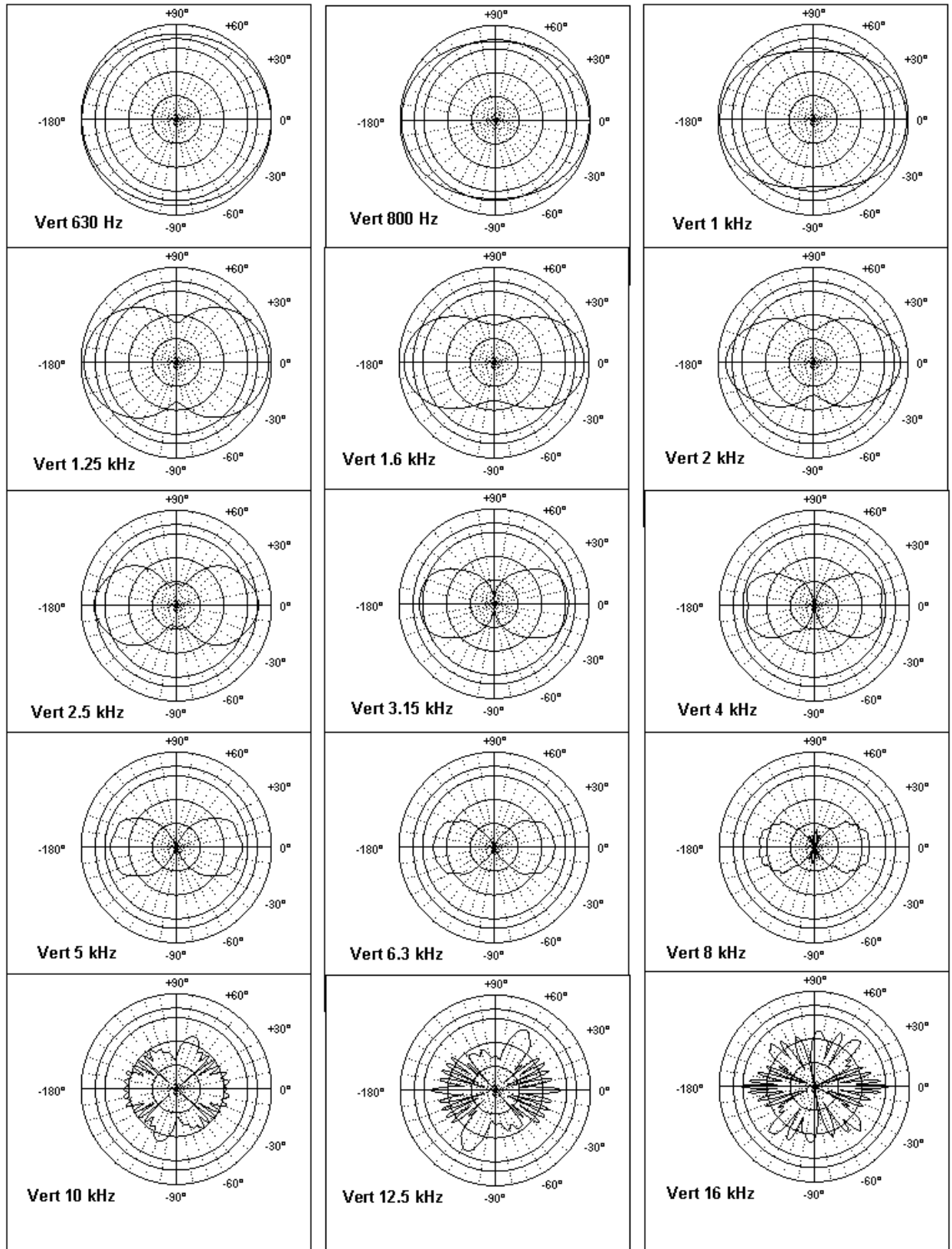Fig. 17. (e) Horizontal polars. . See first figure for full caption.

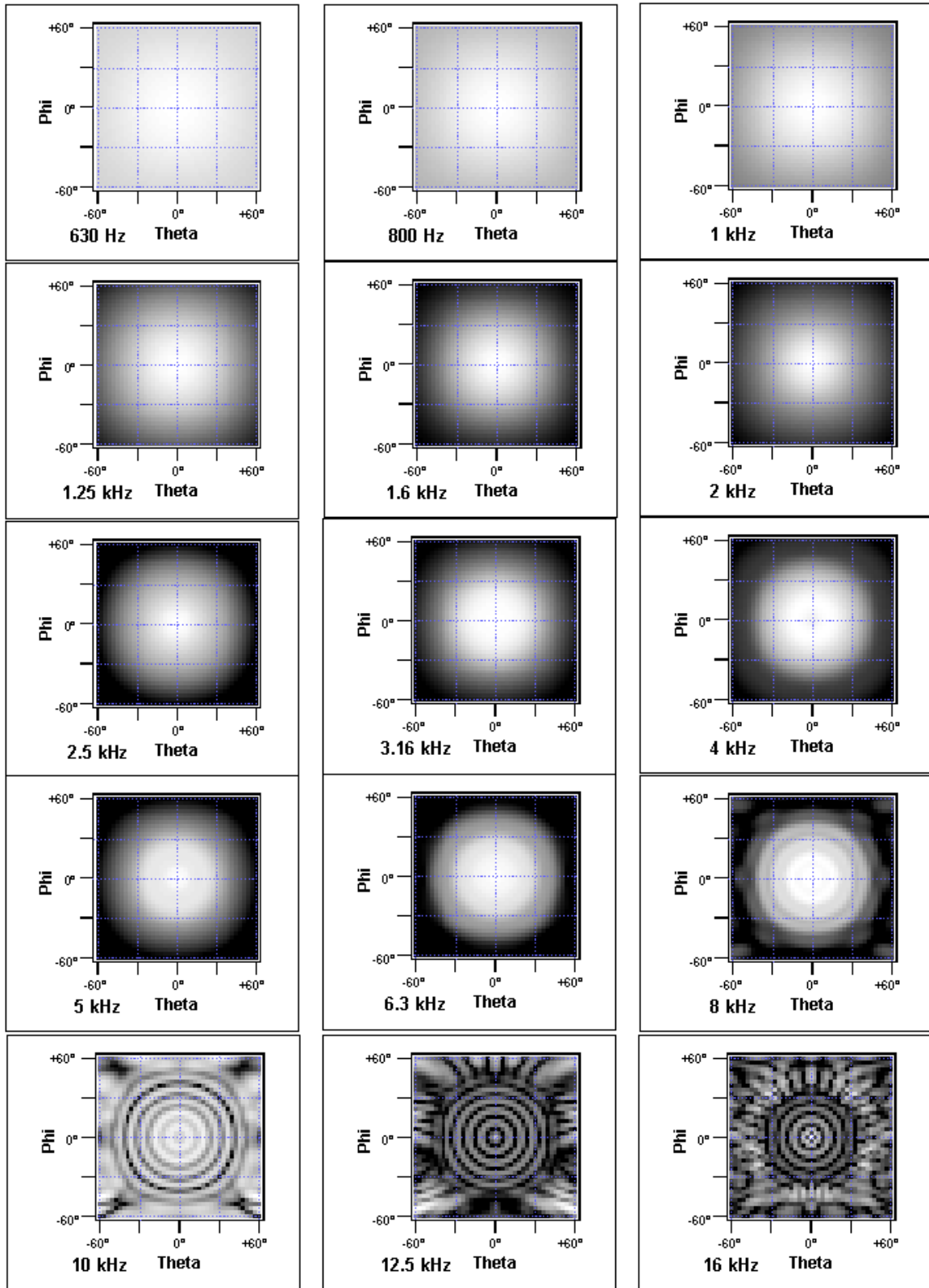Fig. 17. (f) Vertical polars. . See first figure for full caption.

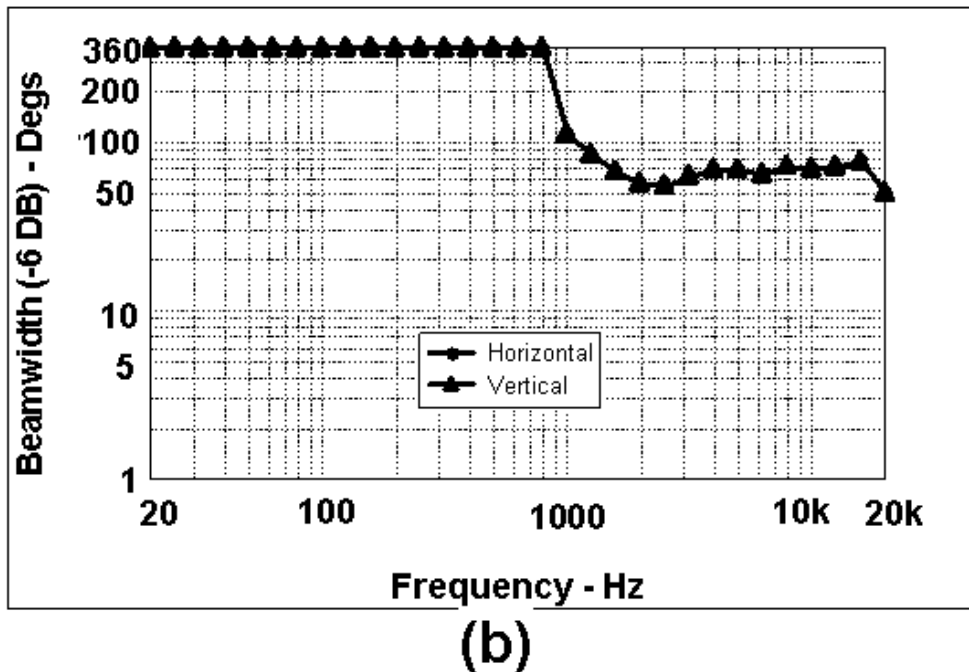Fig. 17. (g) Footprints. See first figure for full caption.

(a)

(b)

Fig. 18. Simulation results of the 81-point circular wedge line array with Legendre shading. (a) Front, top, and side configuration views. (b) Plot of beamwidth vs. frequency. (c) Directivity and Q vs. frequency. (d) On-axis loss plot vs. frequency. (e) Horizontal polar plots of the array from 630 Hz to 16 kHz at one-third-octave centers. (f) Vertical polar plots of the array from 630 Hz to 16 kHz at one-third-octave centers. (g) Footprint plots from 630 Hz to 16 kHz at one-third-octave centers.

(c)

(d)

Fig. 18. (c) Directivity. (d) On-axis loss. See first figure for full caption.

Fig. 18. (e) Horizontal polars. . See first figure for full caption.

Fig. 18. (f) Vertical polars. . See first figure for full caption.

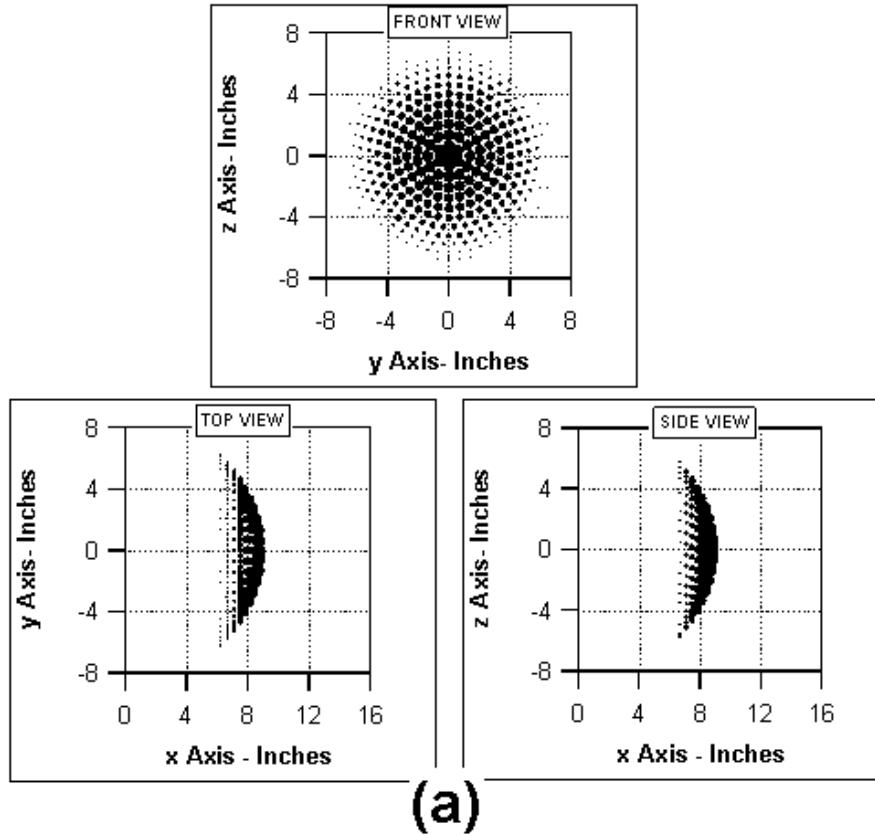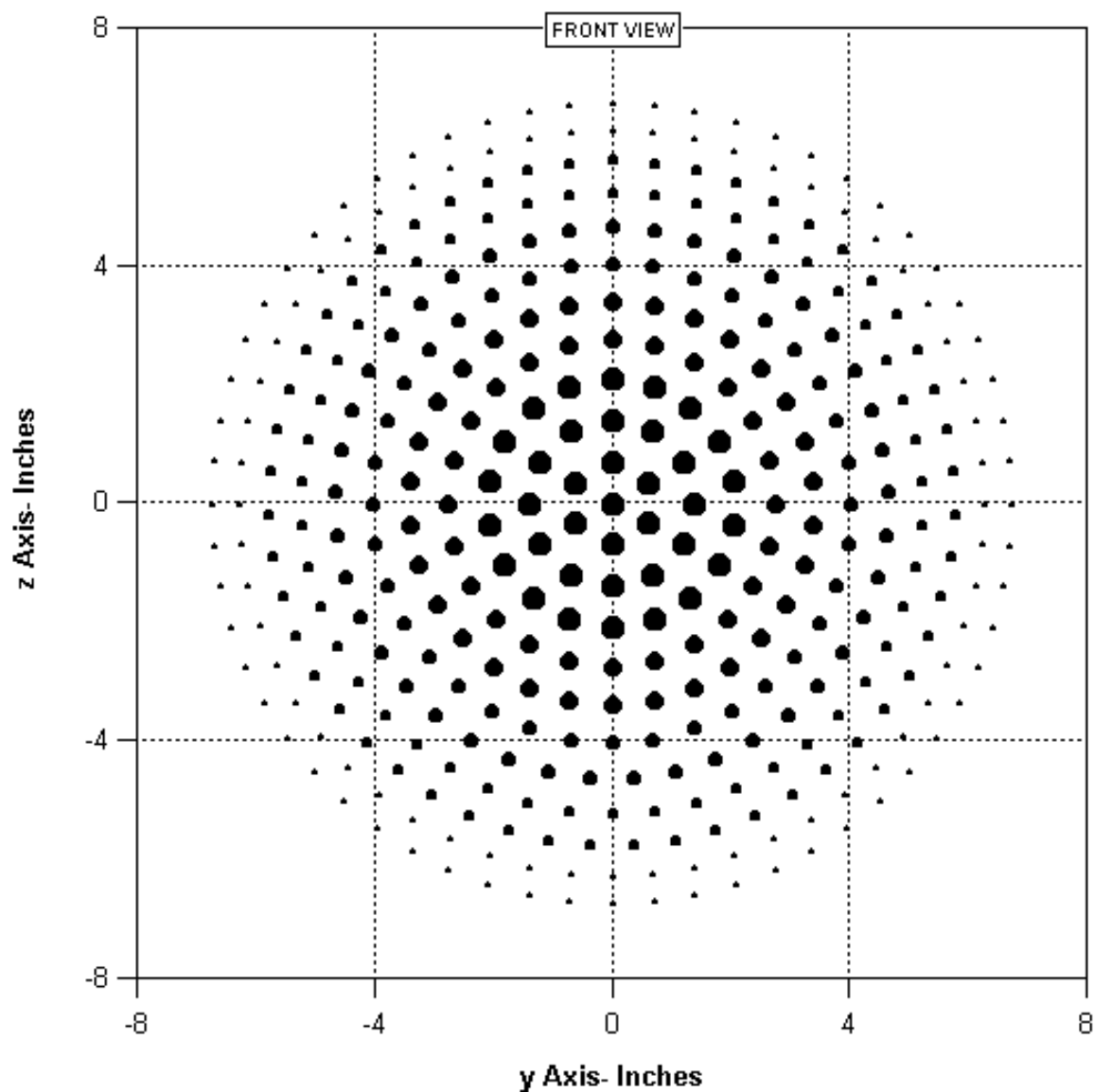Fig. 18. (g) Footprints. See first figure for full caption.
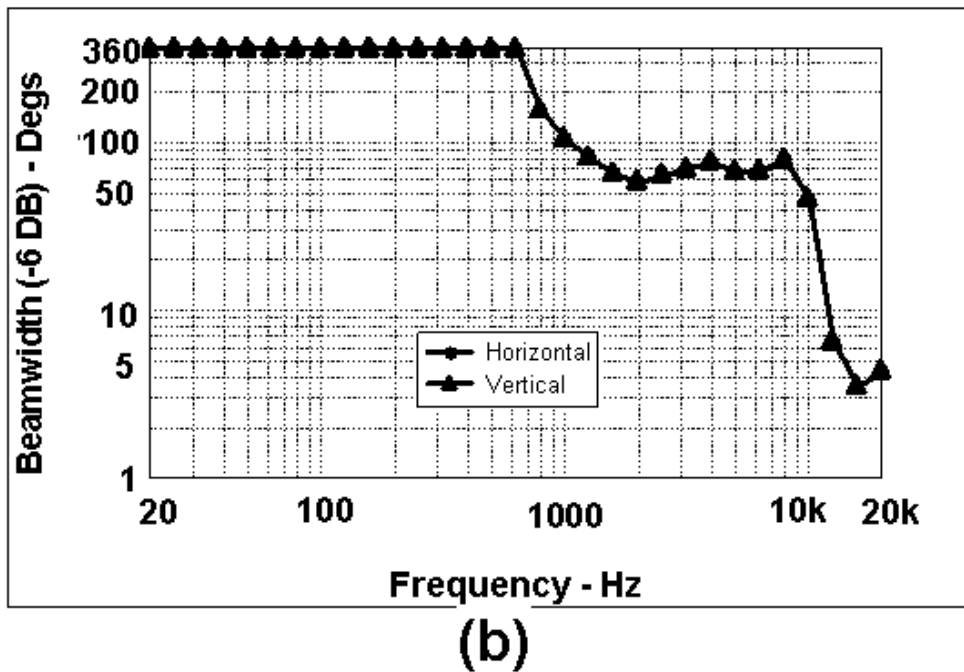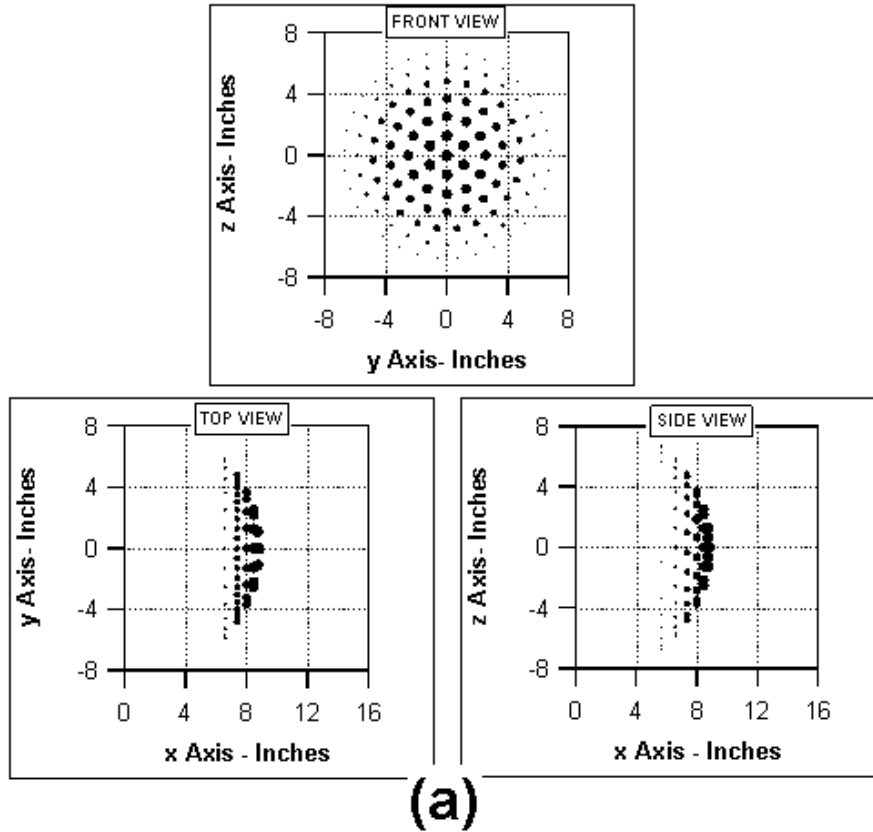
Fig. 19. Simulation results of the 121-point spherical cap array with Legendre shading. (a) Front, top, and side configuration views. (b) Plot of beamwidth vs. frequency. (c) Directivity and Q vs. frequency. (d) On-axis loss plot vs frequency. (e) Horizontal polar plots of the array from 630 Hz to 16 kHz at one-third-octave centers. (f) Vertical polar plots of the array from 630 Hz to 16 kHz at one-third-octave centers. (g) Footprint plots from 630 Hz to 16 kHz at one-third-octave centers.

(c)
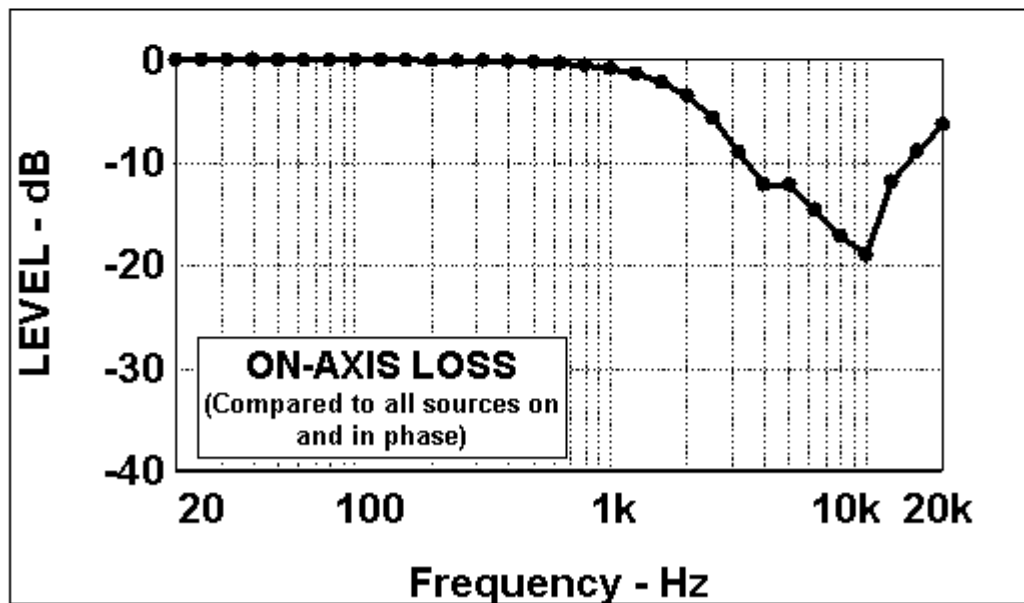
(d)

Fig. 19. (c) Directivity. (d) On-axis loss. See first figure for full caption.

Fig. 19. (e) Horizontal polars. . See first figure for full caption.

Fig. 19. (f) Vertical polars. . See first figure for full caption.
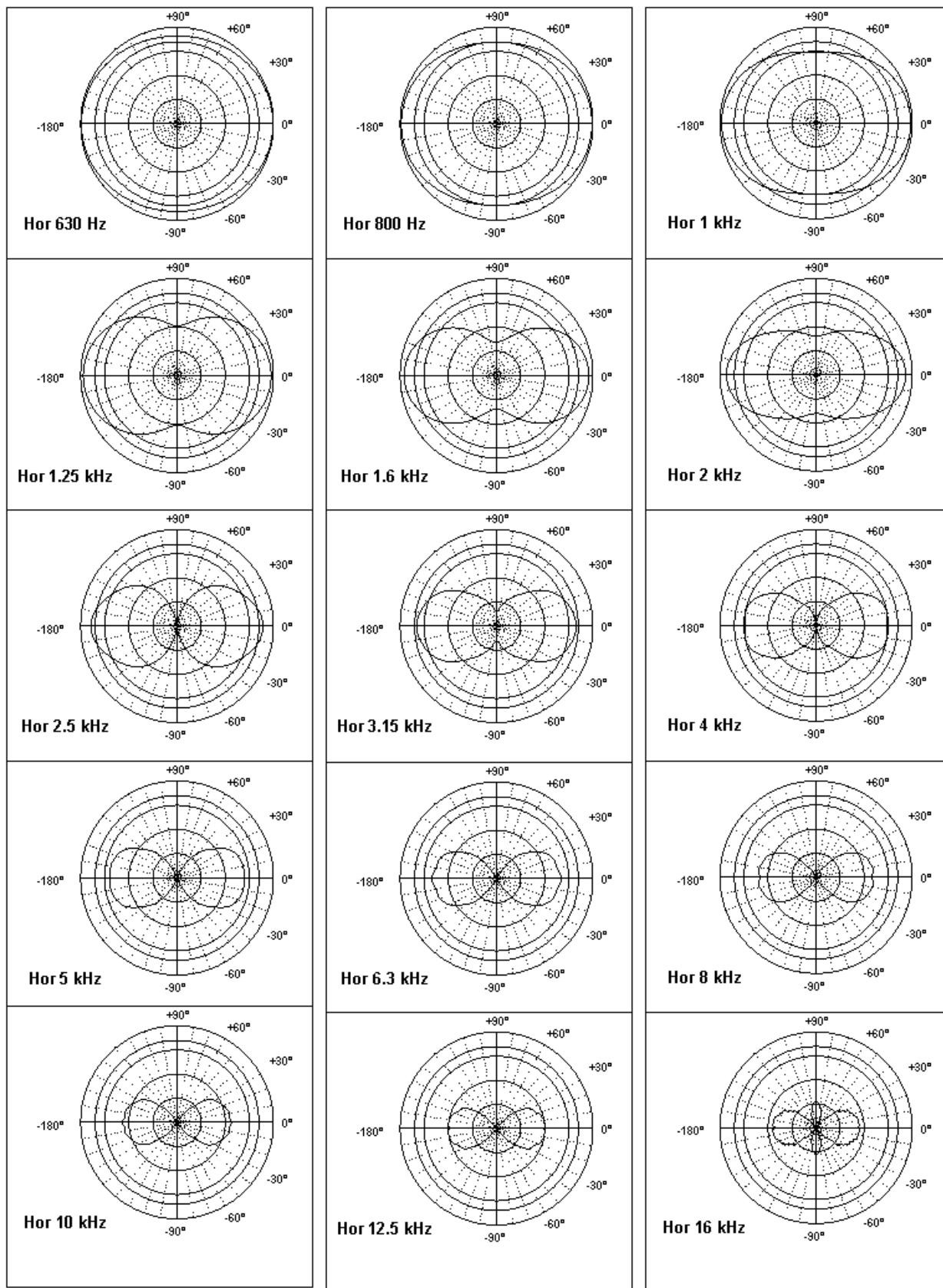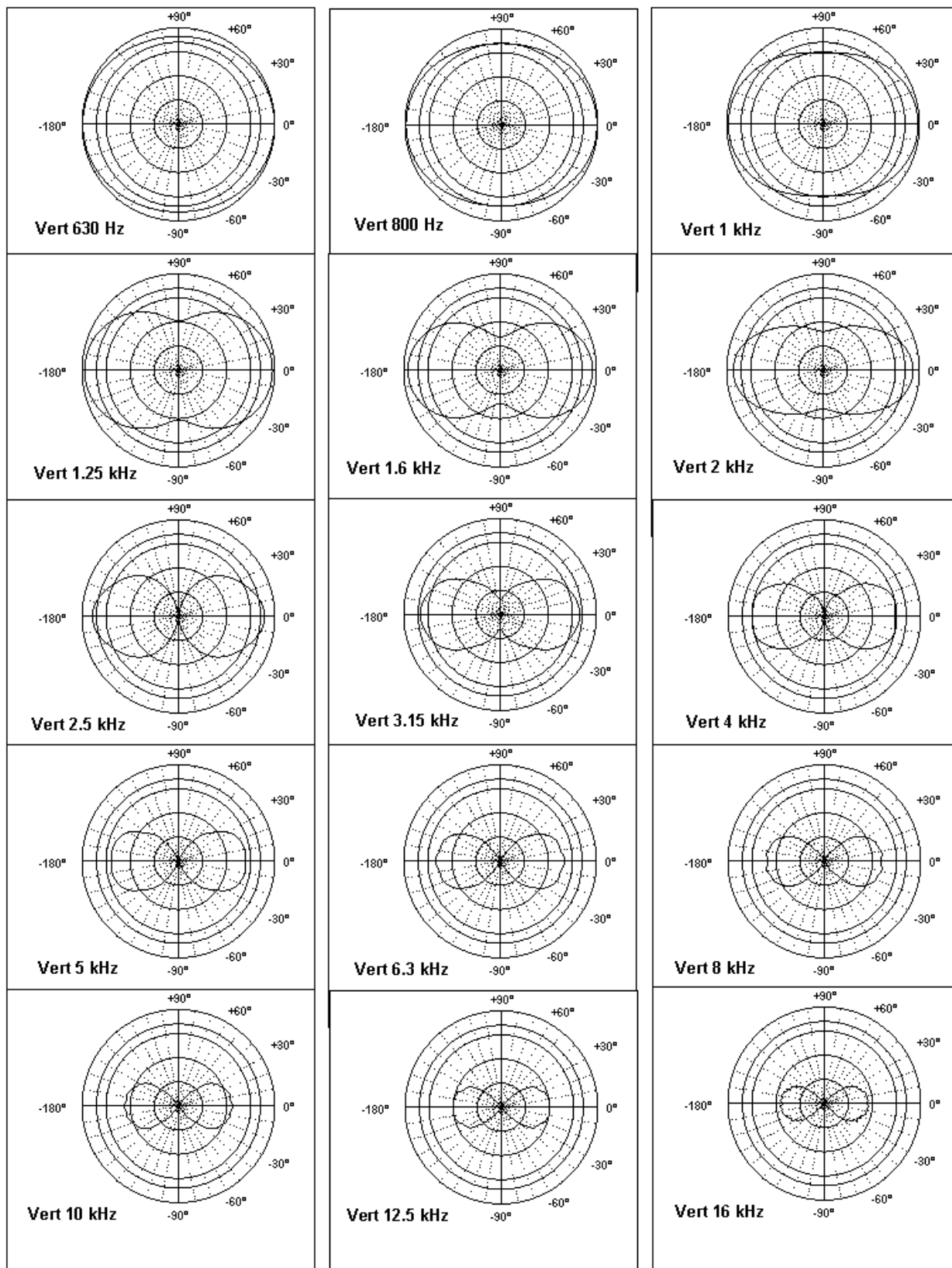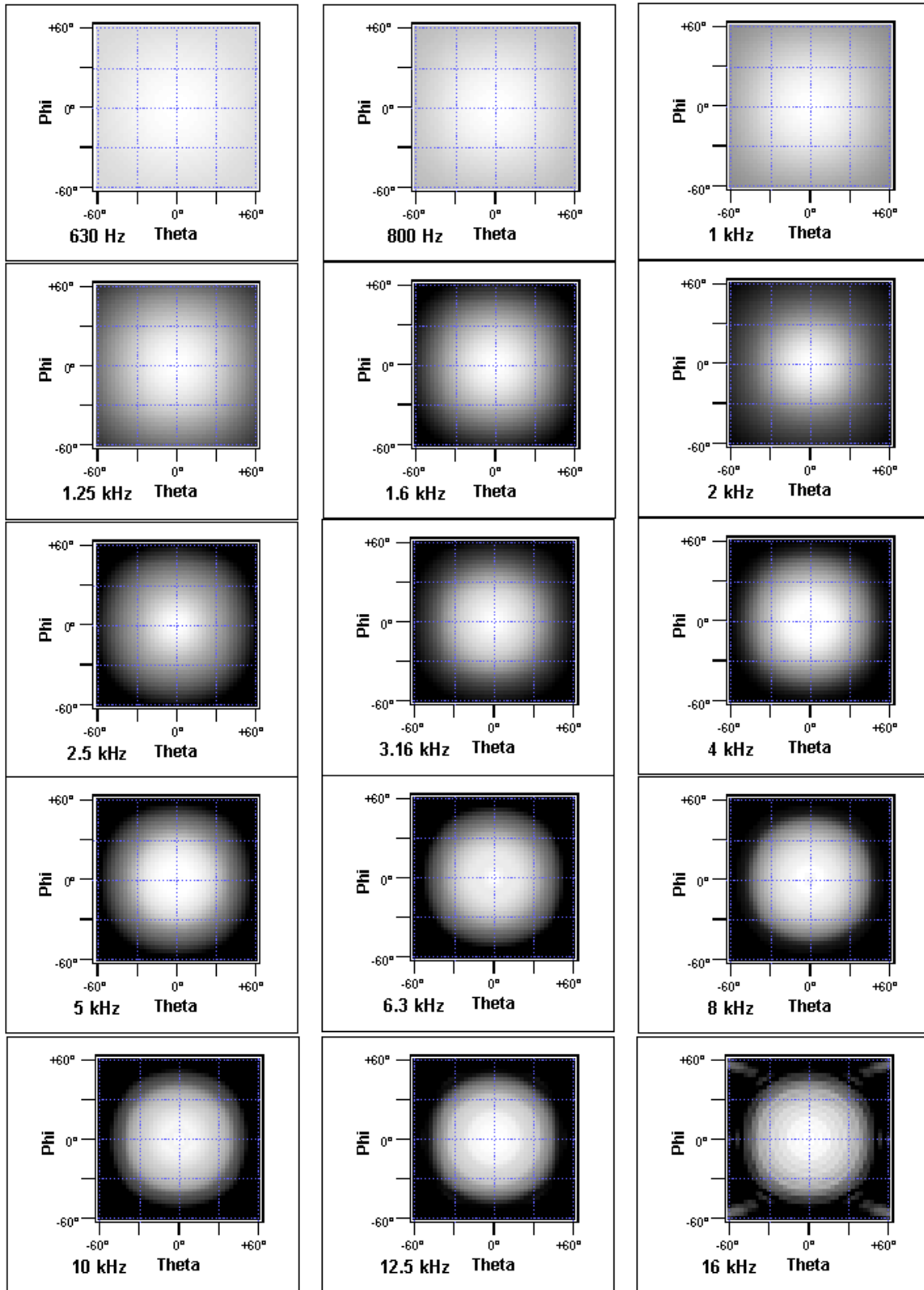
Fig. 19. (g) Footprints. See first figure for full caption.

Fig. 20. Simulation results of the 381-point spherical cap array with Legendre shading. (a) Front, top, and side configuration views. (b) Plot of beamwidth vs. frequency. (c) Directivity and Q vs. frequency. (d) On-axis loss plot vs frequency. (e) Horizontal polar plots of the array from 630 Hz to 16 kHz at one-third-octave centers. (f) Vertical polar plots of the array from 630 Hz to 16 kHz at one-third-octave centers. (g) Footprint plots from 630 Hz to 16 kHz at one-third-octave centers.

Fig. 20. (a) Expanded front configuration view. Approximate source strength is indicated by point size. Sources were laid out in concentric circles with single source at center. See first figure for full caption.
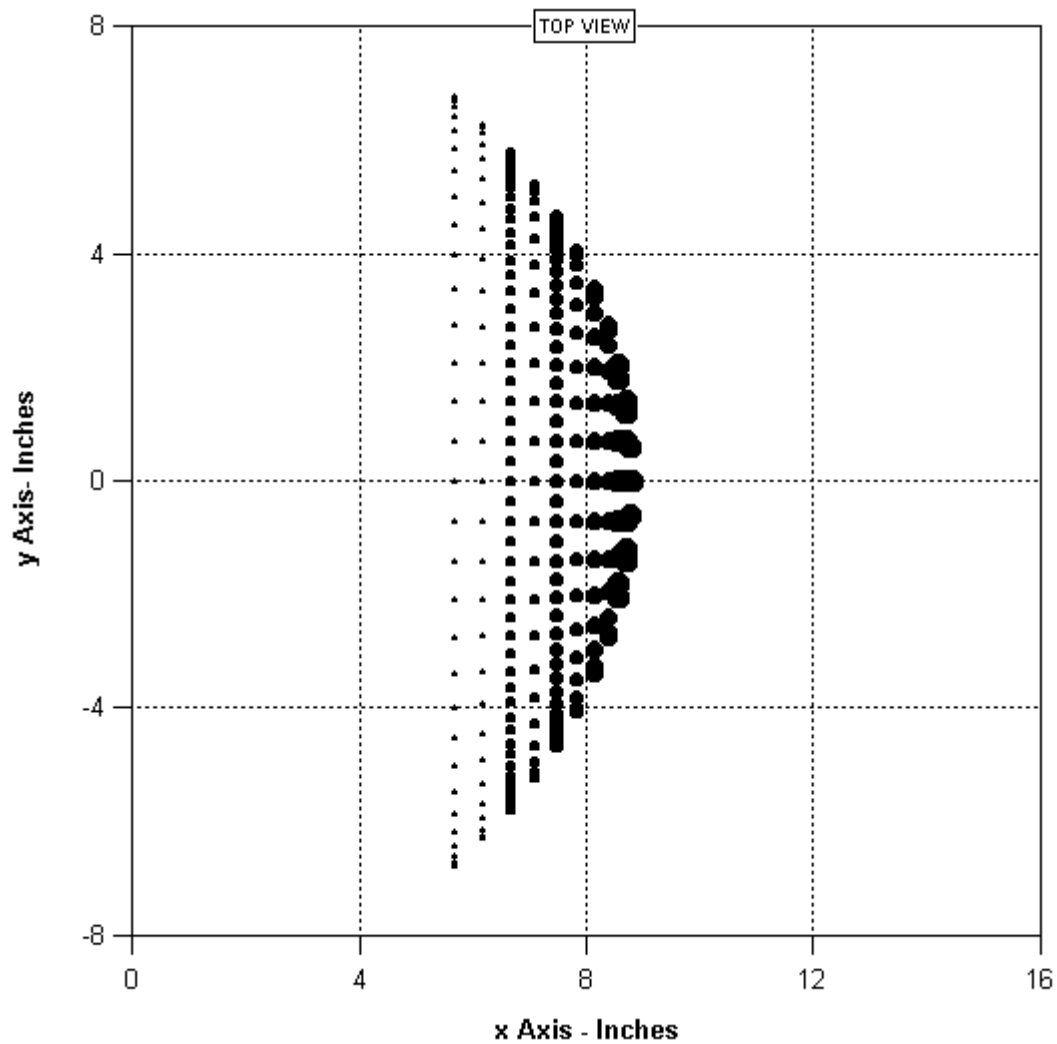
Fig. 20. (a) Expanded top configuration view. Center of spherical cap is at (0, 0, 0). See first figure for full caption.
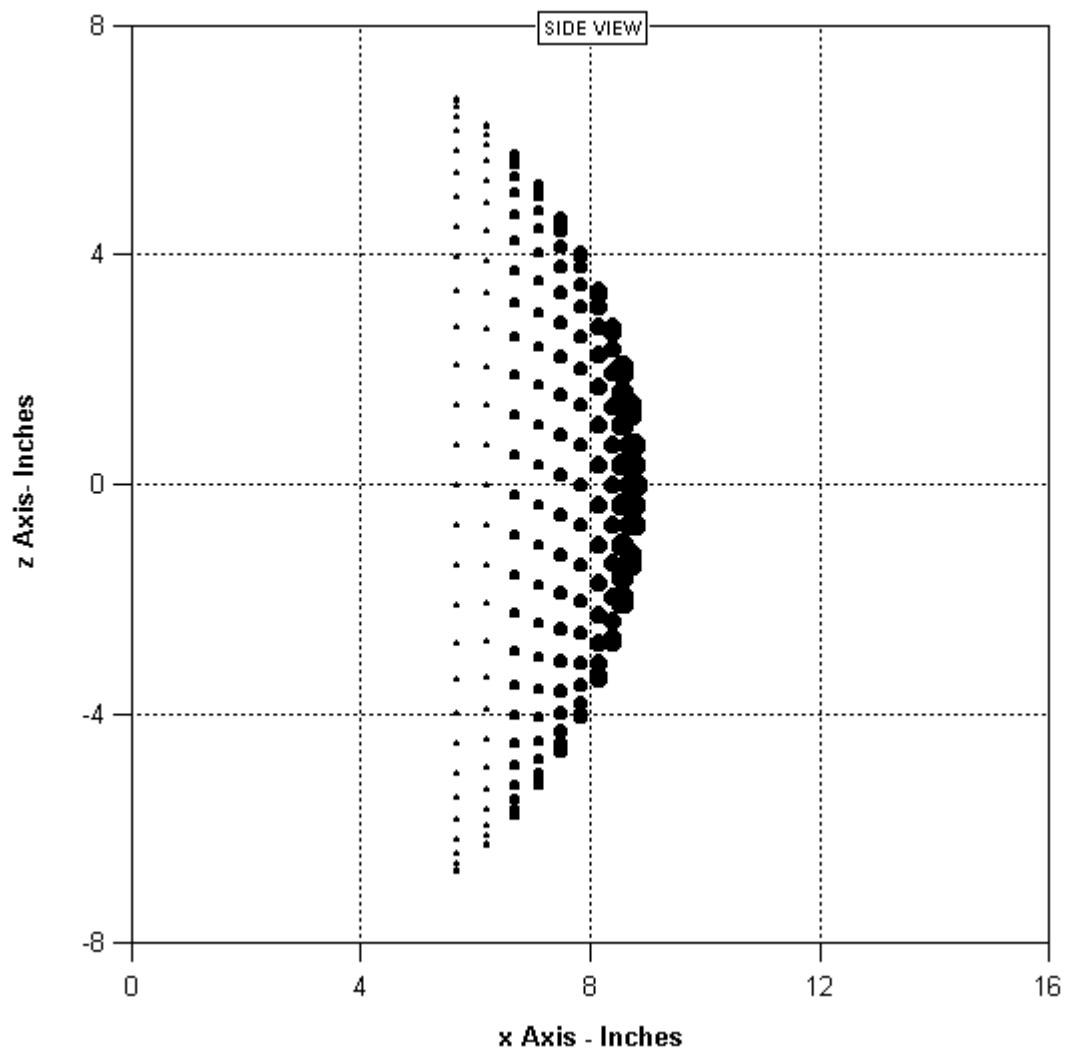
Fig. 20. (a) Expanded side configuration view. See first figure for full caption.
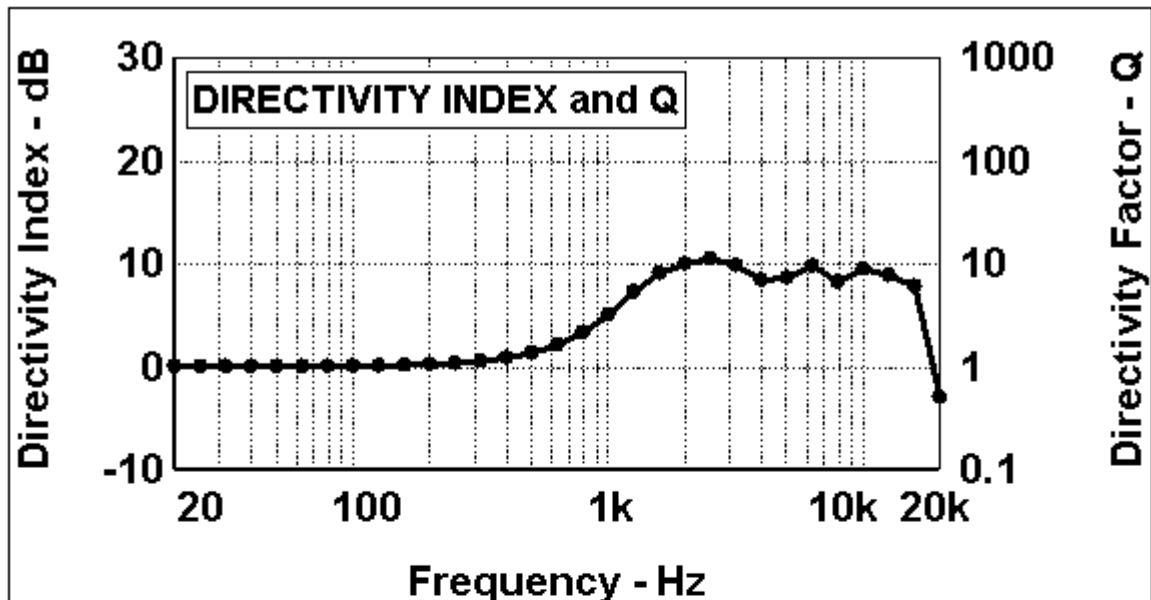
(c)
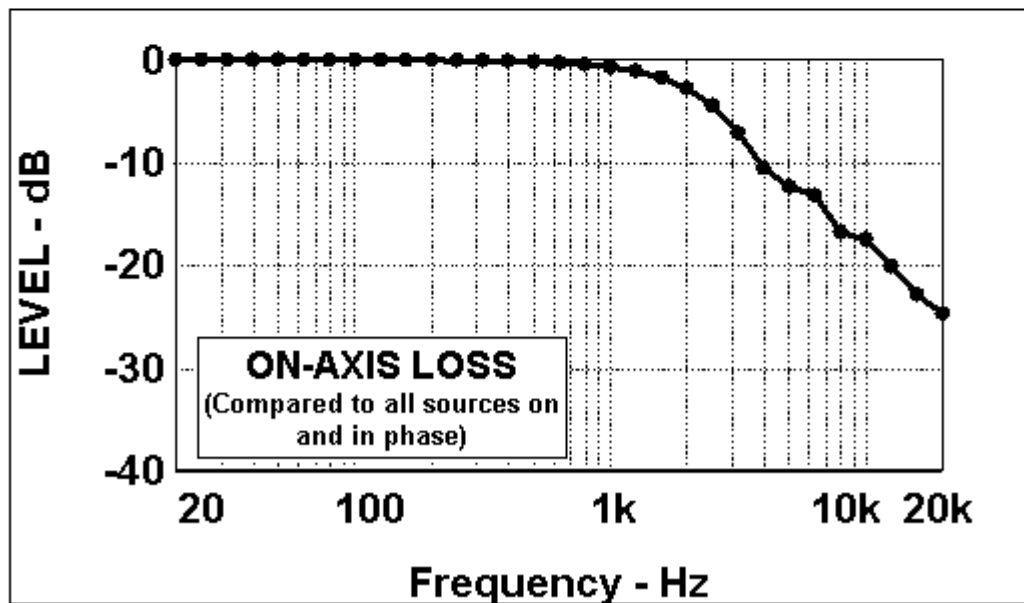
(d)

Fig. 20. (c) Directivity. (d) On-axis loss. See first figure for full caption.

Fig. 20. (e) Horizontal polars. . See first figure for full caption.

Fig. 20. (f) Vertical polars. . See first figure for full caption.
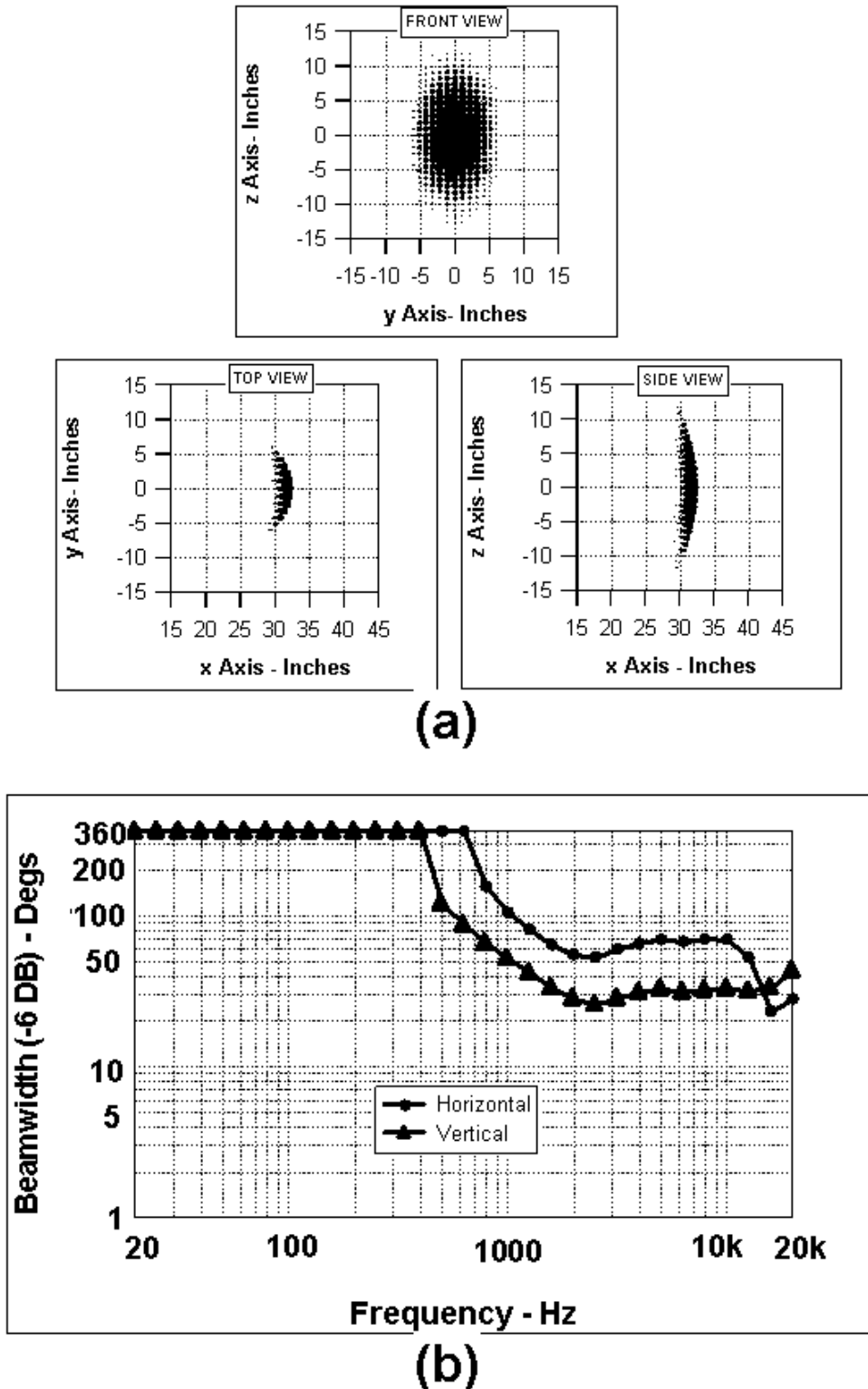
Fig. 20. (g) Footprints. See first figure for full caption.

Fig. 21. Simulation results of the 100º x 50º 372-point elliptical toroidal cap array with Legendre shading. (a) Front, top, and side configuration views. (b) Plot of beamwidth vs. frequency. (c) Directivity and Q vs. frequency. (d) On-axis loss plot vs frequency. (e) Horizontal polar plots of the array from 630 Hz to 16 kHz at one-third-octave centers. (f) Vertical polar plots of the array from 630 Hz to 16 kHz at one-third-octave centers. (g) Footprint plots from 630 Hz to 16 kHz at one-third-octave centers.

Fig. 20. (a) Expanded front configuration view. Approximate source strength is indicated by point size. Sources were laid out on a rectangular grid on an unfolded torus segment at equal angular increments. Shading was applied by superimposing an ellipse and then shade values assigned according to distance from center of ellipse (unity at center and zero at edge of ellipse, etc.). Sources with zero source strength were eliminated. See first figure for full caption.
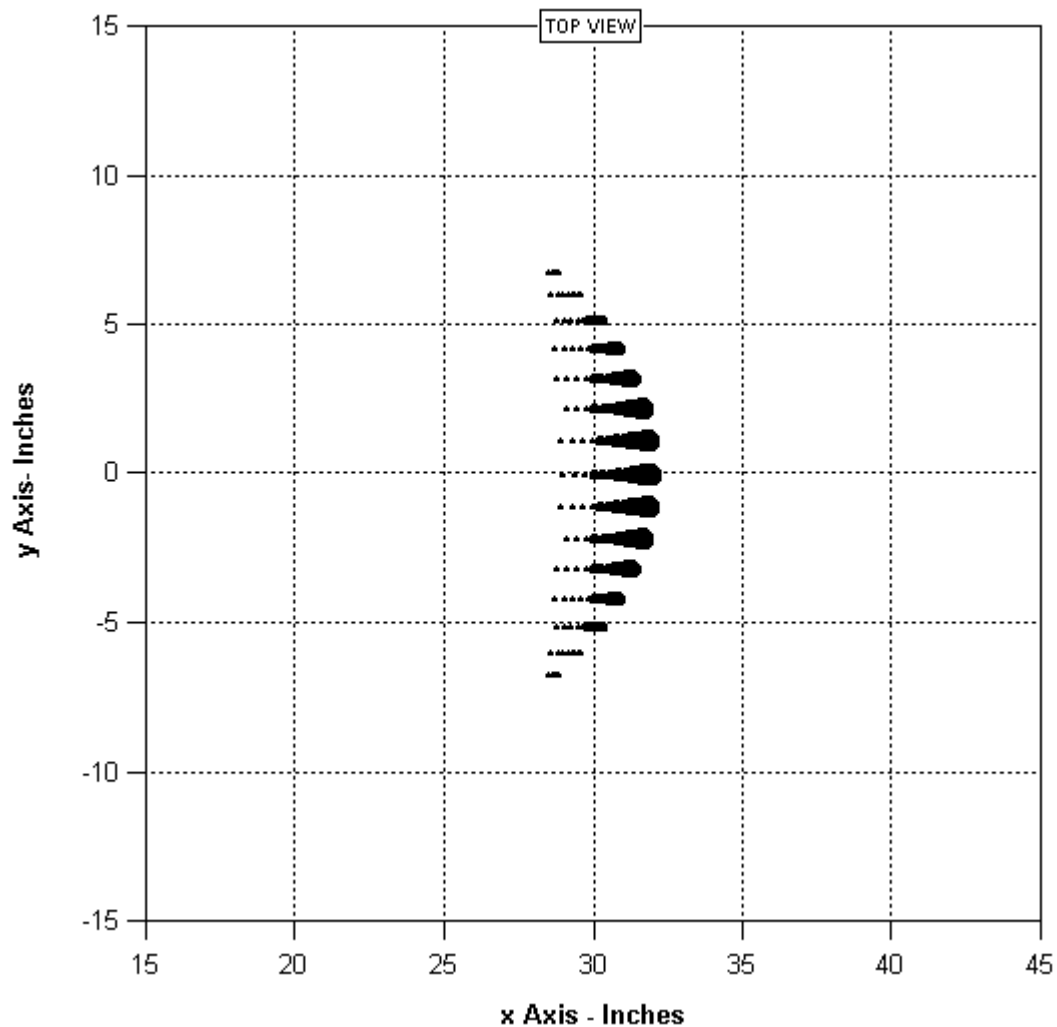
Fig. 21. (a) Expanded top configuration view. Center of curvature for this view is (23.13, 0, *). See first figure for full caption.
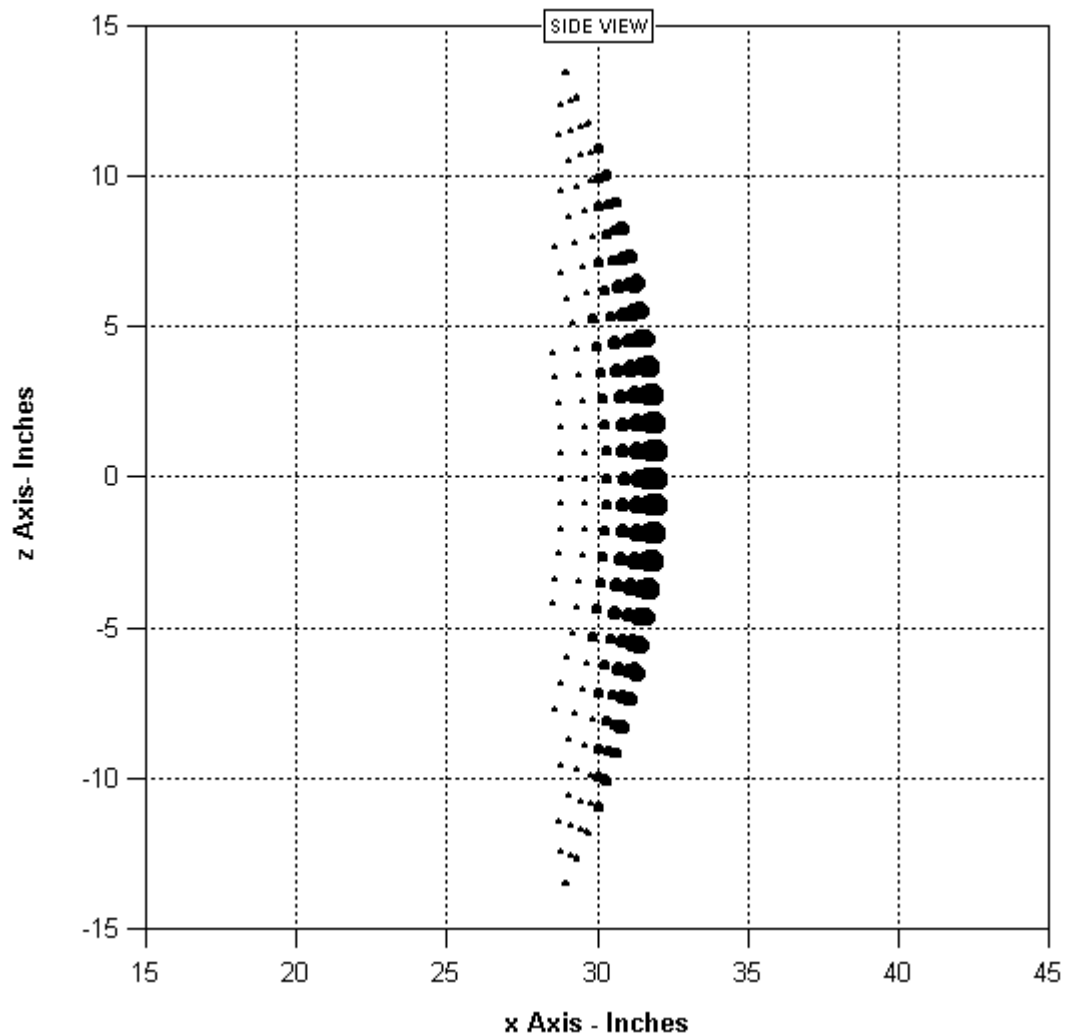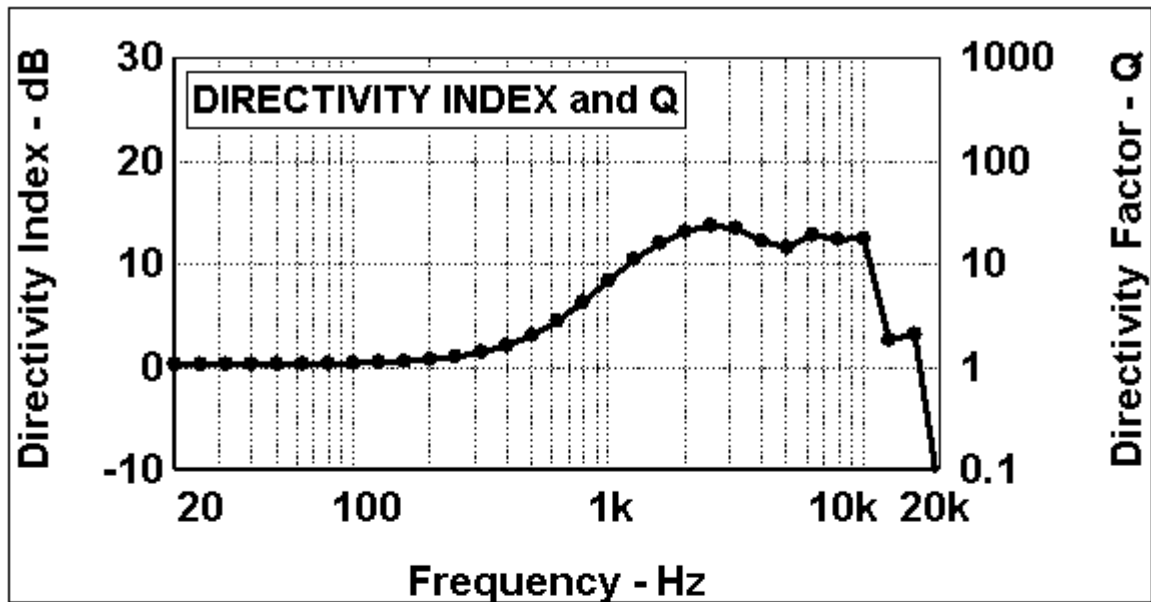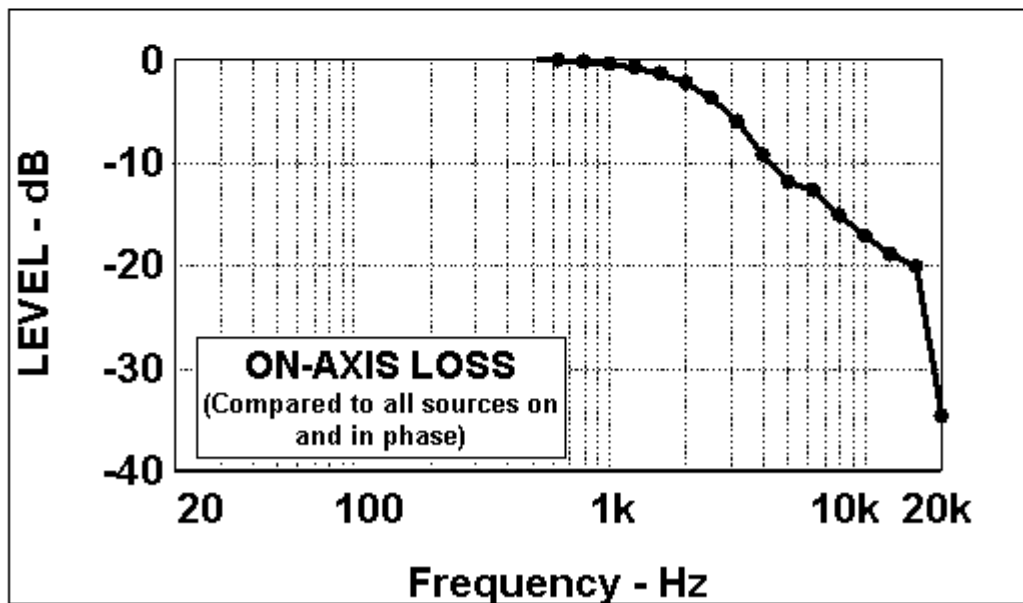
Fig. 21. (a) Expanded side configuration view. Center of curvature (center of torus) for this view is (0, 0, 0). See first figure for full caption.

(c)

(d)

Fig. 21. (c) Directivity. (d) On-axis loss. See first figure for full caption.
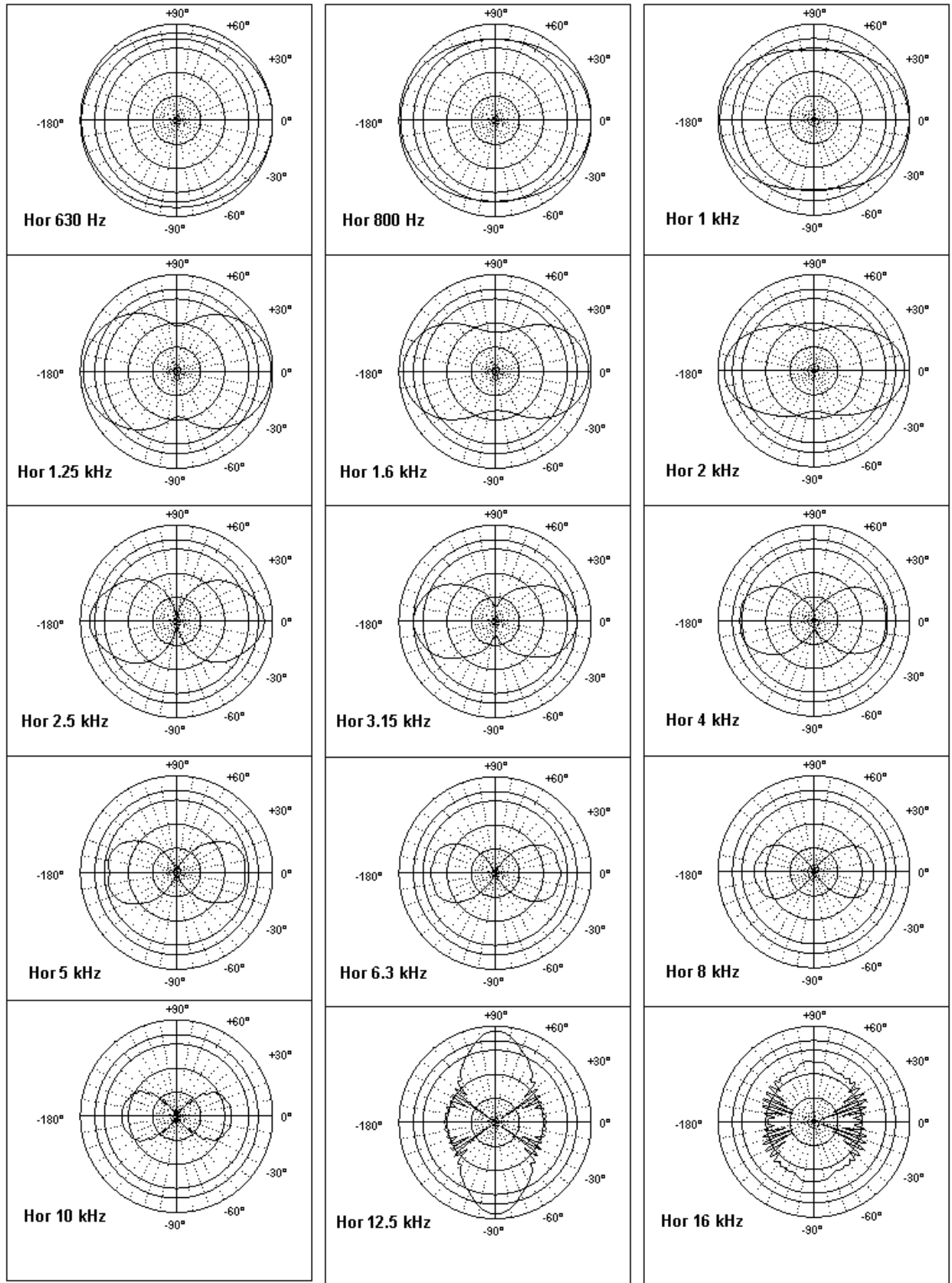
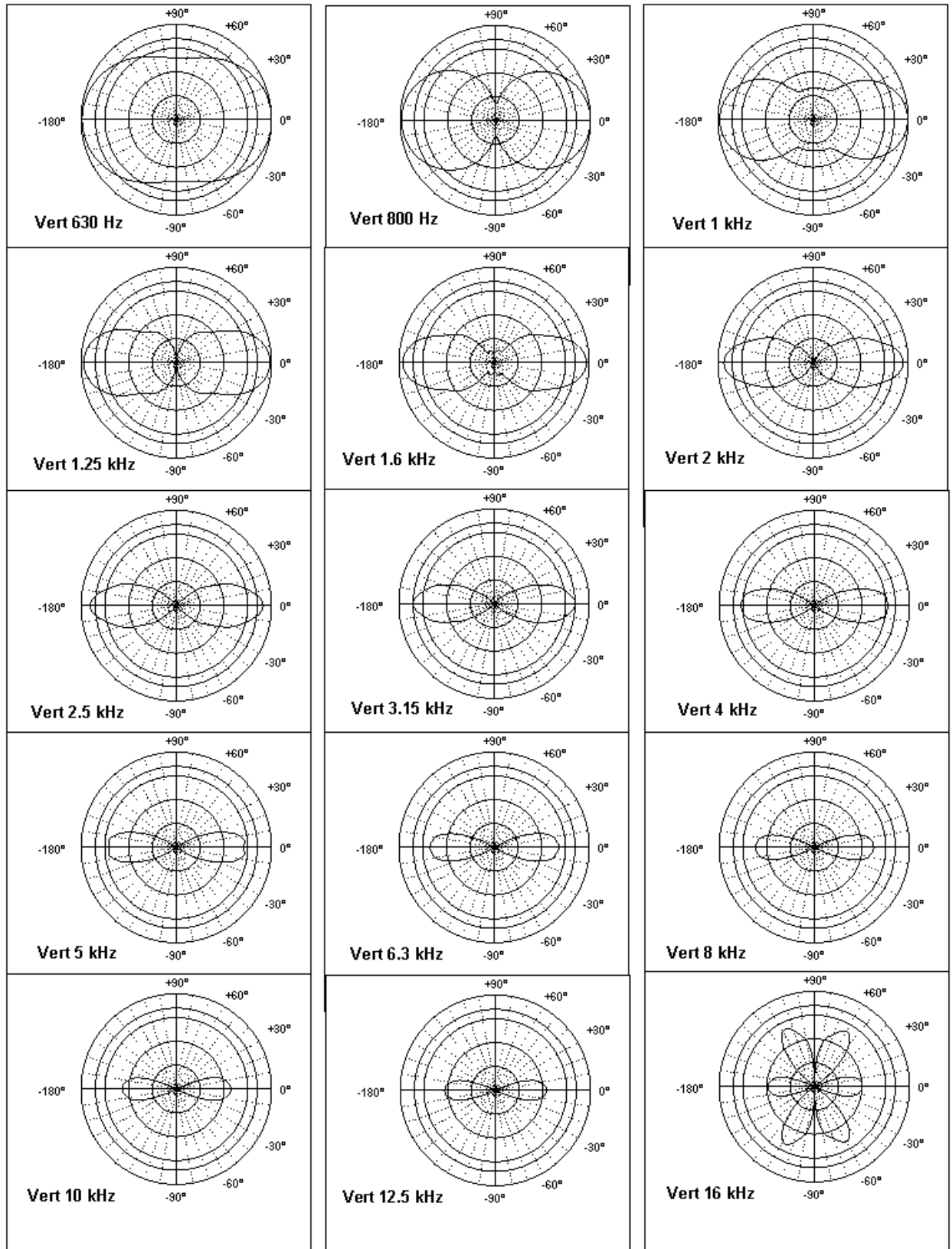Fig. 21. (e) Horizontal polars. . See first figure for full caption.
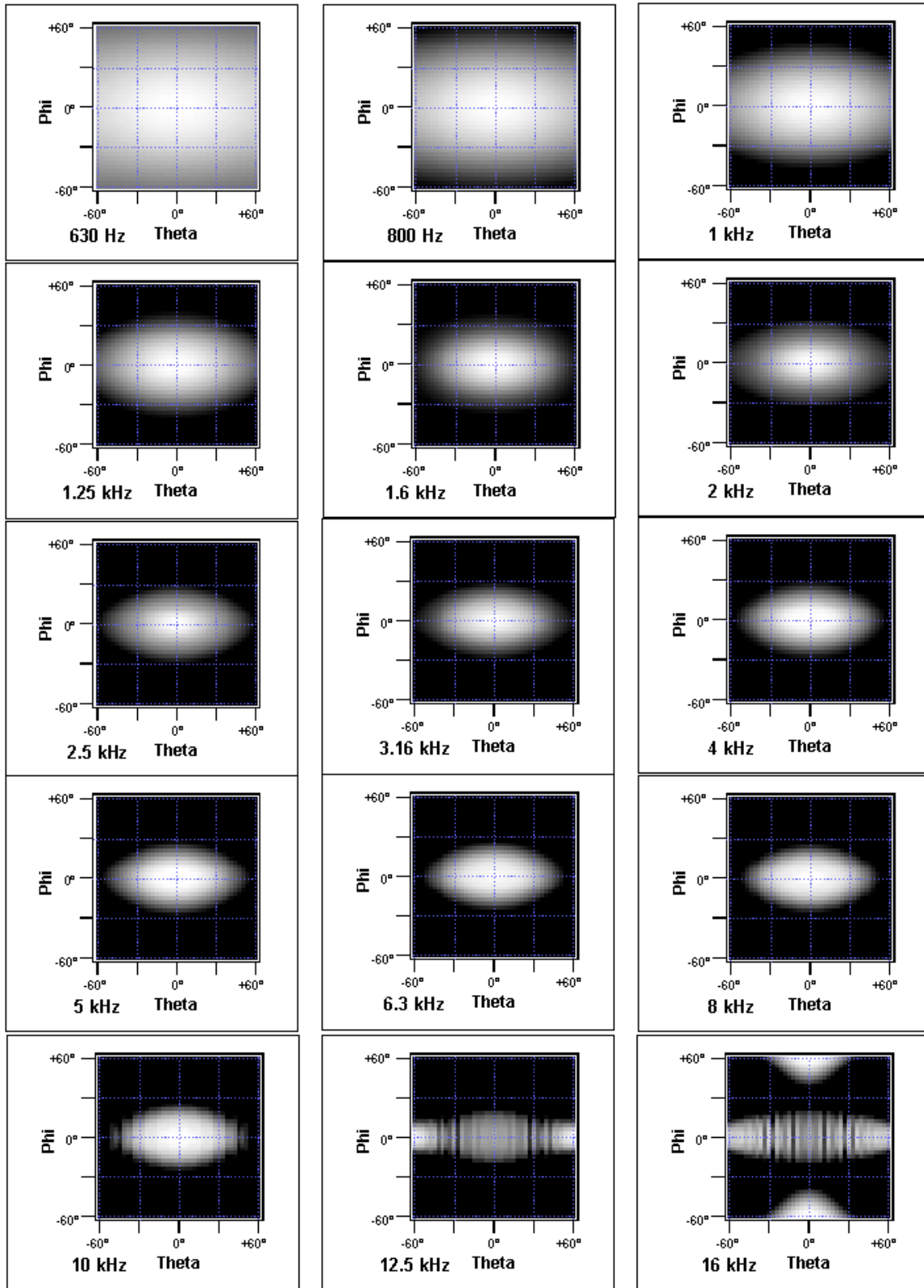
Fig. 21. (f) Vertical polars. . See first figure for full caption.

Fig. 21. (g) Footprints. See first figure for full caption.

KEELE   APPLICATION OF CBT THEORY TO LOUDSPEAKER ARRAYS